The Rheology Of Structured Fluids

by
Jason P. Humm

A thesis submitted to the
University of Warwick
for the degree of
Doctor of Philosophy

Department of Physics
University of Warwick
Coventry
CV4 7AL

October 1993

VARIABLE PRINT QUALITY

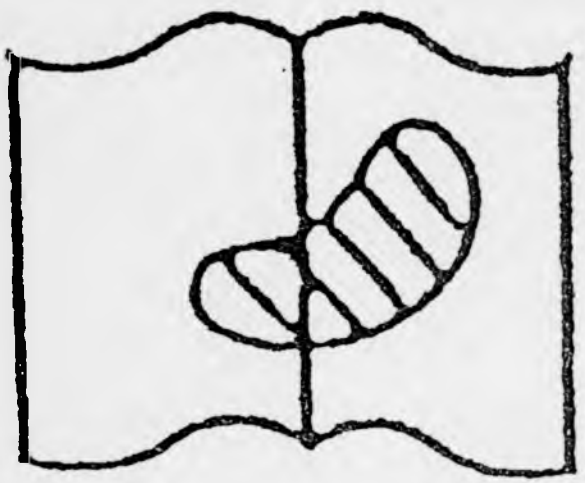

Declaration

This thesis is submitted to the University of Warwick in support of my application for admission to the degree of Doctor of Philosophy. This thesis contains an account of my own independent research carried out in the Department of Physics at the University of Warwick from October 1990 to September 1993 under the supervision of Prof. J.M.F. Gunn of the University of Birmingham and Prof. G. Rowlands of the University of Warwick. No part of this thesis has been previously submitted for a degree anywhere.

Acknowledgments

Firstly I must thank Prof. Mike Gunn for his excellent supervision of this work. His continual enthusiasm for the world of physics has added a great deal to my enjoyment of the three years I have spent on this project.

I must also thank Prof. George Rowlands for the invaluable help he has given me throughout the course of my work.

Thanks also go to the Science and Engineering Research Council and ICI Paints who jointly funded this work. Thanks particularly to Mr. Trevor Strivens and Dr. Stephen Bell for their help during my visits to ICI.

I would also like to thank all the members of the Theory group at Warwick for helping to make my time at Warwick so enjoyable.

Finally, thanks to my Parents and Paula for their support and encouragement, which has helped me throughout my University career.

Abstract

In this thesis we present a theoretical investigation of the rheological properties of gels and colloidal dispersions, subjected to shear stresses.

We present a mean field calculation of the effective shear modulus of an elastic material containing elastic inclusions and use the resulting expression to model a gel under shear. We calculate the stress-strain curve for such a gel and show that the gel is expected to fail along planes parallel to the plates providing the shearing forces.

A model of layered colloidal structures is investigated by considering the sheared flow of many layers of fluid with differing viscosities in each layer. Such flows are shown to be linearly unstable for all systems with more than four layers, when long wavelength perturbations are present.

A microscopic model of a flowing suspension of neutrally buoyant spheres is presented, based on the approach used by Batchelor to describe a fluidised bed. This model takes into the account the lift forces of Vasseur and Cox and the diffusion effects of Brownian motion. The model is used to calculate the equilibrium particle distributions and fluid velocity profiles for a suspension subjected to shear. This equilibrium solution is shown to be stable to small fluctuations of the flow, by a linear stability analysis.

Contents

List of Figures

Chapter 1

Introduction

1.1 The Properties Of Structured Fluids

1.1.1 What is rheology?

Rheology is the study of the deformation and flow of materials when they are subjected to external mechanical forces. Many common substances demonstrate rheological properties which are similar to those of an ordinary liquid at first sight but, on closer inspection, turn out to have much more complicated behaviours than liquids such as water. Many industrially important materials fall into this category making the scientific study of these properties of importance.

1.1.2 Visco-elastic materials

An example of an everyday material which shows unexpected rheological properties is cornstarch or custard powder. This will flow quite freely down a sloping surface but can behave like a solid under rapidly applied stresses such as during a sudden impact. This is an example of a material which shows *visco-elastic* properties . If a visco-elastic material is subjected to a rapid deformation it will behave as an elastic solid but the same material will flow like a viscous fluid if

subjected to a slow deformation. The ratio of the time taken for the material to relax back from a deformation to the time of taken to deform the material is known as the *Deborah number*. For large values of the Deborah number the material will behave as an elastic solid, whilst for small values, the behaviour is that of a viscous fluid. Many structured fluids have a Deborah number of about unity, leading to interesting rheological properties.

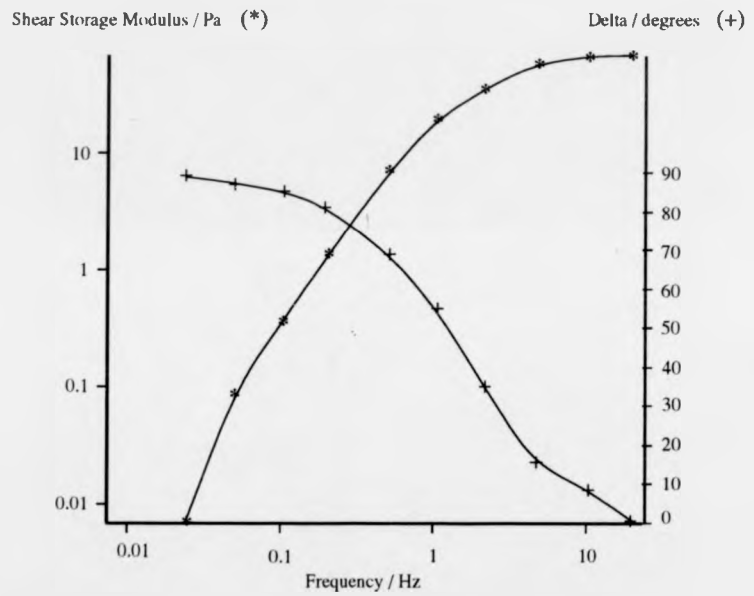

Figure 1.1: *The elastic properties of CTAB subjected to oscillatory shear strains*

An excellent example of a material with strongly visco-elastic properties is cetyl tri-methyl ammonium bromide (CTAB) in solution with salicylic acid. Figure 1.1 shows a plot of the elastic properties of CTAB[1] when subjected to an oscillating shear of varying frequency [1]. The property measured in this case

[1] All the experimental data shown in figures 1.1-1.3 were obtained using a Bohlin controlled stress rheometer in collaboration with the Paints division of ICI.

is the shear storage modulus. Mathematically this is given by the real part of the complex elastic modulus which relates the applied strain to the response stress. Physically this parameter gives a measure of the elasticity of a material. The quantity Delta gives the phase difference between the applied strain and the responding stress. This corresponds to the argument of the complex elastic modulus. (These measurements are described in more detail in appendix A). For a purely elastic material the phase difference should be zero. For a purely viscous fluid the phase difference will be 90 degrees. The figure shows that as the frequency of the oscillation is increased from 0.01 Hz to 10 Hz the phase difference changes from near 90 degrees to almost zero. This clearly demonstrates the tendency for CTAB to behave as a fluid on long time-scales (low frequency) and as an elastic solid on short time-scales (high frequency).

Figure 1.2 shows the behaviour of a non-drip paint when subjected to the same oscillatory strains as CTAB in figure 1.1 [1]. It is seen here that the phase difference changes relatively little over the range of frequencies, showing that the paint is not strongly visco-elastic. The shear storage modulus changes comparatively slowly, increasing by a factor of 10 over the frequency range.

1.1.3 Non-Newtonian Fluids

A simple fluid whose viscosity is a constant under all conditions is known as a Newtonian fluid. By contrast a fluid whose viscosity is a function of stress or time is usually referred to as a non-Newtonian fluid. For the purposes of this discussion it is convenient to discuss non-Newtonian and visco-elastic properties separately, but it should be noted that visco-elastic materials are frequently non-Newtonian and vice versa.

As we have seen, materials such as a non-drip paint do not behave in the same way as visco-elastic fluids but they do show significant differences from simple fluids. These materials behave as solids when small stresses are applied. When

a larger stress is applied, such as by brushing a paint brush across the paint, the material will flow like a liquid. This shows the characteristics of a *shear-thinning* material whose viscosity decreases as the applied stresses are increased.

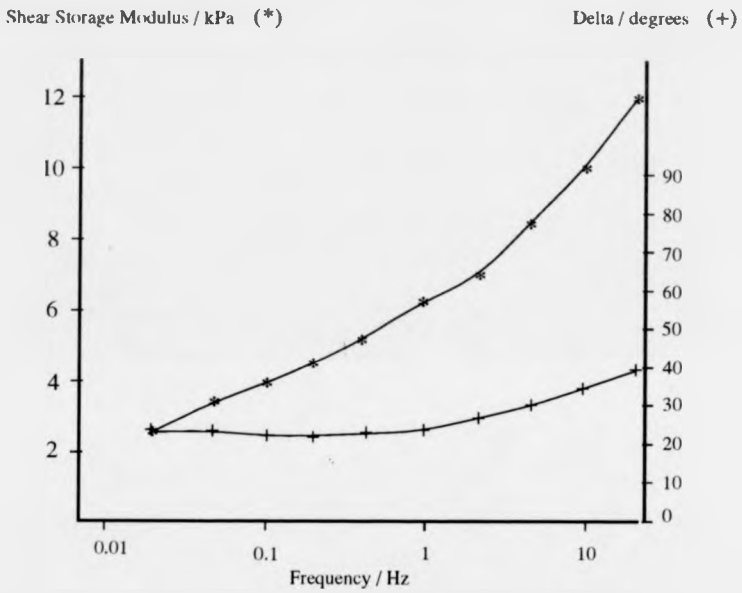

Figure 1.2: *The elastic properties of a non-drip paint subjected to oscillatory shear strains*

Many other types of behaviour can also observed, such as *shear-thickening* or *dilatency*, where the viscosity increases with increasing stresses. Also *thixotropy* is common where the viscosity is a function of the length of time the material is under stress.

An example of a material which shows both shear-thinning and thixotropic properties is given in figure 1.3. This is another type of paint, which shows a decrease in viscosity (the gradient of the stress/ shear-rate curve) as the shear-rate is increased. It also shows that the curve follows a different path when the shear-

rate is decreased from the maximum value to zero. This shows that rheological properties are time (or history) dependent, making the material thixotropic.

All of these different rheological properties are important when considering the industrial uses of structured fluids. For example, a non-drip paint should be solid in the container, yet it must flow easily when sheared by a paint brush so as to be taken up by the bristles of the brush (shear-thinning). It can then be easily applied to the surface. Once on the surface the paint must be fluid enough to flow into any irregularities in the surface and to remove brush marks. It must then regain its viscosity to be strong enough to support its own weight on vertical surfaces (thixotropy), otherwise *sagging* will occur as the paint slides down the surface. Finally the paint must dry to give a tough, durable surface.

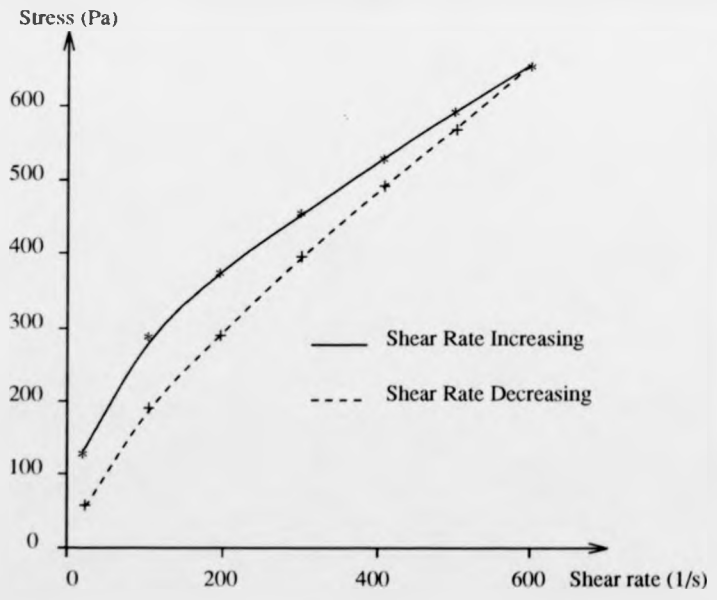

Figure 1.3: *Stress as a function shear-rate for a shear-thinning, thixotropic material*

1.1.4 The structure of complex fluids

The unusually complex behaviour of the materials just described is due to the size and shape of their component molecules. Unlike simple fluids, these fluids are composed of large molecules, with sizes much greater than those of a simple fluid such as water. These structures lead to a very wide range of mechanical behaviours, with the precise behaviour determined by the precise size and shape of the component molecules.

The actual structures which make up these fluids can vary widely. A common form is that of the polymer. Polymers are useful in the creation of structured fluids in several ways. The length of chains in many polymers can be closely controlled and this can be used to produce molecules with quite specific properties. For example, latex spheres can be produced with very small variations in size. Such mono-disperse molecules are ideal for theoretical modelling, since all the molecule's sizes and shapes are known in advance and more simply described than more complex structures.

The non-drip paint, whose visco-elastic behaviour is shown in figure 1.2, is an example of a polymer system. The other paint (figure 1.3) is composed of clay particles, which gives it different rheological properties. The behaviour of CTAB is due to the way the molecules arrange themselves into *micelles*. In this case the micelles are rod-like objects up to 1μm long, although only 20-30 nm wide. These micelles form a network which give CTAB its strongly visco-elastic properties and can clearly be seen in electron micro-graphs, as shown by Vinson and Talmon [2].

The general name for a particle which is in the size range which is interesting for rheology is a colloidal particle. This usually covers particles which lie in the range from 1nm to 1μm. These are not rigid limits but are used to define the scale at which surface effects for each particle are comparable with, or exceed, the effects due to the bulk of the particles. The particle need only have one

dimension in the colloidal size range in order to show colloid like behaviour.

1.2 The Stability Of Colloidal Dispersions

1.2.1 What are colloidal dispersions?

Colloidal dispersions consist of discrete colloidal particles within a continuous dispersing medium. Most of the following discussion will consider dispersions of solid particles within a liquid phase. There are however several different types of dispersions, such as *aerosols* which are dispersions of solids or liquids in a gas, or *emulsions* which are a liquid dispersed within a liquid.

When a large number of colloidal particles are dispersed in a fluid phase, it is usually important that the particles remain dispersed, rather than clumping together in a single large mass. This latter process is known as *aggregation* and can occur to varying degrees. The particles may aggregate into a relatively open network, called a floc, which is easily broken up by stirring or shearing the dispersion. This aggregation process is given the name *flocculation*. When aggregation occurs so that the aggregates cannot be broken up by stirring or shearing the dispersion is said to *coagulate*. The difference between these two behaviours is due to the different inter-particle forces acting in the dispersion and is discussed below.

A colloidal dispersion is said to be stable if flocculation does not occur to a significant extent. In general the stability or otherwise of a dispersion must be considered in terms of the forces which act on the particles within the dispersion. These can occur as inter-particle forces such as electrostatic attraction / repulsion, or as external forces such as gravity. In addition to forces such as these we must consider the effects of Brownian motion which can be very important for particles of colloidal dimensions.

1.2.2 Inter-particle forces

The first group of forces we discuss are Van der Waals forces. These are familiar from the role they play in simple liquids. For colloidal particles it is frequently assumed that the Van der Waals attraction can be calculated by assuming that every molecule in the particle attracts every molecule in a neighbouring particle. This pair-wise summation of single molecule forces results in a total force that acts between colloidal particles [3]. Although this is a crude method of modelling the interaction, it gives a useful guide to the effects of Van der Waals forces. An extra correction is required when the particles are more than about 50nm apart. This is due to the finite speed of light which causes correlations between particles to be reduced. This causes the force to drop more rapidly and is known as *retardation* [4].

Electrostatic forces can be important when the colloidal particles each carry a net electrical charge. The precise effect of electrostatic forces depends very strongly on the dispersion medium, which frequently will contain ionised molecules. This can lead to the formation of an *electrical double layer*, where the charged colloidal particles each attract a layer of oppositely charged ions around themselves. Thus the effects of electrostatic forces can often be controlled by adjusting the pH of the suspending medium.

Steric forces are particularly important when considering polymers. These forces are due to the interaction of polymer chains at the surfaces of colloidal particles. When these chains begin to overlap and inter-penetrate, we get two different effects. Firstly, the concentration of the suspending medium is reduced between the particles, causing osmotic pressures which force more of the medium between the particles, tending to separate the particles. Secondly, the chains become increasingly constrained in their movements, reducing the number of configurations they can adopt. This is equivalent to a reduction of entropy of the system and results in an entropic force tending to separate the particles.

These are the main inter-particles forces which define the stability of colloidal dispersions. The relative importance of these different forces will depend very strongly on the type of dispersion being considered. In general, if we plot the total potential between two colloidal particles we get a curve similar to that shown in figure 1.4. This curve shows the competition between the short range repulsive forces (e.g. steric repulsion) and the longer range attractive forces (e.g. Van der Waals forces). This form of interaction is peculiar to colloidal systems having two minima in the potential curve.

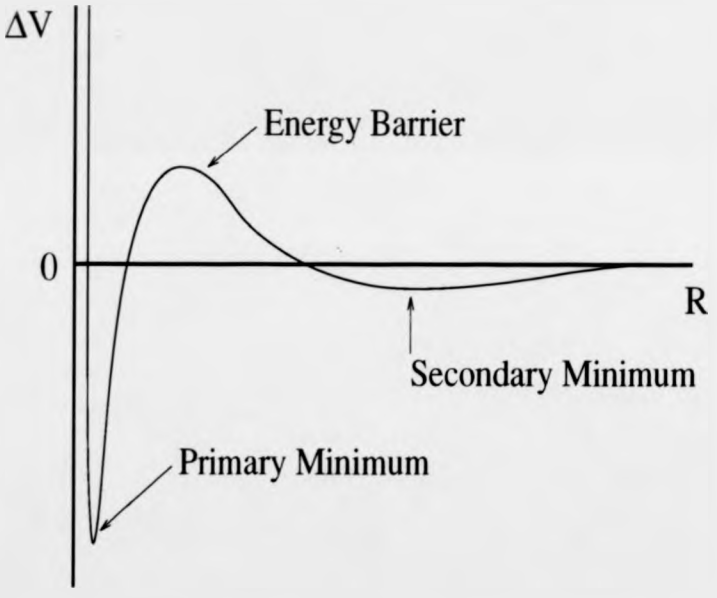

Figure 1.4: *The total interaction potential for two colloidal particles as a function of separation, R*

Figure 1.4 gives an explanation for the difference between flocculation and coagulation. If a particle is in the deeper potential well at small separation (the *primary minimum*) then the particles cannot be separated by stirring. The

secondary minimum) is generally very shallow (maybe a few kT or less) and particles can be removed from it relatively easily by stirring or shearing. Thus to prevent a dispersion from coagulating significantly the energy barrier between the minima should be as high as possible.

It should be emphasised that these descriptions are quite simplistic and that detailed models of colloidal interactions require more specific information about the interactions between particles. Although we shall not say anything about the detailed interactions between particles in the following chapters, these general interactions will act as a background to our modelling.

1.2.3 Brownian motion

The motion of a neutrally buoyant sphere suspended in a fluid and subject to random Brownian forces can be modelled using the Langevin equation [5]. The random forces correspond to the unpredictable forces imparted to the sphere during collisions with the molecules comprising the fluid. If a particle of mass, m, has a radius, a is in a fluid of viscosity, η, then the Langevin equation[2] is,

$$m\frac{\mathrm{d}^2\mathbf{r}}{\mathrm{d}t^2} + 6\pi\eta a\frac{\mathrm{d}\mathbf{r}}{\mathrm{d}t} = \mathbf{L}(t). \tag{1.1}$$

The vector $\mathbf{r}$ is the position vector of the centre of the sphere, at a time t and $\mathbf{L}(t)$ represents the random forces. This corresponds to Newton's second law of motion, with a drag force due to the surrounding fluid (using Stokes' formula) and inertia appearing in the usual way.

Since the exact form of the random forces is unknown, we make two assumptions which are sufficient to characterise $\mathbf{L}(t)$ for our purposes. If, we define the

[2]Equations with a random term such as the Langevin equation are usually referred to as stochastic equations. In some texts a Langevin equation is considered to be a stochastic equation with a random term which does not vary with position.

ensemble average of a process,

$$\langle \mathbf{L}(t) \rangle = \frac{1}{N} \sum_{i=1}^{N} \mathbf{L}_i(t), \tag{1.2}$$

where N is a large number and $\mathbf{L}_i$ is the force for the ith member of the ensemble, where all members have identical initial conditions. We then assume that the ensemble average of the random force is zero,

$$\langle \mathbf{L}(\mathbf{t}) \rangle = \mathbf{0} \tag{1.3}$$

and the average of the square of the force is given by,

$$\langle \mathbf{L}(t)\mathbf{L}(t+\tau) \rangle = \sigma \delta(\tau), \tag{1.4}$$

where σ is a constant and $\delta(\tau)$ is a Dirac delta function. The use of the Dirac delta function here is equivalent to saying that the random forces are completely uncorrelated in time.

Since the random forces have been defined only through averages, we can only use the Langevin equation to obtain information about the average position of the sphere at a given time. This is achieved by integrating the equation once to obtain the velocity, $\mathrm{d}\mathbf{r}/\mathrm{d}t$, and calculating the average of the velocity squared. Then using the equipartition of energy at equilibrium,

$$\frac{m}{2} \langle \frac{\mathrm{d}r_i}{\mathrm{d}t} \frac{\mathrm{d}r_j}{\mathrm{d}t} \rangle = \tfrac{1}{2} kT \delta_{ij}, \tag{1.5}$$

where δ_{ij} is a Kronecker delta, we can obtain an expression for σ. We can then find the root mean square displacement as a function of time, as well as other average properties.

An alternative approach is to obtain a Fokker-Planck equation for the probability distribution, P, of finding the particle at a position, r, at a time t. This is most simply found in the case where the inertia of the particle is very small compared to the viscous forces and so the first term in the Langevin equation can be neglected. The Fokker-Planck equation is then,

$$\frac{\partial P}{\partial t} = \tfrac{1}{2} \sigma \nabla^2 P. \tag{1.6}$$

(See Haken [6] for a full derivation of this result). It can easily be seen that this result has the form of a diffusion equation, with a diffusion constant, $\sigma/2$. In fact, it is the diffusion equation for particles and shows clearly that the random forces cause the sphere to diffuse throughout the fluid. The diffusion constant is found from the equipartition of energy at equilibrium, as before to give,

$$\tfrac{1}{2}\sigma = \frac{kT}{6\pi\eta a}, \tag{1.7}$$

which is the usual Stoke's-Einstein result for the self-diffusion of a sphere.

1.2.4 Sedimentation

One example of where external forces are important in the stability of dispersions is that of sedimentation. If we consider the one-dimensional sedimentation of a single particle under gravity and subjected to Brownian motion, we obtain the equation,

$$6\pi\eta a\frac{\mathrm{d}x}{\mathrm{d}t} - mgx = L(t), \tag{1.8}$$

where g is the the acceleration due to gravity on a particle at a height, x. The Fokker-Planck equation for this system is

$$\frac{\partial P}{\partial t} = \frac{mg}{6\pi\eta a}\frac{\partial P}{\partial x} + D\frac{\partial^2 P}{\partial x^2}. \tag{1.9}$$

It is useful at this point to note that the Fokker-Planck equation can be written as a continuity equation for a probability flux, J:

$$\frac{\partial P}{\partial t} = \frac{-\partial J}{\partial x}. \tag{1.10}$$

If we look for equilibrium solutions, we can put $\partial P/\partial t$ to be zero and integrate once with respect to x to obtain

$$J = \frac{mg}{6\pi\eta a}P + D\frac{\partial P}{\partial x} = \text{constant}. \tag{1.11}$$

Since the probability flux must be zero at the bottom of the container ($x = 0$), the constant of integration must be zero. Integrating once more we obtain

$$P = C \exp\left(\frac{-mgx}{kT}\right), \tag{1.12}$$

where we have used the value of the diffusion constant given by equation 1.7 and C is a constant (this can be found by normalisation of the probability distribution).

Here we have obtained an equilibrium solution. An important question to be answered is how does the system approach equilibrium? Weiland, Fessas and Ramarao [7] have shown experimentally that when two different sizes (or densities) of sedimenting particles are present the system can show *fingering*, where the particles tend to sediment in vertical streams separated by regions of relatively particle free fluid. This shows that uniform sedimentation can be unstable and can give more complex structures which vary in the directions perpendicular to the x direction. These instabilities have been investigated theoretically by Batchelor and Janse Van Rensburg [8] who showed that the fingering can be initiated by small fluctuations in the concentration. The idea that fluctuations in concentration can cause equilibrium solutions to become unstable is very important and will be used to investigate the stability of shear flows in chapters 3 and 5.

1.3 The Elastic Properties Of Gels

The term *gel* can have many different interpretations and has been used for many widely varying systems. We shall use the definition of Almdal [9]. The phenomenological characteristics of gels used by Almdal are:

(a) "They consist of two or more components, one of which is a liquid present in substantial quantity"

(b) "They are soft, solid or solid-like materials."

This definitions excludes dry materials such as *aerogels* but covers a wide range of two phase materials which are of interest.

The mechanical properties of gels are important in many branches of industry. As a result of this, a theoretical understanding of the physics underlying these properties is highly desirable.

Experimental measurements of the elastic properties of gels have been carried out by several groups. The shear moduli of latex gels were measured by Buscall et al [10] as a function of shear strain for various volume fractions of gelled material. They showed that at small strains the gels behaved elastically with constant shear moduli. As the strains were increased, the shear moduli tended to decrease and the gels softened. The shear moduli of gels as a function of particle concentration have also been measured by Buscall et al [11].

Experimental measurement of the properties of gels near the sol-gel transition have also been carried out by Allain and Salomé [12] and Adam et al [13]. Allain and Salomé showed that the elastic modulus of a gel goes to zero below some critical concentration of molecular cross-links. Adam et al showed that above a critical concentration of cross-links the mass distribution of clusters of gel molecules diverged.

The elastic properties of gels have been theoretically investigated using several different approaches. One of the successful methods is the use of various aspects of percolation theory [14]. In its simplest form, percolation theory can be used to calculate the fraction of a system which must be gelled, in order for the system to show a non-zero shear modulus. Percolation theory provides a framework within which to describe the the way the physical properties behave near the gelation point (see for example Adam et al [15]). This concept can be extended from a simple connectivity problem, to include more complex ideas, such as rigidity percolation, as used by Thorpe [16, 17].

Rigidity percolation takes into account the fact that although a gel network may be connected this is not a sufficient condition for the network to support

a stress across it. This allows stronger constraints to be placed on the required gelled fraction.

Work by Duxbury [18] on fuse networks is related to calculations of the elastic properties of gel networks. This work was intended to study the general failure of materials outside the scope of elasticity theory. The equations solved when a network of fuses is subjected to an electric potential, are the scalar equivalent of the vector equations which would describe a material comprised of bonds with a finite yield stress. The applied potential plays the role of an applied stress on a gel and the fuses behave as bonds within the gel. Such calculations are useful in attempting to find patterns of failure within a failed network.

Some other approaches have been less successful. For example models such as that of Denny and Brodkey [19], based on the kinetic equations for bond breakage and reformation, contain too many unknown parameters to be practically useful.

The field of composite materials has also given some useful results. These involve calculations of the elastic properties of two phase materials, where each phase has different elastic properties. Since a gel can be considered as a composite of an elastic medium and regions which are stress free, where no bonds exist, the field of composite materials is potentially very useful for the study of gels. Much of the work in the field of composites uses results due to Eshelby [20], based on the assumption that the materials are composed of ellipsoidal regions within a homogeneous matrix phase. Effective elastic moduli have been calculated using various assumptions about the systems in question. In the case of shear moduli, most of these methods are unable to give precise expressions. Normally, only upper and lower bounds on the moduli can be obtained, such as the result of Hashin [21].

In Chapter 2 a model of a gel under shear is described. We begin by modelling the gel as a homogeneous, isotropic elastic medium with a distribution of spherical voids throughout the medium. Each of these voids is a region which is unable to support any stress and can be thought of as a missing or broken bond within the

structure.

The case of an elastic medium with a single spherical inclusion of elastic material is solved and the result shown to be analogous to the problem of an electric dipole in an electric field. To take into account the effect of the distribution of spheres, a mean field calculation of the stress due to to a distribution of such dipoles is made, by analogy with the Clausius-Mossotti relationship of electromagnetic theory. This allows a precise expression for the effective shear modulus to be obtained in terms of the volume fraction of voids.

A phenomenological model for the void concentration is then used, in conjunction with this result, to obtain a self-consistent result for the stress-strain relationship for the gel. This uses the idea of a distribution of bond yield stresses as used by Duxbury [18]. We then go beyond the mean field arguments and predict the likely patterns of failure of the gel. Inspection of the energy density near a single void shows that failure is expected to be most likely along planes perpendicular to the plane of shear.

Finally, we shall point out the similarity between the equations of elasticity and the equations of slow fluid motions. This similarity will be used to obtain the solution for a spherical void near a fixed boundary.

1.4 The Stability Of Layered Colloidal Structures Under Shear

It has been known since the early 1970's that suspensions of particles can form ordered structures when sheared [22, 23]. Light scattering experiments carried out on sheared latex dispersions [24] have shown that two and three dimensional structures can be formed, consisting of ordered arrays of colloidal particles.

Many different types of ordering have been observed, including string-like structures where particles lie in lines. Structures of this sort have been observed

by Ackerson and Pusey for polymethylmethacrylte (PMMA) spheres in a steady shear flow [25]. They also showed that under oscillatory shearing the particles exhibited a different ordering. In this case structures of face centred cubic and hexagonally packed particles were observed. When shearing was ceased, it was found that the particle structure was lost over a period of about 30 minutes, leaving an amorphous structure. This was described a melting of the crystal structure.

The structures described so far show a crystal-like ordering with colloidal particles behaving as the units of the crystal. A different type of ordering has also been observed where the colloidal particles are concentrated in layers several particle diameters thick. These layers are separated by regions which are depleted of particles [26]. These structures will behave less as crystals and can be thought of as alternating layers with different rheological properties.

The viscosity of a suspension depends strongly on the concentration of the suspended particles. Hence we would expect these layered suspensions to have different viscosities in each layer. Such a suspension could then be thought of as a system of layered Newtonian fluids, with different viscosities and densities attributed to each layer. The regions where the particles tend to congregate will have a high viscosity and the depleted layers will have a correspondingly lower viscosity. Using such a model, one can calculate the time independent configurations of a suspension.

The study of the stability of such layered configurations has a long history, with many systems having been considered. The case of layers of inviscid fluids was investigated by Taylor [27], who considered stability of a fluid with a density which varied as a function of height. For the case where the density profile was constant in an upper and lower layer and varied linearly within a central layer a form of resonance instability was identified. This occurs when a disturbance on one interface forces a disturbance on the other.

A result obtained by Squire [28] allows one to simplify the stability analysis

of such systems greatly. He showed that any instability which exists for a three dimensional disturbance also exists for a two dimensional disturbance, with a lower value of the critical Reynold's number. This means that the stability of any three dimensional fluid bounded by parallel, plane walls could be found by considering the equivalent two-dimensional problem.

Squire's result was used by Yih [29] and Li [30] to investigate the stability of two and three layer viscous flows respectively. They both identified instabilities for long wavelength disturbances.

In Chapter 3, we use the long wavelength perturbation technique of Yih to calculate the stability of N layers of fluid in a Couette system. The neutral stability curves are discussed and a resonance instability identified. We shall show that this layered model is unstable when more than four layers of fluid are considered.

1.5 A Microscopic Model Of Flowing Suspensions

There have been many different models of flowing suspensions of particles suggested over the last 20 years. A variety of different approaches have been used with varying degrees of success. Most of these models rely on a knowledge of the behaviour of single particles in a flowing material and so we begin with a brief discussion of the forces acting on single spherical particles.

There are various hydrodynamic forces which act on single spheres. Possibly the most familiar of these is the Stoke's drag [31] which tends to slow the motion of a particle relative to the surrounding fluid. Another important hydrodynamic force is known as the Faxén force [32] and is proportional to $\nabla^2\mathbf{V}$, where $\mathbf{V}$ is the fluid velocity which would exist without the particle. Both of these forces occur in the limit of zero Reynolds number, but they are unable to make a particle cross

streamlines within a flow. (This is a general result at zero Reynolds number, due to Bretherton [33]).

The existence of transverse forces, which allow particles to cross streamlines, is well known in inviscid fluids and is described using the Bernoulli equation. At low Reynolds number when viscous effects become important the same effects are more difficult to calculate. This type of force is often known as a lift force and has been considered by many workers, both experimentally and theoretically. The lift force on a sphere in an unbounded shear flow was obtained by Saffman [34]. The lift force in a bounded flow was discussed by Cox and Brenner [35] who obtained a lift force in integral form. The first explicit calculation of a lift force in a bounded fluid was obtained by Ho and Leal [36] although the result was later corrected by Vasseur and Cox [37]. These forces have been incorporated into several different types of model.

One model that we shall discuss is that used by Nozières and Quemada [38], who considered a continuous fluid containing discrete spherical particles. This approach allows the fluid to be described using a form of the Navier-Stokes equations. The particle distributions are defined using a diffusion equation, with the additional assumption that the particles are subject to a force acting to move them towards regions of lower shear rate. This force was justified by reference to the work of Ho and Leal but the from of the force used was significantly different to that predicted by Ho and Leal. Nozière and Quemada carried out a linear stability analysis for the model and showed that Plane Couette flow of a suspension could be unstable above a critical shear rate.

An alternative approach was used by McTigue, Givler and Nunziato [39], who modelled the particles as a second fluid which penetrates throughout the true fluid. This model incorporated all of the hydrodynamic forces mentioned above but required an extra constitutive relation to be assumed in order to make any physical predictions.

A more rigorous approach was used by Batchelor [40], for a 1 dimensional

fluidised bed. In a fluidised bed the particles fall under gravity while supported in a vertical upward fluid flow. Batchelor considered the detailed conservation of momentum for the particles, to obtain an equation which treats the particles as a fluid but removes the requirement for the additional assumptions used by McTigue et al.

In Chapter 4 we shall present more detailed review of these models and the important hydrodynamic forces. We shall then use an approach similar to that used by Batchelor to obtain a model of a flowing suspension. In Chapter 5 we apply our model to the problem of Plane Couette flow of a suspension. An equilibrium solution is given and the stability of the solution considered using linear stability theory.

Chapter 2

The Softening Of Gels Under Shear

2.1 A Model For Gels

It is well known that a gel will behave as an elastic body when subjected to small shear stresses and strains. This has been shown by Buscall et al in the specific case of latex gels [10]. With this in mind, it is reasonable to model a gel, initially, as an elastic medium. As the stress is increased the structure of the gel begins to break down and the shear modulus decreases. Microscopically this is a result of bonds breaking within the gel structure. Regions near a failed bond are then unable to support a shear stress and further straining occurs. Such a region can be modelled as a cavity within a general elastic medium.

We begin by modelling a gel as a homogeneous, isotropic, elastic medium. When this gel is subjected to a given stress, a fraction of the bonds within the structure will fail. This is represented by a distribution of spherical cavities within the elastic medium. The actual volume fraction of cavities is determined by the applied stress. A schematic diagram of the system is shown in Figure 2.1.

We must first consider the stress field associated with a single spherical cavity

when the medium is subjected to a homogeneous shear. This result is obtained from the calculation of the stress field for a spherical inclusion of elastic material, with a shear modulus which is different from the surrounding elastic medium. We may then use the limiting case that the shear modulus of the inclusion equals zero. This result is used to show that an elastic inclusion, in an elastic material can be treated by an approach analogous to that of a polarisable molecule, in a dielectric material.

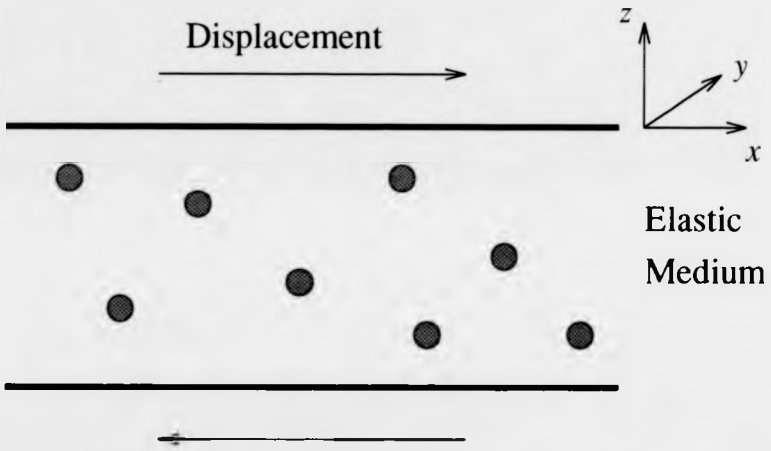

Figure 2.1: *The geometry of the gel system*

An equation analogous to the Clausius-Mossotti relation [41, 42] from dielectric theory is obtained for a system of many inclusions. This relates the elastic constants of the entire system to those of the medium and the inclusions. A self-consistent argument is used next, to obtain the stress-strain relationship for a gel, when the number of cavities present is a function of the applied stress. We next consider the most likely modes of failure of a gelled system, when the distribution of cavities is not homogeneous, as is assumed in the previous mean field calculation. Finally we point out some mathematical similarities between

the equations of elasticity and those of a fluid moving at low Reynolds number. This analogy is used to calculate the displacement field of a single cavity near a fixed boundary.

2.2 The Stress Field Due To A Single Inclusion

We begin with a description of some well known results, which we will make use of in our calculation. The first result is a calculation of the stress due to a single spherical inhomogeneity in an infinite elastic medium. We shall refer to this situation as a spherical inclusion within an elastic matrix. This result has been obtained independently by many workers. The approach used here combines results obtained by Landau and Lifshitz[43], for a spherical void, and Eshelby[20], for general, elliptical inclusions.

The equation of equilibrium for an elastic material subjected to a distribution of body forces, $\mathbf{F}$, is

$$\mu\nabla^2\mathbf{u} + \frac{\mu}{(1-2\nu)}\nabla(\nabla\bullet\mathbf{u}) = -\mathbf{F}. \tag{2.1}$$

This equation involves Poisson's ratio for the matrix, ν, and the shear modulus, μ. Poisson's ratio can vary between values of -1 and $\frac{1}{2}$. These limits are due to the requirement that the strain energy of an isotropic elastic material must always be positive. The upper limit corresponds to an incompressible solid whose volume cannot be altered, although the shape may be changed. Conversely, the lower limit is for a material whose volume can be changed but which cannot be sheared (i.e. the body's shape cannot be changed). Materials with a negative Poisson's ratio are rare but a few examples are known (see for example [44]).

If the forces are only applied at the surface of a body then the right-hand side of the equation of equilibrium is zero. Taking the divergence of the resulting equation gives

$$\nabla^2(\nabla\bullet\mathbf{u}) = 0. \tag{2.2}$$

Taking the Laplacian of the equilibrium equation instead of the taking divergence (still with $\mathbf{F} = 0$) gives the result that the equilibrium displacement vector must satisfy the biharmonic equation,

$$\nabla^2 \nabla^2 \mathbf{u} = 0. \tag{2.3}$$

Hence the volume change during a deformation $\nabla \cdot \mathbf{u}$ is a harmonic function while $\mathbf{u}$ is a biharmonic function.

If we now consider a spherical elastic inclusion in an elastic medium then we can use the fact that $\mathbf{u}$ satisfies the biharmonic equation to obtain a general expression for the displacement vector in the region outside the inclusion. Landau and Lifshitz stated the result in terms of derivatives of the distance from the centre of the sphere, r. We give the expression here using the notation, $\partial_k = \partial/\partial r_k$. (The Einstein summation convention is used subsequently, unless otherwise stated).

$$u_i = -4A(1-\nu)\sigma^0_{ip}\partial_p\left(\frac{1}{r}\right) + A\sigma^0_{pq}\partial_p\partial_q\partial_i\, r \tag{2.4}$$

Here a term of order $1/r^5$ has been neglected. This form is the most general biharmonic vector which depends on the applied stress and vanishes at infinity. The stress at distances far from the inclusion, is given by σ^0_{ip}, and A, is an unknown constant. Once the displacement vector is known then the stress is derived in the usual way using Hooke's law,

$$\nu_{ik} = \frac{E}{1+\nu}\left(u_{ik} + \frac{\nu}{1-2\nu}u_{ll}\delta_{ik}\right), \tag{2.5}$$

where u_{ik} is the strain tensor, given by, $u_{ik} = \frac{1}{2}(\partial_k u_i + \partial_i u_k)$.

Eshelby showed that if a homogeneous strain is applied to a matrix, an ellipsoidal inclusion will be in a state of homogeneous strain. The form of this strain is given by the strain at large distances from the region. Using this result, the displacement vector within the inclusion can be written in terms of the stress at large distances, σ^0_{ip}:

$$u'_i = \frac{B}{2\mu_0}\sigma^0_{ip}r_p. \tag{2.6}$$

This expression involves the shear modulus of the matrix, μ_0, and an unknown constant, B.

The constants A and B are calculated using the boundary conditions at the surface of the sphere. The appropriate conditions are that the displacement and the resulting stress must be continuous across the boundary. This leads to the following expression for A and defines the stress within the matrix, due to the inclusion.

$$A = \frac{5R^3(1-\mu/\mu_0)}{4[2(4-5\nu)\mu + (7-5\nu)\mu_0]} \tag{2.7}$$

The stress within the inclusion is defined by B, which in terms of A is given by

$$B = 1 + \frac{8\mu_0}{5R^3}(4-5\nu)A \tag{2.8}$$

Here μ is the shear modulus of the inclusion and R is the radius of the inclusion. We note at this point that since we are applying a pure shear, Eshelby's result says that the inclusion is in a state of pure shear. Hence only the shear modulus of the inclusion is involved in the calculation.

2.3 An Inclusion As An Elastic Dipole

In order to calculate the effective shear modulus of a matrix with inclusions, we treat each of the inclusions as a dipolar system of forces. The description of the inclusion contributions as dipolar is consistent with the term polarisation stress, used by Shtrikman[45], to describe additional stresses due to inclusions within a matrix.

The fact that the inclusion stress field has a dipolar character can be seen by a multipolar expansion of the Green's function, in the convolution integral for the displacement vector:

$$u_i = \frac{1}{16\pi\mu(1-\nu)} \int F_j(\mathbf{r}') \left(\frac{(3-4\nu)\delta_{ij}}{|\mathbf{r}-\mathbf{r}'|} + \frac{(\mathbf{r}-\mathbf{r}')_i(\mathbf{r}-\mathbf{r}')_j}{|\mathbf{r}-\mathbf{r}'|^3} \right) d\mathbf{r}' \tag{2.9}$$

A derivation of this result is given in Appendix B.

To obtain a multipolar expansion, we use a Taylor expansion of the Green's function, which is equivalent to writing the force distribution as,

$$F_k(\mathbf{r}') = F_k^{(0)}\,\delta(\mathbf{r}') - F_{kj}^{(1)}\partial_j\,\delta(\mathbf{r}') + \tfrac{1}{2}F_{kjl}^{(2)}\partial_j\partial_l\,\delta(\mathbf{r}') - \ldots, \tag{2.10}$$

where

$$F_k^{(0)} = \int F_k\,d\mathbf{r}', \qquad F_{kj}^{(1)} = \int F_k r_j'\,d\mathbf{r}', \qquad F_{kjl}^{(2)} = \int F_k r_j' r_l'\,d\mathbf{r}', \tag{2.11}$$

are the moments of the force distribution about $\mathbf{r}' = \mathbf{0}$. From symmetry arguments, we would expect zero contribution from the 'monopole' term, i.e. $\mathbf{F}^{(0)}$. Thus the void should provide no net force acting on the gel. The leading order contribution is therefore expected to come from $\mathbf{F}^{(1)}$. If this term is substituted into equation 2.9, and the integral evaluated using the properties of the Dirac delta function, then after some manipulation we obtain,

$$u_i = -\frac{1}{4\pi\mu}\left(F_{ij}^{(1)}\partial_j\left(\frac{1}{r}\right) - \frac{1}{4(1-\nu)}F_{jk}^{(1)}\partial_j\partial_k\partial_i r\right). \tag{2.12}$$

If this expression is compared to the expression given by Landau and Lifshitz then it is quickly shown that we have obtained the two terms of order $1/r^2$, provided that the elastic 'polarisation tensor' $\mathbf{F}^{(1)}$ is proportional to the applied stress $\sigma^{(0)}$. This can be seen to be reasonable by considering the following system of forces, as a tends to zero.

$$\mathbf{F} = \frac{\hat{\mathbf{z}}}{a}\delta(\mathbf{r} - a\hat{\mathbf{x}}) - \frac{\hat{\mathbf{z}}}{a}\delta(\mathbf{r} + a\hat{\mathbf{x}}) + \frac{\hat{\mathbf{x}}}{a}\delta(\mathbf{r} - a\hat{\mathbf{z}}) - \frac{\hat{\mathbf{x}}}{a}\delta(\mathbf{r} - a\hat{\mathbf{z}}). \tag{2.13}$$

If we now use the definition of the elastic dipole moment,

$$F_{ij}^{(1)} = \int F_i r_j d\mathbf{r}, \tag{2.14}$$

then we find that $\mathbf{F}^{(1)} = 2(\hat{\mathbf{x}}\hat{\mathbf{z}} + \hat{\mathbf{z}}\hat{\mathbf{x}})$, which is indeed proportional to the applied stress.

If the stress is thought of as the equivalent of the electric field, then the constant of proportionality which relates the stress, σ_{ij} and the elastic polarisation,

$\mathbf{F}^{(1)}$, is the equivalent of the polarisability of an electric dipole. In this case the constant of proportionality is $16\pi\mu(1-\nu)A$, where A is defined in equation 2.7. Hence we can define the *elastic polarisability*, α, by

$$\alpha = \frac{20\pi R^3(1-\nu)(\mu_0-\mu)}{[\mu_0(7-5\nu)+2\mu(4-5\nu)]}. \tag{2.15}$$

2.4 Effective Shear Modulus Of An Elastic Matrix With Many Inclusions.

We now have a useful expression for the relationship between the applied stress, at long distances from an inclusion, and the resulting stress due to an inclusion. Following the analogy with electromagnetic theory we can now derive a relationship between the microscopic polarisablility and the elastic equivalent of the dielectric constant of the material. This is the Clausius-Mossotti relationship of electromagnetic theory. Since we consider only the case of pure shear deformations the *elastic dielectric constant* is a scalar. This quantity turns out to be equal to the ratio of the effective shear modulus, μ^{eff}, and the matrix shear modulus, μ_0.

The Clausius-Mossotti approach needs a calculation of the local field within the medium. This local field consists of contributions from the applied field and the dipoles induced by that field. The method used to obtain this local field is based on an elegant derivation of the Clausius-Mossotti relation by Hannay [46]. Hannay noted that each dipole has an extended electric field and a point field concentrated on the dipole itself. The singular contribution is conveniently represented by a Dirac delta function situated at the site of the dipole. Thus the electric field, $\mathbf{E}(\mathbf{r})$ due to dipole moment, $\mathbf{p}$ can be written as

$$\mathbf{E}(\mathbf{r}) = \frac{1}{4\pi}\left(\frac{3(\mathbf{p}\bullet\mathbf{r})\mathbf{r}}{r^5} - \frac{\mathbf{p}}{r^3}\right) - \frac{\mathbf{p}}{3}\delta(\mathbf{r}) \tag{2.16}$$

The magnitude of the delta function contribution is calculated by integrating

the electric field over a sphere centred on the dipole. Hannay states that the local field near a dipole will be given by the average field with the delta function contribution, due to the dipoles, subtracted. This is due to the fact that a single dipole will not feel these contributions, although the average field will include them.

The same arguments can be used in the case of elastic inclusions. An integral of the stress due to a void, over a spherical volume centred on the void, can be converted to a surface integral to give

$$\int \sigma_{ik}\, dV = \frac{2(4-5\nu)}{15(1-\nu)} f_{ik}. \tag{2.17}$$

Here we have assumed that a single void has an elastic polarisation, f_{ik}, defined in the same way as $F^{(1)}$ in equation 2.10. This contribution to the macroscopic stress is due only to the delta functions, which are produced by the derivatives of the radius vector.

Following Hannay, the local stress field is obtained by subtracting these contributions from the average stress. The elastic polarisation for the void, f_{ik}, is then related to the local stress field by the polarisability, α, such that

$$f_{ik} = \alpha \left[\sigma_{ik} - \frac{2(4-5\nu)}{15(1-\nu)} f_{ik} \right]. \tag{2.18}$$

The link between the macroscopic stress and the average elastic polarisation can then be calculated from the Green's function (equation 2.9), by analogy with the derivation used in electromagnetic theory. In electromagnetic theory, the relation is obtained from the Green's function for the electric potential. This gives the familiar $\mathbf{D} = \mathbf{E} + 4\pi\mathbf{P}$, where $\mathbf{E}$ is the electric field, $\mathbf{P}$ is the polarisation and $\mathbf{D}$ is the electric displacement vector (See for example [47]).

For a number density of voids, n, we can define $F_{ik} = nf_{ik}$ as the average elastic polarisation, with G_{ik} as the *elastic displacement* field due to the inclusions, then we obtain (see Appendix B)

$$G_{ik} = \sigma_{ik} - F_{ik}. \tag{2.19}$$

This gives us the relation between the average polarisation and the average stress applied. In electromagnetic theory $\nabla \cdot \mathbf{D}$ gives the free charge density. In our case the divergence of G_{ik} gives the "free force" density, ie. the force applied externally to the medium. Hence this relation can be interpreted as saying that the total stress, σ_{ik}, is given by the sum of the external stresses and the polarisation stresses.

If we assume that the elastic displacement field, G_{ik}, is proportional to the stress field, then we can introduce a scalar *elastic dielectric constant*, γ. This is a legitimate assumption since we are considering only pure shear deformations. This gives us the macroscopic relation,

$$nf_{ik} = -(\gamma - 1)\sigma_{ik} \tag{2.20}$$

Using this definition of γ as the ratio of the total stress and the applied stress means that we can interpret γ as the ratio of the effective shear modulus to the matrix shear modulus.

We now use equations 2.18 and 2.20 to eliminate the microscopic polarisation, f_{ik} and the average stress, σ_{ik}, to obtain the following expression[1] for the elastic dielectric constant, γ:

$$\gamma = \frac{\mu^{\text{eff}}}{\mu_0} = 1 - \frac{15\phi(1-\nu)(1-\mu/\mu_0)}{(7-5\nu) + 2(4-5\nu)[\mu/\mu_0 - (\mu/\mu_0 - 1)\phi]}. \tag{2.21}$$

Here we have introduced the volume fraction of the inclusions, $\phi = 4\pi R^3 n/3$.

This result is the same as an expression obtained by Hashin[21]. Hashin obtained the expression as a representative formula which satisfies bounds on the shear modulus, calculated by a variational approach. This method shows that the expression chosen has more physical significance than other possible expressions, which are also bounded by the variational approach.

It is interesting to note at this point the behaviour of the result we have obtained in the limit that the inclusions become rigid and the matrix becomes

[1] This result has been independently obtained using a similar approach by Felderhof and Iske [48]

incompressible. Hence we allow $\mu \to \infty$ and $\nu \to \frac{1}{2}$. For small volume fractions this gives

$$\mu^{\text{eff}} = \mu_0(1 + \tfrac{5}{2}\phi). \tag{2.22}$$

This equation is of the same form as the Einstein relation for the effective viscosity of a sheared fluid containing a small volume fraction of rigid spheres [49]. The incompressibility of the matrix is important, since fluids are usually considered to be incompressible.

In fact the Einstein relation can be derived in similar way to our result [50, 51]. This is because the Green's function for the velocity field of a slow moving fluid, due to a point force, is very similar to that for the displacement vector due to a point force in an elastic medium. As for our result, the Einstein relation is due to spheres acting as dipolar systems of forces. In the fluid mechanics terminology, the solution for a point force is known as a *Stokeslet*, and the symmetric force dipole known as a *Stresslet*. (There can also exist anti-symmetric force dipoles which are known as *Couplets* or *Rotlets*). The similarity between the elastic and fluid Green's functions is exploited later in this chapter in order to calculate the displacement field for an inclusion near a boundary.

2.5 Self-Consistent Shear Moduli For Gels.

In order to obtain a more complete model of a gel under shear, it is necessary to model the failure of bonds within a gel structure. When a bond fails in a gel, the region it occupies is unable to support any stress. If this region is assumed to be spherical, then the previously calculated expression for the effective shear modulus can be used for the gel. In order that no stress exists in the region, the shear modulus of the cavity is taken to be zero.

Once this limit has been taken a self-consistent argument is necessary to calculate the actual volume fraction of the gel which has failed. There is no

generally accepted model of bond failure within gel structures, so the following phenomenological approach is used.

It is assumed that the bonds within a gel have a distribution, P, of yield stresses, σ_Y. Whenever the average stress within the gel exceeds a bond's yield stress, then that bond is said to have failed. The volume fraction of failed gel can then be expressed as the integral of the distribution, P, up to the applied average stress. We assume the following form for the normalised distribution, P.

$$P(\sigma_Y) = \frac{(A+1)}{\sigma_M}\left(\frac{\sigma_Y}{\sigma_M}\right)^A \theta(\sigma_M - \sigma_Y). \tag{2.23}$$

The function $\theta(\sigma_M - \sigma_Y)$, is a step function, being unity for a positive argument and zero otherwise, with σ_M the maximum yield stress of the bond distribution. We have introduced a parameter, A, which can be adjusted to give a suitable distribution. For $A = 0$ all bond strengths are equally probable up to the maximum yield stress. For $A = 1$ the probability increases linearly with yield stress. For increasing values of A the distribution becomes increasingly weighted toward higher yield stresses. We restrict A to having positive values to avoid a divergence in the probability distribution function at $\sigma_Y = 0$.

The volume fraction, ϕ of failed bonds is now given by the integral of this function up to the applied stress.

$$\phi = \int_0^\sigma P(\sigma_Y)d\sigma_Y = \left(\frac{\sigma}{\sigma_M}\right)^{A+1}. \tag{2.24}$$

Using the expression for the effective shear modulus 2.21, with $\mu = 0$ to represent a matrix with cavities, we can now calculate the effective shear modulus as a function of the applied stress.

$$\mu_{\text{eff}} = \mu_0\left(1 - \frac{15(1-\nu)(\sigma/\sigma_M)^{A+1}}{(7-5\nu) + 2(4-5\nu)(\sigma/\sigma_M)^{A+1}}\right) \tag{2.25}$$

Since the effective shear modulus is equal to $d\sigma/d\epsilon$, where ϵ is the strain, we can integrate this expression to obtain a stress-strain relationship for a gel.

$$\epsilon = \frac{1}{\mu_0}\int_0^\sigma \frac{1 + J(\sigma'/\sigma_M)^{A+1}}{1 - (\sigma'/\sigma_M)^{A+1}}d\sigma', \tag{2.26}$$

where we have taken $J = 2(4 - 5\nu)/(7 - 5\nu)$. If we re-write this expression in terms of the normalised stress, Z, such that $Z = \sigma/\sigma_M$, we obtain

$$\epsilon = \frac{\sigma_M}{\mu_0}\left(-JZ + (J+1)\int_0^{\sigma/\sigma_M} \frac{dZ}{(1 - Z^{A+1})}\right). \tag{2.27}$$

For $A = 0$, the solution obtained is as follows.

$$\epsilon = -\frac{\sigma_M}{\mu_0}\left[JZ + (J+1)\ln|1 - Z|\right] \tag{2.28}$$

Inspection of this solution shows that the strain diverges when $\sigma = \sigma_M$. In other words, the gel is unable to support a stress greater than the yield stress of its strongest bonds, as one would intuitively expect.

Analytic expressions for the integral are available for the cases where A is an integer. Gradsteyn and Ryzhik [52] give the following expression for positive even values of A:

$$(A+1)\int \frac{dZ}{1 - Z^{A+1}} = \tag{2.29}$$
$$\ln\left[\frac{1+Z}{1-Z}\right] - \sum_{k=1}^{(A+1)/2} P_k \cos\left(\frac{2k\pi}{A+1}\right) + \sum_{k=1}^{(A+1)/2} Q_k \sin\left(\frac{2k\pi}{A+1}\right)$$

where

$$P_k = \ln\left(Z^2 - 2Z\cos\left(\frac{2k\pi}{A+1}\right) + 1\right), \quad Q_k = 2\arctan\left(\frac{z - \cos\left(\frac{2k\pi}{A+1}\right)}{\sin\left(\frac{2k\pi}{A+1}\right)}\right). \tag{2.30}$$

A similar expression can be obtained for odd integer values of A.

As A is increased it can be seen that these solutions become progressively more complicated, but we can obtain the asymptotic behaviour of these solutions by considering expansions of the integrand near $Z = 1$ and $Z = 0$. If we put $Z = 1 - \delta$ then our integral becomes

$$\int_0^{\sigma/\sigma_M} \frac{dZ}{(1 - Z^{A+1})} = -\int_1^{1-\sigma/\sigma_M} \frac{d\delta}{(1 - (1-\delta)^{A+1})}. \tag{2.31}$$

Near $Z = 1$ we have a small value of delta and can expand the denominator of the integrand to first order in δ. Thus the integrand becomes $1/\delta(A+1)$ which

when integrated gives a logarithmic term. When Z is near zero the denominator is approximately unity. When this contribution is integrated and the limits applied, the logarithmic term dominates for stresses near σ_M. The integral then has the following form as $\sigma \to \sigma_M$.

$$\int_0^{\sigma/\sigma_M} \frac{dZ}{(1 - Z^{A+1})} = -\frac{1}{(A+1)} \ln\left|1 - \frac{\sigma}{\sigma_M}\right|. \tag{2.32}$$

Thus we see a logarithmic divergence as σ approaches σ_M for all positive values of A, not just the integer values. This shows that the strain will diverge logarithmically for any positive value of A, when the applied stress approaches σ_M.

This expression has also been integrated numerically, for non-integer values of A with the matrix Poisson's ratio taken to be one half (J=2/3), and taking σ_M/μ_0 to be unity. Plots of the behaviour of the stress-strain curves are given in figure 2.2. These confirm that the stress divergence, predicted by the analytic solutions, is a general feature of this model.

As the value of A is increased it can be seen the stress-strain curve turns over increasingly rapidly. This is due to the fact that increasing the value of A reduces the number of weaker bonds in the distribution throughout the gel. Because of this the effective modulus does not change significantly until the normalised stress approaches unity. In the limit $A \to \infty$ we would expect the stress/strain ratio to be a constant until the stress equals σ_M, when the strain will diverge as all the bonds fail simultaneously. This tendency is clear in the figure by $A = 5$. The opposite limit, with $A = 0$, shows a smooth turn-over with the effective modulus decreasing smoothly with increasing stress or strain.

It should be noted that this model has assumed that the applied stress is the controlled quantity. A model which assumes that the strain is the fixed quantity would need to be more complicated. For example, application of a fixed strain will induce a stress causing bond failures. These failures will then act to reduce the average stress within the gel and lead to over estimation of the average stress.

A detailed algorithm would be needed to overcome such difficulties, and is not attempted here.

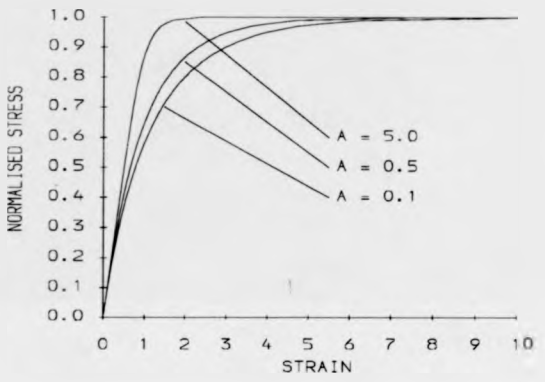

Figure 2.2: *Plots of stress as a function of strain, varying the parameter A (Poisson's ratio of matrix = 1/2, $\mu_0/\sigma_M = 1$)*

2.6 Modes Of Gel Failure

We now have a mean field theory approach to calculate the stress-strain relationship for a gel. In order to go beyond the mean field theory, we have attempted to find specific patterns of failure to which gels are susceptible.

In a real gel, we would expect bond failures to occur in regions where the stresses are highest. Since the stress tensor is a multi-component object it is difficult to define a 'higher' level of stress. Instead we have looked at the elastic energy density as an indicator of the average stress at any point. Since the energy

density is a scalar, this can more easily be used to discuss the likelihood of bond failures at a given point.

The elastic energy density for a material under strain is given by

$$E = \tfrac{1}{2}\left(\sigma_{xx}u_{xx} + \sigma_{yy}u_{yy} + \sigma_{zz}u_{zz} + \sigma_{xy}u_{xy} + \sigma_{zx}u_{zx} + \sigma_{yz}u_{yz}\right). \tag{2.33}$$

Calculation of the elastic energy density near a single void in a gel, shows that there is a strong directional dependence of this density.

We take the total strain to be the sum of the applied strain, u^0_{ik}, and the strain due to a single cavity, u^1_{ik}. For the case of pure shear we can use $u^0_{ik} = \alpha(\hat{\mathbf{x}}\hat{\mathbf{z}} + \hat{\mathbf{z}}\hat{\mathbf{x}})$, where α is a constant. We can now use Hooke's law to calculate the stress and hence the energy density, E, can be written as

$$E = \mu_0\left(u^0_{ik}u^0_{ik} + 2u^0_{ik}u^1_{ik} + H.O.T.\right). \tag{2.34}$$

The first term is the energy density without a cavity. The second term is the leading order correction which is of order $1/r^3$. Since r is greater than unity outside the vacancy, we ignore the subsequent terms which are of order $1/r^6$.

If we subtract the energy density due to the deformation at infinity, then we get the change in energy density, ΔE, due to the cavity. Using spherical polar coordinates as defined in figure 2.3, for a void at the origin of the coordinate system, we can write ΔE in the following form.

$$\Delta E = \frac{4\mu A\alpha^2}{r^3}[2(1-2\nu) + 6\nu(\sin^2\theta\cos^2\phi + \cos^2\theta) - \tfrac{15}{2}\sin^2 2\theta\cos^2\phi] \tag{2.35}$$

Here, A is the constant defined by equation 2.7.

We now wish to find the maxima and minima of this energy as θ and ϕ are varied. To achieve this, we differentiate this expression and look for zeroes of the result.

$$\frac{\partial\Delta E}{\partial\phi} = -\frac{4\mu A\alpha^2}{r^3}(2\cos\phi\sin\phi[6\nu\sin^2\theta - \tfrac{15}{2}\sin^2 2\theta]), \tag{2.36}$$

$$\frac{\partial\Delta E}{\partial\theta} = -\frac{4\mu A\alpha^2}{r^3}(\cos^2\phi[12\nu\sin\theta\cos\theta - 30\sin 2\theta\cos 2\theta] - 12\nu\sin\theta\cos\theta). \tag{2.37}$$

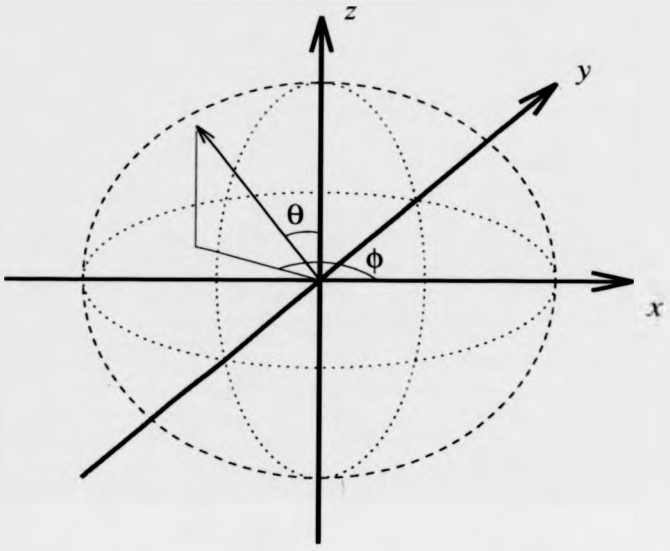

Figure 2.3: *The Spherical Polar Coordinate System*

The first differential is zero when $\phi = n\pi/2$, where n is an integer. The second is generally zero when $\theta = n\pi/2$. In addition, for $\phi = n\pi$, the second differential goes to zero when $\theta = n\pi/4$.

Inspection of ΔE near these turning points shows that the energy is minimised for four sets of (θ, ϕ) coordinates. These are $(\frac{\pi}{4}, 0), (\frac{\pi}{4}, \pi), (\frac{3\pi}{4}, 0)$ and $(\frac{3\pi}{4}, \pi)$. Reverting to a Cartesian coordinate description, these correspond to the lines $x = z$ and $x = -z$. The energy density is maximised for directions along the z axis, and the x axis.

As a result of this, the total energy density is reduced in the directions near the lines $x = z$ and $x = -z$, making bond failures less likely in those regions. The regions near the $x - y$ and $y - z$ planes have an increased energy density and therefore bond failures are more likely to occur in those regions.

The failure of bonds in the $y-z$ planes will not cause a catastrophic failure of the gel, and will merely add to the softening. Failure in the $x-y$ plane will result in the complete failure of the gel since no stress can be passed between the upper and lower plates in this case. Because of these effects, we would expect most failures of the gel to occur along the $x-y$ planes.

2.7 Elasticity and Slow Fluid Motion

2.7.1 The method of images

The results presented so far in this chapter apply for a material subjected to a uniform shear at infinity. This is a good approximation for voids within the bulk of the gel but near the surface of the gel we should consider the effect of more realistic boundary conditions.

The true geometry of a gel under shear is likely to be a slab geometry as shown in figure 2.1. In order to solve the problem for a spherical cavity in a slab geometry it is necessary to use the method of images [53]. This allows the correct boundary conditions to be obtained at the surfaces of the slab. A reasonable boundary condition to apply is that the displacement vector, u_i, due to the presence of the void must be zero on the upper and lower boundaries. This is equivalent to assuming that no slip conditions occur between the gel and the plates applying the shear.

With a single boundary a single image is sufficient to enforce the correct condition. At a second boundary then the first image will give rise to the need for corrections which are obtained with a second image. This in turn requires corrections at the first boundary and so on. This results in an infinite series of images at increasing distances from the boundary.

2.7.2 A comparison with Stokes' fluid flows

As we mentioned earlier in this chapter problems of this form in elasticity theory are closely related to equivalent problems in low Reynold's number fluid flows (known as Stokes' or creeping flow problems). It is convenient at this point to discuss both the problem of elastic images and the equivalent problem in Stokes' flows. This will allow us to point out several similarities between the approaches used and introduce concepts which will be useful later.

If we begin with the fluid problem, we note that the velocity and pressure fields, v and p, for Stokes' flow must satisfy

$$\eta \nabla^2 \mathbf{v} = \nabla p, \qquad \nabla \cdot \mathbf{v} = 0, \tag{2.38}$$

where η is the viscosity of the fluid. At first sight these equations may seem quite different from the equivalent elasticity equation of equilibrium. One important difference is that fluids are considered to be incompressible and hence $\nabla \cdot \mathbf{v} = 0$. This is not the case in elasticity problems since elastic bodies are generally considered to be compressible (unless they have a Poisson's ratio of one half).

The similarity is emphasised if we rewrite the equation of equilibrium in the following form.

$$\mu \nabla^2 \mathbf{u} = -\frac{\mu}{(1-2\nu)} \nabla (\nabla \cdot \mathbf{u}). \tag{2.39}$$

This form makes the elastic equivalent of pressure the quantity $(\mu \nabla \cdot \mathbf{u})/(1-2\nu)$.

The similarities are further emphasised by inspecting the Green's function for the velocity field, v_i, due to a point force

$$v_i = \frac{1}{8\pi\eta} \left[\frac{\delta_{ik}}{r} + \frac{r_i r_k}{r^3} \right] F_k. \tag{2.40}$$

This is very similar to the Green's function for the elastic displacement, although slightly simpler. In fact putting Poisson's ratio to be one half in the elastic Green's function makes the Green's function differ only by the constant of proportionality (ie. the viscosity replaces the shear modulus).

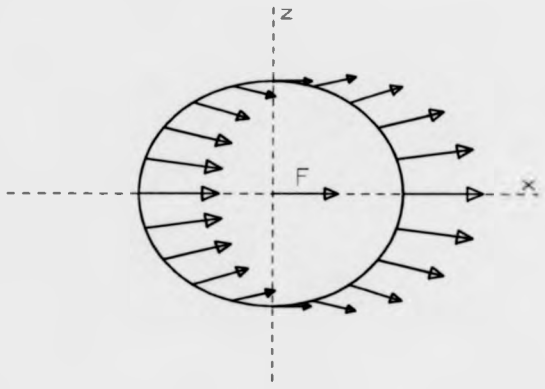

Figure 2.4: *Elastic displacement at a constant distance from a point force, with Poisson's ratio* $= 0.5$

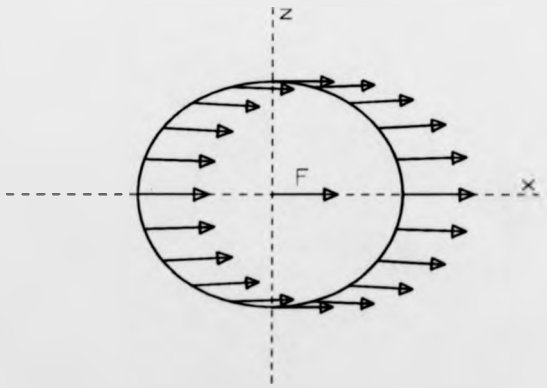

Figure 2.5: *Elastic displacement at a constant distance from a point force, with Poisson's ratio* $= -1.0$

The following image calculations give a further illustration of the similarity between between problems in elasticity and in Stokes' flows.

2.7.3 The image of a point force

First we shall derive the image for a point force in an elastic medium, near a single boundary. The equivalent fluid problem is described as the image of a Stokeslet and has been studied by Blake [54] for a single, no-slip boundary condition. Blake obtained the following velocity field, v_j:

$$\begin{aligned} v_j &= \frac{F_k}{8\pi\eta}\left\{\left(\frac{1}{r}-\frac{1}{R}\right)\delta_{jk}+\frac{r_j r_k}{r^3}-\frac{R_j R_k}{R^3}\right. \\ &\left. +2d(\delta_{k\alpha}\delta_{\alpha l}-\delta_{k3}\delta_{3l})\frac{\partial}{\partial R_l}\left[\frac{dR_j}{R^3}-\left(\frac{\delta_{j3}}{R}+\frac{R_j R_3}{R^3}\right)\right]\right\}, \end{aligned} \tag{2.41}$$

where $\mathbf{R}$ is defined in figure 2.7 and d is the distance of the force from the boundary (an alternative derivation is given in the review article by Hasimoto and Sano [55]). The summation convention used for this expression and the rest of this chapter is that roman indices are summed over 1-3 as normal, while greek indices are summed over 1,2 only. This is a useful convention as the normal to the interface is a distinguished direction.

We now use method similar to Blake's to find the image of a point force in an elastic medium at a distance d from a single boundary[2]. We use the coordinate system shown in figure 2.7, with the boundary along $r_3 = z = 0$.

The Green's function (equation 2.9) for the displacement vector due to a point force is defined by the Green's tensor

$$u_{ik} = \frac{1}{16\pi\mu(1-\nu)}\left[(3-4\nu)\frac{\delta_{ik}}{r}+\frac{r_i r_k}{r^3}\right]. \tag{2.42}$$

(The directional behaviour of this is shown in figures 2.4 and 2.5). Using this

[2]The image of a point force has been found by other methods [56], but we use this approach as a demonstration of the connections between fluid and elasticity problems

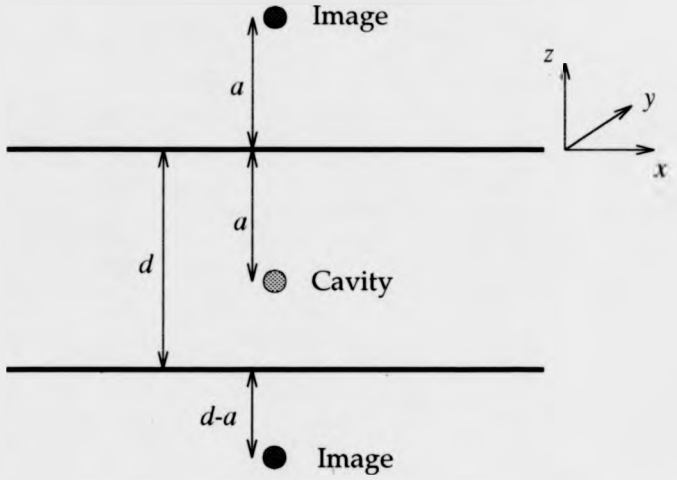

Figure 2.6: *A cavity within an elastic medium and its first two images*

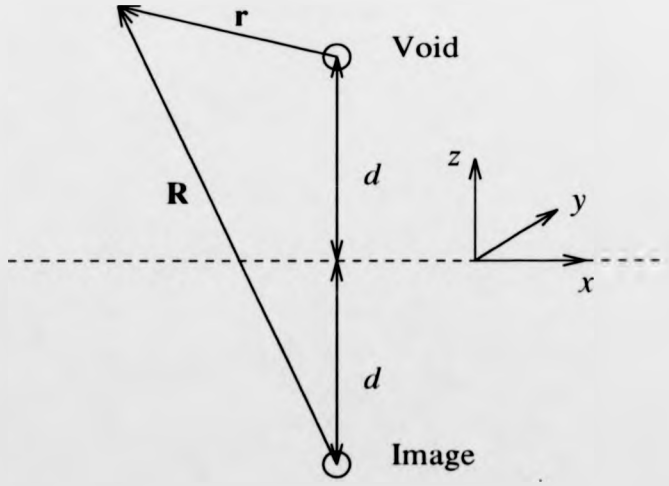

Figure 2.7: *The coordinate system for a force and its image at a single boundary*

we can construct a Green's tensor of the form

$$u_{ik} = \frac{1}{16\pi\mu(1-\nu)}\left[(3-4\nu)\left(\frac{1}{r}+\frac{1}{R}\right)\delta_{ik} + \frac{r_i r_k}{r^3} + \frac{R_i R_k}{R^3} + t_{ik}\right]. \qquad (2.43)$$

Here t_{ik} is to be found and $\mathbf{R}$ is the vector from the image to the required point in the medium (See figure 2.7).

For u_i to be zero on the boundary ($R_3 = d$) then t_{ik} must satisfy the following boundary condition,

$$t_{ik} = 2d\left(\delta_{i3}\delta_{k\alpha} + \delta_{k3}\delta_{i\alpha}\right)\frac{R_\alpha}{R_0^3}, \qquad (2.44)$$

where $R_0 (= (R_1^2 + R_2^2 + d^2)^{1/2})$ is the distance from the image to a point on the boundary.

The problem is approached using two-dimensional Fourier transforms defined by

$$\hat{f}(\lambda_1, \lambda_2, R_3) = \frac{1}{2\pi}\iint_{-\infty}^{\infty} f(R_1, R_2, R_3) e^{i\lambda_\beta R_\beta} dR_1 dR_2. \qquad (2.45)$$

Since t_{ik} must satisfy the equation of equilibrium, with no force term, we Fourier transform the left-hand side of equation 2.1 to obtain

$$Q\left(\frac{\partial^2}{\partial R_3^2} - \xi^2\right)\hat{t}_{ik} + \left(-i\lambda_\alpha\delta_{\alpha i} + \delta_{i3}\frac{\partial}{\partial R_3}\right)\left(-i\lambda_\beta\delta_{\beta j} + \delta_{j3}\frac{\partial}{\partial R_3}\right)\hat{t}_{jk} = 0, \qquad (2.46)$$

where $Q = 1 - 2\nu$.

In addition to the equation of equilibrium we know that the bi-harmonic equation must be satisfied, giving

$$\left(\frac{\partial^2}{\partial R_3^2} - \xi^2\right)^2 \hat{t}_{ik} = 0, \qquad (2.47)$$

where $\xi^2 = \lambda_1^2 + \lambda_2^2$. The general solution to this equation can be written in the form

$$\hat{t}_{ik} = [B_{ik} + C_{ik}(R_3 - d)]e^{-\xi R_3} + [E_{ik} + F_{ik}(R_3 - d)]e^{\xi R_3}. \qquad (2.48)$$

We require E_{ik} and F_{ik} to be equal to zero, since $\hat{t}_{ik}$ should go to zero as R_3 tends to infinity.

Having obtained the necessary equations in Fourier space, we now require the correct boundary condition in Fourier space. The most convenient way of obtaining this is to use the following relationship between 2-dimensional Fourier transforms and 1-dimensional Hankel transforms,

$$\frac{1}{2\pi}\iint_{-\infty}^{\infty} f(r)e^{\lambda_1 r_1+\lambda_2 r_2}dr_1dr_2 = \int_0^{\infty} rf(r)J_0(\xi r)dr, \tag{2.49}$$

where J_0 is a zeroth order Bessel function, $r = (r_1^2 + r_2^2)^{1/2}$ and $\xi = (\lambda_1^2 + \lambda_2^2)^{1/2}$. The real space boundary condition can now be written in terms of derivatives of R_0, and transformed to give,

$$\hat{t}_{ik} = 2d\,(\delta_{i3}\delta_{k\alpha} + \delta_{k3}\delta_{i\alpha})\,\frac{i\lambda_\alpha}{\xi}e^{-\xi d}. \tag{2.50}$$

Comparison of this condition with the general solution for $\hat{t}_{ik}$ when $R_3 = d$ immediately gives

$$B_{ik} = 2d\,(\delta_{i3}\delta_{k\alpha} + \delta_{k3}\delta_{i\alpha})\,\frac{i\lambda_\alpha}{\xi}. \tag{2.51}$$

Next, we must find the C_{ik}'s by substituting the general solution for $\hat{t}_{ik}$ into the Fourier transformed equation of equilibrium and using the known expression for B_{ik}, at $R_3 = d$. This results in the following expression for the C_{ik}'s.

$$C_{ik} = \frac{1}{2Q+1}\,(\xi\delta_{i3} + i\lambda_\beta\delta_{\beta i})\,(i\lambda_\alpha\delta_{\alpha k} - \xi\delta_{k3})\,\frac{1}{\xi}. \tag{2.52}$$

Back Fourier transforming, $\hat{t}_{ik}$ gives,

$$\begin{aligned}\hat{t}_{ik} &= 2d\left\{(\delta_{i3}\delta_{k\alpha} + \delta_{k3}\delta_{i\alpha})\,\frac{R_\alpha}{R_0^3}\right. \\ &- \left.\frac{(R_3-d)}{2Q+1}\left[(\delta_{k\alpha}\delta_{\alpha l} - \delta_{k3}\delta_{3l})(\delta_{i\alpha}\delta_{\alpha p} + \delta_{i3}\delta_{3p})\frac{\partial^2}{\partial R_l\partial R_p}\left(\frac{1}{R}\right)\right]\right\}\end{aligned} \tag{2.53}$$

Finally, after some manipulation, we get

$$\begin{aligned}\hat{t}_{ik} &= 2d\left\{(\delta_{k\alpha}\delta_{\alpha l} - \delta_{k3}\delta_{3l})\,\frac{\partial}{\partial R_l}\left[\frac{d}{(3-4\nu)}\left(\frac{R_i}{R^3}\right)\right.\right. \\ &\left.\left. - \left(\frac{\delta_{i3}}{R} + \frac{1}{(3-4\nu)}\frac{R_iR_3}{R^3}\right)\right] - 2\frac{(1-2\nu)}{(3-4\nu)}\delta_{k3}\frac{\partial}{\partial R_i}\left(\frac{1}{R}\right)\right\}.\end{aligned} \tag{2.54}$$

This result reduces to Blake's solution in the the incompressible limit, $\nu = \frac{1}{2}$. In general the expression is different due to the fact that the elastic material is compressible, although a similar interpretation of the result can be made for this solution. The first term in the square brackets is identified by Blake as a source doublet and has exactly the same form here, except for a numerical factor. The second term in the square brackets was termed a stresslet by Blake and corresponds to our elastic dipole solution. The final term does not occur in Blake's solution and corresponds to a source, as defined by Blake and Chwang [57]. This final term disappears as $\nu \to \frac{1}{2}$.

2.7.4 The image of a void

We now consider the image of a void at a distance d from a single boundary. In the creeping flow terminology, this is equivalent to finding the image of a Stresslet. Taking the elastic dipole moment to have the form $\mathbf{F}^{(1)} = 2(\hat{\mathbf{x}}\hat{\mathbf{z}} + \hat{\mathbf{z}}\hat{\mathbf{x}})$, we can write the displacement vector in the form

$$u_i = \frac{1}{4\pi\mu}\left[\frac{M}{r^3}(\delta_{i3}r_1 + \delta_{i1}r_3) + P\frac{r_i r_1 r_3}{r^5} - \frac{M}{R^3}(\delta_{i3}R_1 + \delta_{i1}R_3) - P\frac{R_i R_1 R_3}{R^5} + t_i\right]. \tag{2.55}$$

Again t_i is unknown, $M = 1 - 1/[2(1-\nu)]$, $P = 3(1-M)$, and $\mathbf{R}$ is the vector from the image to the required point in the medium (See figure 2.7).

As before for u_i to be zero on the boundary, $R_3 = d$, then t_i must satisfy the following boundary condition,

$$t_i = 2d\left(\frac{\delta_{i1}}{R_0^3} + \frac{P\delta_{i\alpha}}{3}\frac{R_\alpha R_1}{R_0^5}\right), \tag{2.56}$$

where $R_0 = (R_1^2 + R_2^2 + d^2)^{1/2}$ is the distance from the image to a point on the boundary.

Using the same approach as for the point force we can obtain a general solution for $\hat{t}_i$ of the form

$$\hat{t}_i = [B_i + C_i(R_3 - d)]e^{-\xi R_3}, \tag{2.57}$$

where

$$B_i = 2\left(\delta_{i3} - \frac{Pd}{3}\frac{\lambda_\alpha \lambda_1}{\xi}\delta_{i\alpha}\right) \tag{2.58}$$

and

$$C_i = \frac{2}{2Q+1}\left[1 - \frac{Pd}{3}\xi\right](\xi\delta_{i3} + i\lambda_\alpha\delta_{i\alpha})\frac{i\lambda_1}{\xi}. \tag{2.59}$$

A back Fourier Transform gives the following result:

$$\begin{aligned} t_i \;=\; 2\Bigg\{ & -\delta_{i1}\frac{\partial}{\partial R_3}\left(\frac{1}{R}\right) + \frac{Pd}{3}\delta_{i\alpha}\frac{\partial^2}{\partial R_\alpha \partial R_1}\left(\frac{1}{R}\right) \\ & -\frac{(R_3 - d)}{2Q+1}\left[1 + \frac{Pd}{3}\frac{\partial}{\partial R_3}\right]\frac{\partial^2}{\partial R_i \partial R_1}\left(\frac{1}{R}\right)\Bigg\}. \end{aligned} \tag{2.60}$$

This result is considerably more complicated than would be expected for the equivalent electric dipole system with which we made our initial analogy. This is due to the more complicated tensor structure which is required for elasticity problems. The first image due to the second boundary can be obtained in a similar fashion. The secondary images are more difficult to calculate since the correction term t_i must also have a resulting image which complicates the situation further.

Although in principle further images could be obtained to obtain the exact boundary condition, this is unlikely to improve our understanding of the problem and is not attempted here. We shall merely emphasise the similarities between the tensor objects which occur in our elasticity calculation and the objects such as Stokeslets and Stresslets which are common in problems involving slow fluid flows.

Chapter 3

The Stability Of Layered Colloidal Structures Under Shear

3.1 The model

We have shown in the previous chapter that we expect a gelled structure to fail along planes parallel to the plates which provide the shearing motion. This will result in parallel layers of alternating high and low concentrations of colloidal particles. This effect has been seen experimentally [26]. In order to find out whether these structures persist for significant times, or are merely a transient phenomenon, it is necessary to study the stability of such layered structures.

To model such a situation we consider the structure to be composed of many layers of fluid under shear. The viscosity of the layers are chosen to alternate between two values. The layers of higher viscosity represent layers with higher concentrations of colloidal particles, as would be expected. We are interested particularly in the cases where the number of layers is odd, since we would expect the structures to be symmetrical about the centre plane of the shear flow. Using

this model we are able to calculate the velocity profile of the system and study its stability when subjected to small perturbations. If the layered structure is to exist for a significant time, then it must be stable when subjected to perturbations.

We assume that the particles under consideration are neutrally buoyant. This is not unrealistic for appropriate colloidal particles and has the advantage that the density in each of the fluid layers will be the same and constant. In this case gravity does not affect the stability of the system.

3.2 Previous results

We are interested in the stability of a three-dimensional, layered system, undergoing plane Couette flow. It was shown by Squire [28] that it is sufficient to consider two-dimensional disturbances of fluids in a parallel plate geometry, since any instability which exists in the three-dimensional case will also exist for the two-dimensional case, although the critical Reynold's number will be reduced. As a result of this we restrict our analysis to two spatial dimensions.

The linear stability of two layer, plane Couette flow was investigated by Yih [29] for the viscous case. He used a perturbation technique appropriate to small amplitude, long wavelength disturbances, and showed that two layer flows could be unstable at the first order of perturbation if the viscosity was different in each layer. This instability occurs at all values of the Reynold's number. The same approach was used by Li [30] for the case of three layers. Li showed that due to a form of resonance between the fluid interfaces, the 3-layer system could be unstable even at the zeroth order of perturbation. A similar resonance instability has been identified by Weinstein and Kurz [58] for three-layer flow down an inclined plane. This is analogous to the instability of three layers of inviscid fluid, originally identified by Taylor [27].

Hooper and Grimshaw [59] have shown that the introduction of surface tension effects lead to stabilization. However in the present treatment, which is restricted

to long-wavelength disturbances, such effects are small.

The physical reason for the instability, as explained by Yih [60], is the discontinuity in vorticity which occurs near the interface between two layers. This allows interfacial waves to draw energy from the main flow. A mechanism for this type of behaviour was given by Hinch for an unbounded shear flow, albeit with an emphasis on short wavelength disturbances [61]. The mechanism is illustrated in figure 3.1. A perturbing wave produces vorticity perturbations of one sign near the peaks of the wave and of the opposite sign near the troughs. This vorticity is then advected along by the background shear flow, resulting in vorticity perturbations of differing signs at adjacent positions either side of the interface. These opposing vorticities interact so as to increase the amplitude of the original wave. The whole process is repeated and this leads to the amplification of the amplitude of any initial wave and corresponds to instability.

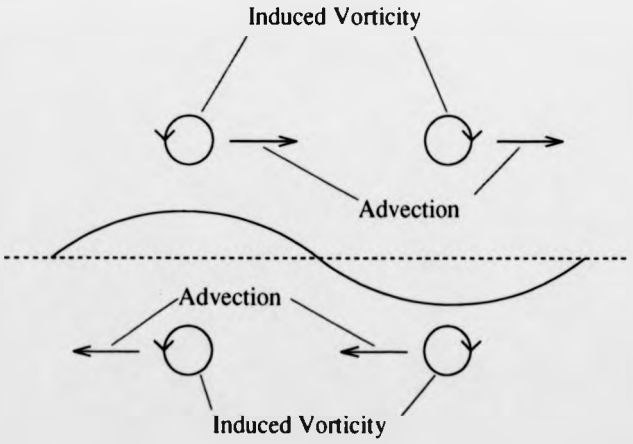

Figure 3.1: *The advection of vorticity in a shear flow*

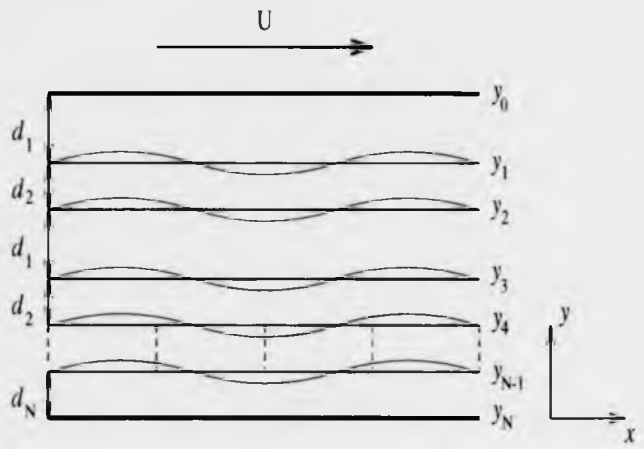

Figure 3.2: *The Problem Geometry*

3.3 The equilibrium solution for N layers

The Navier-Stokes equations for the jth layer of fluid are

$$\left(\frac{\partial}{\partial t} + \mathbf{u}_j.\nabla\right) u_j = -\frac{1}{\rho}\frac{\partial p}{\partial x} + \eta_j \nabla^2 u_j \tag{3.1}$$

$$\left(\frac{\partial}{\partial t} + \mathbf{u}_j.\nabla\right) v_j = -\frac{1}{\rho}\frac{\partial p}{\partial y} + \eta_j \nabla^2 v_j, \tag{3.2}$$

where u_j and v_j are the x and y components of the velocity $\mathbf{u}_j$, p is the pressure and η_j is the viscosity of the jth layer. The interfacial boundary conditions are the continuity of velocity and stress, $\eta_j du_j/dy$. The usual no-slip boundary conditions apply at the walls of the system.

For convenience we introduce dimensionless variables by the making following substitutions;

$$\mathbf{u}_j \to \mathbf{u}_j/U, \quad (x,y) \to (x,y)/w, \quad p \to p/\rho U^2, \quad t \to tU/w, \tag{3.3}$$

where U is the velocity of the upper plate and w is the width of the system. It is also convenient to choose the coordinate system such that $y_0 = 1$ and $y_N = 0$

The viscosity is assigned a value η_1 in odd numbered layers and a value η_2 in even numbered layers, the layers being numbered from the side nearest the moving wall as shown in figure 3.2. In a similar fashion the equilibrium layer thickness alternates between d_1 and d_2. The system can then be described in terms of the two parameters, $m = \eta_2/\eta_1$ and $d = d_2/d_1$. The positions of the interfaces, y_j, can now be written as

$$y_j = 1 - \frac{j(1+d) + \frac{1}{2}(1-(-1)^j)(1-d)}{N(1+d) + \frac{1}{2}(1-(-1)^N(1-d)}. \tag{3.4}$$

We must first find the equilibrium velocity profile. We assume that the flow is unidirectional, hence $\bar{v}_j = 0$ and $\bar{u}_j$ depends only on y. (We use the over-bar to indicate equilibrium values from here on). The equation for the equilibrium flow is then

$$\frac{d^2\bar{u}_j}{dy^2} = K_j, \tag{3.5}$$

where K_j is the pressure gradient, taken to be constant in each layer. The resulting time-independent velocities are polynomial in y;

$$\bar{u}_j = \bar{a}_j + \bar{b}_j y + \bar{c}_j y^2. \tag{3.6}$$

Since there is no external pressure gradient in plane Couette flow the constants $\bar{c}_j$ are zero.

Using the interfacial boundary conditions, we find that

$$\bar{b}_j = \bar{b}_1 \eta_1/\eta_j, \tag{3.7}$$

and

$$\bar{a}_j = \bar{a}_1 + \nu \bar{b}_1 \sum_{p=1}^{n-1} (-1)^p y_p, \tag{3.8}$$

where y_p is the position of the pth interface and $\nu = (1/m) - 1$. The values of $\bar{b}_1$ and $\bar{a}_1$ are then chosen to satisfy the no-slip boundary conditions at the walls which can be expressed as:

$$\bar{a}_1 + \bar{b}_1 = 1, \qquad \bar{a}_N = 0. \tag{3.9}$$

3.4 The stability analysis

3.4.1 The wavy interface approximation

We now apply the stability analysis introduced by Yih [29] to the above flow geometry. We allow perturbations to occur in the velocity field, these being u'_j and v'_j in the x and y directions respectively, and define these in terms of a stream-function ψ_j such that

$$u'_j = \frac{\partial \psi_j}{\partial y}, \quad v'_j = -\frac{\partial \psi_j}{\partial x}. \tag{3.10}$$

The disturbances in the pressure p and stream-function, ψ, are then of the form

$$(p, \psi_j) = (f_j(y), \phi_j(y)) \exp i\alpha(x - ct). \tag{3.11}$$

Here α is the wave number of the disturbance and c the complex velocity. If the imaginary part of the velocity c_I is greater than zero then the disturbances will increase in time and the system will be unstable. Substituting the primary flow plus the perturbations into the Navier-Stokes equations and linearizing gives the following equations:

$$i\alpha \left\{ (\bar{u}_j - c)\frac{\partial \phi_j}{\partial y} - \frac{\partial \bar{u}_j}{\partial y}\phi_j \right\} = -i\alpha f_j + R_j^{-1} \left(\frac{\partial^3 \phi_j}{\partial y^3} - \alpha^2 \frac{\partial \phi_j}{\partial y} \right) \tag{3.12}$$

and

$$\alpha^2 (c - \bar{u}_j)\phi_j = f'_j + \frac{i\alpha}{R_j} \left(\frac{\partial^2 \phi_j}{\partial y^2} - \alpha^2 \phi_j \right). \tag{3.13}$$

Differentiating the first equation and eliminating the pressure term f_j leads to the Orr-Sommerfeld equation:

$$\frac{\partial^4 \phi_j}{\partial y^4} - 2\alpha^2 \frac{\partial^2 \phi_j}{\partial y^2} + \alpha^4 \phi_j = i\alpha R_j \left\{ (\bar{u}_j - c)\left(\frac{\partial^2 \phi_j}{\partial y^2} - \alpha^2 \phi_j \right) \right\}. \tag{3.14}$$

Here R_j is the Reynolds number $\rho U w/\eta_j$, where w is the channel width, ρ the fluid density, U the velocity of the upper plate, and η_j the viscosity of the jth layer. The elimination of the pressure perturbation is achieved by effectively

taking the curl of the perturbed Navier-Stokes equation. Since we have only two dimensions this gives a single equation in the direction perpendicular to the flow. Using this interpretation we see that the Orr-Sommerfeld equation is equivalent to a linearised vorticity equation for two-dimensional disturbances [62].

To specify the problem completely, the correct boundary conditions must be applied. The rigid wall boundary conditions are

$$\phi_1|_{y=1} = 0, \qquad \left.\frac{\partial \phi_1}{\partial y}\right|_{y=1} = 0, \tag{3.15}$$

and

$$\phi_N|_{y=0} = 0, \qquad \left.\frac{\partial \phi_N}{\partial y}\right|_{y=0} = 0. \tag{3.16}$$

The interfacial boundary conditions must be applied at the deformed interfaces, ξ_j. As the perturbations are small a Taylor expansion of the interface positions, about the mean positions, can be made. Continuity of velocity and stress in both the x and y directions then gives four conditions at each interface. Continuity of the y component of velocity gives

$$\phi_{j+1}(y_j) = \phi_j(y_j). \tag{3.17}$$

At each interface we must satisfy

$$\left(\frac{\partial}{\partial t} + \bar{u}_j \frac{\partial}{\partial x}\right) \xi = v'_j. \tag{3.18}$$

Using the definition of v', the interfacial position can be written as

$$\xi = \frac{\phi_j(y_j)}{c_j} \exp(i\alpha(x - ct)), \tag{3.19}$$

where c_j is given by $c - \bar{u}_j(y_j)$. Using this result the continuity of the x component gives a more complicated condition due to the curvature of the interface:

$$\frac{\partial \phi_{j+1}}{\partial y} - \frac{\partial \phi_j}{\partial y} = \frac{\phi_j}{c_j}\left(\frac{\partial u_j}{\partial y} - \frac{\partial u_{j+1}}{\partial y}\right). \tag{3.20}$$

Here all the functions are evaluated at y_j.

The continuity of shear stress can be applied at the interfaces themselves since the gradient of the shear stress is the same in all layers. This gives

$$\eta_{j+1}\left(\frac{\partial^2\phi_{j+1}}{\partial y^2}+\alpha^2\phi_{j+1}\right)=\eta_j\left(\frac{\partial^2\phi_j}{\partial y^2}+\alpha^2\phi_j\right). \tag{3.21}$$

Finally, the continuity of hydrostatic pressure gives the condition

$$\eta_{j+1}\left(\frac{\partial^3\phi_{j+1}}{\partial y^3}-3\alpha^2\frac{\partial\phi_{j+1}}{\partial y}\right)-\eta_j\left(\frac{\partial^3\phi_j}{\partial y^3}-3\alpha^2\frac{\partial\phi_j}{\partial y}\right)=i\alpha^3\frac{T_j}{V}\frac{\phi_j}{e_j}. \tag{3.22}$$

Here we have introduced the effect of surface tension, T_j, at the jth interface. However such terms do not contribute to the analysis given below since they are only significant at short wavelengths.

It is important to note that only one boundary condition contains the wave velocity itself; the condition for continuity in u'. It occurs there because a correction has to be made for the curvature of the interface. In the next section we shall show that at long wavelengths this is the only place that c appears and so any instability must be due to the curvature of the interfaces.

3.4.2 The long wavelength approximation

The Orr-Sommerfeld equation is investigated using the perturbation method of Yih. The eigenfunctions ϕ_j and eigenvalue c are expanded as a power series in the wave number α.

$$\phi_j=\phi_{0,j}+\alpha\phi_{1,j}+\ldots \tag{3.23}$$

$$c=c_0+\alpha c_1+\ldots \tag{3.24}$$

These expressions are then substituted into the Orr-Sommerfeld equation and collected into terms of the same order of α. The zeroth order equation is

$$\frac{\partial^4\phi_{0,j}}{\partial y^4}=0, \tag{3.25}$$

which has a polynomial solution

$$\phi_{0,j}=A_{0,j}+B_{0,j}\,y+C_{0,j}\,y^2+D_{0,j}\,y^3. \tag{3.26}$$

We now apply the boundary conditions at zeroth order. Continuity of v_j' gives

$$\phi_{0,j+1} = \phi_{0,j}\big|_{y=y_j} \tag{3.27}$$

and continuity of u_j' gives

$$\frac{\partial \phi_{0,j+1}}{\partial y} - \frac{\partial \phi_{0,j}}{\partial y} = \frac{\phi_{0,j}}{c_{0,j}} \left(\frac{\partial \bar{u}_j}{\partial y} - \frac{\partial \bar{u}_{j+1}}{\partial y} \right)\Bigg|_{y=y_j}, \tag{3.28}$$

where $c_{0,j} = c_0 - \bar{u}_j(y_j)$.

Continuity of stress gives

$$\eta_{j+1} \frac{\partial^2 \phi_{0,j+1}}{\partial y^2} = \eta_j \left. \frac{\partial^2 \phi_{0,j}}{\partial y^2} \right|_{y=y_j} \tag{3.29}$$

and

$$\eta_{j+1} \frac{\partial^3 \phi_{0,j+1}}{\partial y^3} = \eta_j \left. \frac{\partial^3 \phi_{0,j}}{\partial y^3} \right|_{y=y_j}. \tag{3.30}$$

This results in a linear, homogeneous, system of algebraic equations for the coefficients of equation 3.26. The only non-trivial solution of such a system occurs when the determinant of the system is zero. Using this fact we can construct the characteristic equation for the system which is a polynomial of order $N-1$ in c_0. Thus there are $N-1$ possible eigenvalues for the system at zeroth order. If all these eigenvalues are real then the system is neutrally stable. Since the characteristic polynomial has real coefficients, if the eigenvalues are not real, they will appear in complex conjugate pairs, with one eigenvalue always giving an unstable mode. The results of Yih [29] show that to lowest order we cannot get instability for two layers, but Li [30] has shown that for three layers we obtain an instability.

If the zeroth order wave velocity is real, then we have neutral stability and the first order approximation must be considered. This has the following form:

$$\frac{\partial^4 \phi_{1,j}}{\partial y^4} = i\alpha R_j \left\{ (\bar{u}_j - c) \frac{\partial^2 \phi_{0,j}}{\partial y^2} - \frac{\partial^2 u_j}{\partial y^2} \phi_{0,j} \right\}. \tag{3.31}$$

This equation can also be integrated directly to produce a polynomial solution

$$\phi_{1,j} = A_{1,j} + B_{1,j}\, y + C_{1,j}\, y^2 + D_{1,j}\, y^3 + i\alpha R_j h_j(y). \tag{3.32}$$

The first three terms are the complementary solution for which the coefficients are found from applying the boundary conditions to order α. The final term is the particular solution, which has the following form:

$$h_j(y) = C_{0,j}(a_j - c_0)\frac{y^4}{12} + \{C_{0,j}\bar{b}_j + 3D_{0,j}(a_j - c_0)\}\frac{y^5}{60} + D_{0,j}\bar{b}_j\frac{y^6}{60}. \qquad (3.33)$$

The boundary conditions to be applied are the same as for the zeroth order case, with $\phi_{0,j}$ becoming $\phi_{1,j}$, with the exception of equation 3.28 which has an additional correction to become

$$e_{0,j}\left(\frac{\partial\phi_{1,j+1}}{\partial y} - \frac{\partial\phi_{1,j}}{\partial y}\right) + \phi_{1,j}\left(\frac{\partial\bar{u}_j}{\partial y} - \frac{\partial\bar{u}_{j+1}}{\partial y}\right) = c_1\left(\frac{\partial\phi_{0,j+1}}{\partial y} - \frac{\partial\phi_{0,j}}{\partial y}\right). \qquad (3.34)$$

For each zeroth order eigenvalue there exists a corresponding first order eigenvalue c_1. If the zeroth order eigenvalue is real then it can be shown (see Appendix D) that the first order eigenvalue is of the form

$$c_1 = i\alpha R_1 J, \qquad (3.35)$$

where J is a real function of the number of layers, the viscosity ratio and the depth ratio. Thus the first order eigenvalue is wholly imaginary. The condition for instability is that $J > 0$.

3.5 Numerical Calculations

3.5.1 The zeroth order calculation

The algebraic analysis involved in solving the stability problem for more than three layers becomes unwieldy and hence we have resorted to a numerical treatment.

The primary flow coefficients are first evaluated for the given values of the viscosity ratio $m = \eta_2/\eta_1$ and depth ratio $d = d_2/d_1$. This involves solving the recurrence relations 3.7 and 3.8 so as to satisfy the no slip boundary conditions.

The interfacial conditions can also be expressed in terms of recurrence relations. At each order in the perturbation, the coefficients of the polynomial solution must satisfy these recurrence relations and also the boundary conditions at the upper and lower walls. At zeroth order the relations are

$$A_{0,j+1} = A_{0,j} + y_j(B_{0,j} - B_{0,j+1}) + y_j^2(C_{0,j} - C_{0,j+1}) + y_j^3(D_{0,j} - D_{0,j+1}), \tag{3.36}$$

$$B_{0,j+1} = B_{0,j} + 2y_j(C_{0,j} - C_{0,j+1}) + 3y_j^2(D_{0,j} - D_{0,j+1}) + F_j(A_{0,j} + y_j B_{0,j} + y_j^2 C_{0,j} + y_j^3 D_{0,j}), \tag{3.37}$$

$$C_{0,j} = C_{0,1}\frac{\eta_1}{\eta_j}, \tag{3.38}$$

and

$$D_{0,j} = D_{0,1}\frac{\eta_1}{\eta_j}, \tag{3.39}$$

where $F_j = (b_j - b_{j+1})/e_{0,j}$. Unlike for the primary flow, these recurrence relations cannot be separated to obtain a general solution and hence we use a purely numerical method to find the eigenvalues c_0.

We can take the value of $A_{0,1}$ to be unity since the zeroth order solution is only defined up to an arbitrary multiplicative constant. The coefficients $C_{0,1}$ and $D_{0,1}$ are then calculated in terms of $B_{0,1}$ using the upper wall boundary conditions:

$$1 + B_{0,1} + C_{0,1} + D_{0,1} = 0 \tag{3.40}$$

and

$$B_{0,1} + 2C_{0,1} + 3D_{0,1} = 0. \tag{3.41}$$

Thus we can iterate the recurrence relations if we first specify the values for $B_{0,1}$ and c_0. However by making the change of variables

$$A_{0,j} = \hat{A}_{0,j} + B_{0,1}\tilde{A}_{0,j}, \qquad B_{0,j} = \hat{B}_{0,j} + B_{0,1}\tilde{B}_{0,j}, \tag{3.42}$$

and applying the new boundary conditions

$$\hat{A}_{0,1} = 1, \quad \hat{A}_{0,1} = 0, \quad \hat{B}_{0,1} = 0, \quad \hat{B}_{0,1} = 1, \tag{3.43}$$

we need only specify the value of c_0 before we start the iteration scheme. The transformed recurrence relations are given in Appendix D.

The value of c_0 is obtained by iterating the recurrence relations and applying the boundary condition at the lower wall. This condition can be expressed as

$$\hat{A}_{0,N}\hat{B}_{0,N} - \hat{B}_{0,N}\hat{A}_{0,N} = G(c_0) = 0. \tag{3.44}$$

The evaluation of the eigenvalue is now equivalent to finding the zeroes of the function $G(c_0)$. This function is equivalent to the characteristic equation for the system of equations which as previously stated is polynomial in c_0. Using this fact we look for $N-1$ real solutions to the boundary condition. If fewer solutions are found then we know that the remaining solutions exist as complex conjugate pairs. In this case one of the eigenvalues must correspond to an unstable mode. Thus we can determine whether the system is stable or unstable using only real variables, a significant simplification over using complex algebra. We can now take a range of real values for c_0, evaluate $G(c_0)$ and plot it as a function of c_0. The zeroes of the function $G(c_0)$ are obtained by using a bisection algorithm [63].

Some plots of $G(c_0)$ are shown in figures 3.3 and 3.4. It is found that the zeroes of the function always lie in the range from 0 to 1. (This result has been proven for the Orr-Sommerfeld equation applied to a single fluid [64]). It can also be seen that the function goes to infinity whenever c_0 takes the value of an undisturbed interface velocity. This is due to the term proportional to $1/e_{0,j} = 1/(c_0 - u_j)$ in equation 3.37.

Figures 3.3(a)-(c) show that as the depth ratio is varied the number of zeroes of G goes from two (neutral stability) to zero (instability). It can also be seen that at the point at which the system goes unstable the two eigenvalues converge to a common value. This behaviour means that just as the two interfaces go

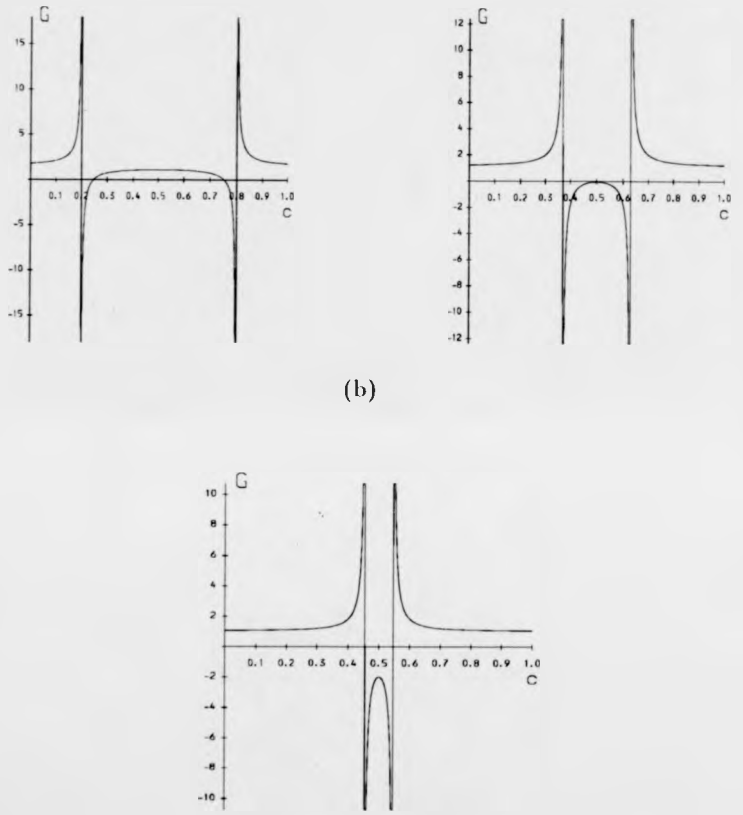

Figure 3.3: *The boundary function, G, as a function of the wave velocity, c, for three layers. (a) m=0.5, d=1.5 (b) m=0.5, d =0.35 (c) m=0.5, d =0.1*
(Note the vertical lines are asymptotes and their crossings do not represent zeroes of $G(c_0)$.)

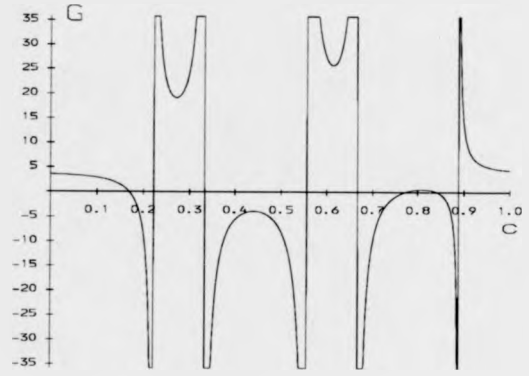

(a)

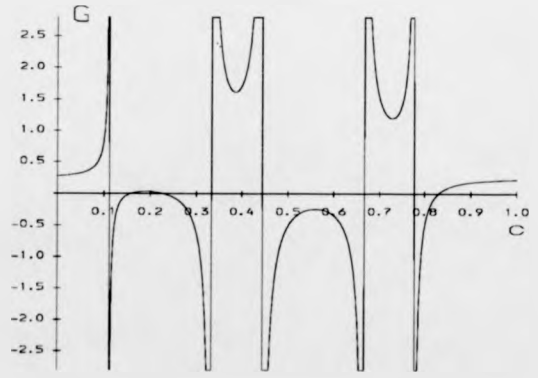

(b)

Figure 3.4: *The boundary function, G, as a function of the wave velocity, c, for six layers. (a) m=0.25, d=0.5 (b) m=4.0, d =2.0*
(Note the vertical lines are asymptotes and their crossings do not represent zeroes of $G(c_0)$.)

unstable the waves at the interfaces (defined by ξ) have the same velocity. Thus we can associate the instability with a resonance phenomenon. Similar results are obtained for $N > 3$ and are illustrated in figure 3.4.

There are certain symmetries which the system must show. For an odd number of layers the function $G(c_0)$ must be symmetrical about $c_0 = 1/2$, since the primary flow has this property. For an even number of layers the transformations $m \to 1/m$ and $d \to 1/d$ must not alter the stability of the system. This transformation is equivalent to a physical reflection of the system about the centre-line of the flow. The effect of this transformation is demonstrated for six layers in figure 3.4. The zeroes of the function are seen to go from c_0 to $1 - c_0$ as would be expected for the reflection. These symmetries are obeyed by our numerical results.

3.5.2 Discussion of stability at zeroth order

From the above numerical results we can find the values of the two parameters m and d for which $G(c_o)$ loses two real zeroes. A plot of these critical values of m and d against one another gives a neutral stability curve. Such a curve divides the parameter space (m, d) into regions corresponding to stability and instability.

Figure 3.5 shows the neutral stability curves at zeroth order for systems with four and five layers. When the viscosity ratio m is less than unity the curves almost overlap and furthermore are of the same general form as those for the three layer case as calculated by Li. Each of these systems is neutrally stable for all depth ratios when m tends to zero. More significantly, the four and five layer systems also have an instability region when m is greater than unity. This is not the case for three layers, which is stable if m is greater than unity.

The curve for the four layer system satisfies the symmetry $m \to 1/m$ and $d \to 1/d$ as it has an even number of layers. This means that the values for $m > 1$ can be obtained from the curve for $m < 1$. This is the case for all our

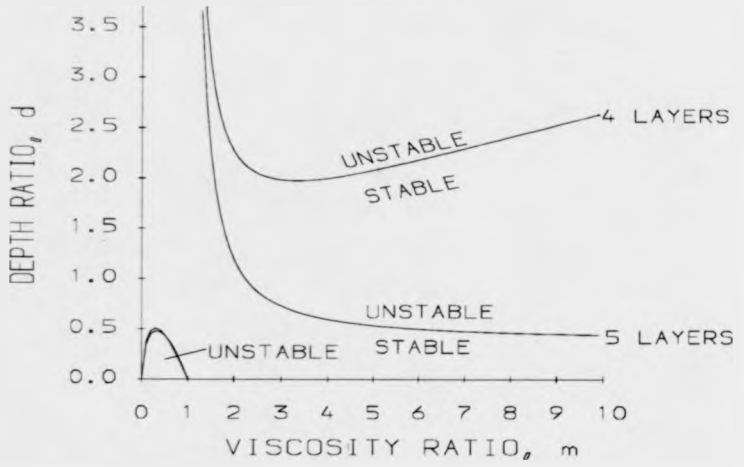

Figure 3.5: *Zeroth order neutral stability curves as a function of depth ratio and viscosity ratio for 4 and 5 layers*

results for even numbers of layers (e.g. 8 layers in figure 3.6)

For six or more layers the system is found to be unstable for finite depth ratios even as m tends to zero. Figure 3.6 shows this and also gives an example of the pairing of neighbouring curves for large values of m. It is seen that as m gets large the eight layer and seven layer curves converge. This phenomenon occurs for all pairs of curves for $2N$ and $2N-1$ layers, where N is an integer. As m tends to zero a similar pairing occurs for systems with $2N$ and $2N+1$ layers. This pairing occurs when two systems differ by the addition of an extra layer of fluid near the lower wall. As m becomes very small or very large this fluid is much more viscous than its neighbouring layer. All the zeroth order perturbation terms in such a layer tend to zero as m tends to zero and this prevents the layer from altering the stability of the system overall. Using these arguments, it follows that

the behavior of the three layer case at $m = 0$ is governed by the stability of the two fluid case in the same limit. Using the symmetry for even numbers of layers, $m \to 1/m, d \to 1/d$, in addition to this argument, gives that the behaviour of the four and five layer cases, as m tends to zero, is restricted by the behaviour of the three layer case as m tends to infinity.

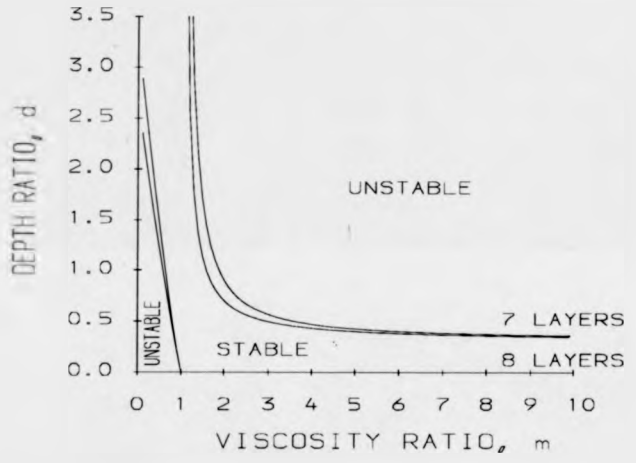

Figure 3.6: *Zeroth order neutral stability curves as a function of depth ratio and viscosity ratio for 7 and 8 layers*

It can also been seen from figure 3.6 that for seven and eight layers the system is unstable at finite depth ratios as m tends to zero. This property is shown for all cases with six or more layers. It is also found that the range of unstable d values increases as the number of layers is increased (subject to the requirement that cases with $2N$ and $2N + 1$ layers must pair off in this limit, as previously described).

All the systems show neutral stability, to zeroth order, when m approaches

unity, as would be expected. As the number of layers is increased the unstable regions get larger, as shown by figures 3.5 and 3.6. It should be noted that the 'stable' regions at zeroth order are neutrally stable and not truly stable, since the eigenvalues are purely real. For those regions which are stable to lowest order the analysis has been extended to first order and the growth rate function, J, calculated. This is used to obtain the growth rates using equation 3.35.

3.5.3 The first order calculation

In the same way as for the zeroth order calculation the first order calculation results in a series of recurrence relations. The first order recurrence relations are analyzed by using a similar transformation as for the zeroth order calculation. This makes it easy to show that the first order eigenvalue is wholly imaginary as long as the zeroth order eigenvalue is wholly real. For the sake of brevity we omit the first order recurrence relations here and give a detailed discussion in Appendix D.

The first order results were checked using certain symmetries which the system must satisfy at both zeroth and first order. Again, if the number of layers is even, then changing m and d to $1/m$ and $1/d$ respectively does not alter the first order eigenvalues. If the number of layers is odd, then the first order eigenvalues will occur in pairs with the same value c_1. This is due to the symmetry of the odd number of layers about the centre line of the flow.

The numerical results were also checked for the cases of two layer and three layer flow by comparing with the results of Yih [29] and Li [30] respectively.

3.5.4 Discussion of stability at first order

The growth rate function for the cases of the four and six layers are shown in figures 3.7 and 3.8. It is found that for all systems with greater than three layers, at least one eigenvalue corresponds to an unstable mode for any value of the

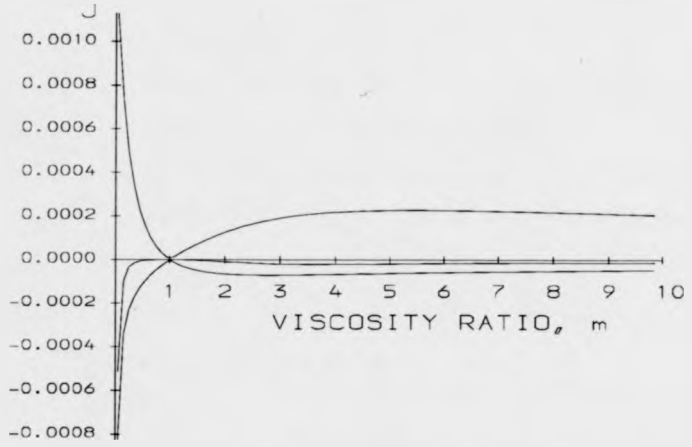

Figure 3.7: *The growth rate function J as a function of viscosity ratio m. (4 layers, d=1.5) The three curves correspond to the three zeroth order eigenvalues for the system*

viscosity ratio. The actual mode which is unstable depends on whether m is greater than or less than unity. The growth rate function is not shown for m less than unity in the six layer case as the system is unstable at zeroth order in most of this region. For the three layer system the modes are stable for $m > 1$ and unstable for $m < 1$. Again the eigenvalues are zero when the viscosity ratio is unity, giving the expected neutral stability.

If we consider the time scale for this instability to manifest itself we must calculate the value of αc_1 in a dimensional form. If we take as representative values those for water sheared at a shear rate of $10s^{-1}$, with a channel width of 1cm and a dimensionless wave number of 0.1, we get a maximum dimensional growth rate of approximately $0.1s^{-1}$. Since the perturbation is initially small this

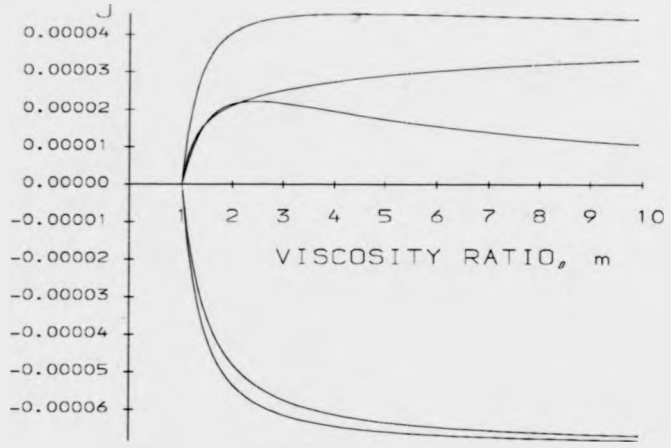

Figure 3.8: *The growth rate function J as a function of viscosity ratio m. (6 layers, d=0.3) The five curves correspond to the five zeroth order eigenvalues*

would mean that time scales of order 10^3 seconds would be required to visually identify the instability. We have not calculated the zeroth order growth rates but would expect them to be about an order of magnitude larger than this, (from the form of the expansion). This would imply a time scale of 100s to observe any instability.

3.6 Conclusions of the stability analysis

The analysis discussed in this chapter has shown several new types of behaviour for multi-layer plane Couette flows. We have identified instabilities for multi-layer flows which are analogous to the resonance instability identified by Li for three layer flow (at the lowest order of perturbation). However, for four or more

layers the neutral stability curves show much more structure. Importantly new regions of instability appear in the viscosity ratio / depth ratio parameter space. For example a region of instability occurs when the viscosity ratio is greater than unity, a result not found for three layers. It is also found, somewhat unexpectedly, that a system with six or more layers is unstable for finite depth ratios as the viscosity ratio approaches zero. This is unlike the cases with three, four or five layers. These are stable at zeroth order for all depth ratios as the viscosity ratio goes to zero. Furthermore, using first order perturbation theory it is found that systems with four or more layers are unstable for all values of the viscosity ratio and depth ratio. This result differs significantly from the result for three layers, where Li showed that stable configurations existed to lowest and first order.

When the system has a large, odd number of layers and the viscosity ratio is small, we find (except for unrealistic depth ratios) the system to be unstable to zeroth order. This is the configuration which models colloidal structures most closely and thus predicts such physical systems to be unstable.

3.7 Discussion of the model

The original motivation for this chapter was to determine the stability of flows in concentrated, colloidal dispersions with layers of different concentrations (and hence viscosities). The results show that in the limit of a large number of layers (appropriate for a macroscopic sample) all such layered profiles are unstable. This behaviour is seemingly in contrast with that observed experimentally, where layered structures are found to exist for finite periods of time.

It is possible that these instabilities do occur but that they evolve too slowly to be observed in the experimental work carried out to date. An alternative explanation for the discrepancy is that the observed layering is truly a time independent phenomenon in which case the model is not adequate to capture the true behaviour of the system. An improved model should take into account

the microscopic behaviour of the suspended particles. A more detailed model of flowing colloidal suspensions will be discussed in the next chapter.

Chapter 4

A Microscopic Model Of Flowing Suspensions

4.1 The Hydrodynamic Forces Acting On Colloidal Particles

4.1.1 The forces present in creeping flow

In order to make a microscopic model of a flowing suspension it is essential to know how the suspending fluid interacts with the particles within it. This means that a knowledge of the hydrodynamic forces acting on particles is necessary. We begin by considering the forces acting on single spherical particles in slow fluid flows.

The most commonly known force which a fluid can exert on a spherical particle is the Stokes' drag [31]. This is a force which tends to equalise the velocity of a particle with the surrounding fluid. Its magnitude is $6\pi\eta a(V_f - V_p)$, where η is the viscosity, a is the particle radius and $V_f - V_p$ is the difference between the fluid and particle velocities. This form is applicable at low Reynolds numbers.

The Stokes' force can be obtained as a special case of the force obtained by

Faxén [32]. The approach of Faxén treats the particle as a distribution of point forces in a fluid. The resulting velocity field is integrated over the surface of the sphere to obtained the total force acting on the sphere. The form of the force on a particle moving with a velocity $\mathbf{V}_p$ in a fluid with a velocity $\mathbf{V}_f$ is

$$\mathbf{F} = 6\pi\eta a([\mathbf{V}_f + \tfrac{1}{6}a^2\nabla^2\mathbf{V}_f]_0 - \mathbf{V}_p). \tag{4.1}$$

The subscript zero means that the object in square brackets should be evaluated at the centre of the sphere. In the case that $\nabla^2\mathbf{V}_f = 0$ this immediately reduces to Stokes force.

Both of these forces are important in creeping flow but they are unable to explain all of the observed behaviour of particles in a fluid, such as particles moving across the streamlines of a uni-directional flow. This is clear for the Faxén force since the force is parallel to the fluid velocity. More generally the equations of creeping flow are linear, leading to a symmetry under the reversal of the direction of a flow. Thus particles cannot cross streamlines when the fluid is undergoing creeping flow. This result was obtained by Bretherton [33] for all uni-directional laminar flows. Therefore, in order to explain observations of particles crossing streamlines, the inertial effects of a non-zero Reynolds number must be considered.

4.1.2 The migration of particles across streamlines

The migration of particles across stream lines was first observed experimentally by Segré and Silverberg [65, 66] for neutrally buoyant, rigid spheres in Poiseuille flow. The experiments of Segré and Silverberg also showed that the spheres did not migrate all the way to the pipe axis, but reached an equilibrium position at approximately 0.6 of the pipe radius from the axis.

Similar observations were made by Halow and Wills [68, 69] for neutrally buoyant spheres in a Couette system. In their experiment it was found that the spheres migrated to a position midway between the annular container walls.

More recent experiments by Jefri and Zahed [70] have shown that the equilibrium position of spheres in plane-Poiseuille flow also depends on the elastic properties of the suspending fluid. For a non-Newtonian (shear-thinning) fluid, they found that the equilibrium position was near the container walls. Several different equilibrium positions were observed as the elastic properties of the suspending fluid were varied.

4.1.3 Theoretical investigations of particle migration

The existence of transverse forces on particles moving in *inviscid* fluids is well known and is described using the Bernoulli equation. At low Reynolds number when viscous effects become important the same effects are more difficult to calculate. Many workers have theoretically investigated the migration of particles at low Reynolds number, with varying degrees of success. Most workers have begun their investigations by considering the case of a single rigid sphere in Poiseuille or Couette flows. In all of the approaches described in this chapter inertial effects are taken into account by using asymptotic expansions valid for small, but non-zero, Reynolds numbers.

Rubinow and Keller [71] and Saffman [34], were among the first to calculate the migration force on a sphere moving through an unbounded fluid. Rubinow and Keller assumed that the sphere was both spinning, with an angular velocity, ω, and moving through a stationary, viscous fluid, with velocity, $\mathbf{V}$. They obtained a migration force, $\mathbf{F}_L$, of the form

$$\mathbf{F}_L = \rho\pi a^3(\omega \times \mathbf{V}). \tag{4.2}$$

The fluid density is ρ and the particle radius a.

Saffman's calculation was for a sphere in a simple, unbounded shear flow, with a shear rate, β. He obtained an expression for a migration force which is

independent of the rate of rotation of the sphere:

$$F_L = 6.46\eta V a^2 \left(\frac{\rho\beta}{\eta}\right)^{\frac{1}{2}}. \tag{4.3}$$

This result was obtained by making an inner and outer expansion of the equations in powers of the Reynolds number. The matching criterion for the two expansions led to the dominant contribution being proportional to the square root of the Reynolds number (the quantity in brackets in the expression is the Reynolds number). Unlike for the calculation by Rubinow and Keller the force is found to be independent of the rate of rotation of the sphere. An analysis was also made by Halow and Wills [68] based on Saffman's solution, which was somewhat unsatisfactory in that they introduced an arbitrary factor, in order to gain agreement with experiment.

Cox and Brenner [35] considered the more general case of bounded, three dimensional, Poiseuille flow. The approach used a double expansion in terms of the Reynold's number and the ratio of the particle size to the pipe size. This result assumed that the boundaries lay within the region of the inner expansion, making the outer expansion unnecessary. The results obtained were not explicit, but were left in integral form without specifying the magnitude or direction of any migration force.

Ho and Leal [36] used a similar approach to Cox and Brenner, involving the method of reflections and the generalised reciprocal theorem of Lorentz [72] to obtain actual values for the migration force. This allowed them to obtain equilibrium positions for particles in plane Poiseuille and shear flows, which are in agreement with experiment. Two distinct effects were pointed out by Ho and Leal. Firstly for plane Couette flow, a force directed towards the centre of the flow, proportional to the square of the shear rate. Secondly a force due to the curvature of the velocity profile which tends to move particles away from the centre of a plane Poisseuille flow.

Later calculations by Vasseur and Cox [37] gave different asymptotic values

of the forces near the boundaries. The numerical results of Vasseur and Cox were found to agree with an analytic calculation of the force on a sphere near a single boundary carried out by Cox and Hsu [73]. The differences between the results of Vasseur and Cox and those of Ho and Leal were attributed to numerical errors and do not significantly alter the equilibrium positions which were predicted by Ho and Leal. The lift force obtained by Vasseur and Cox can be written in the following form for the case of plane Couette flow with a velocity profile V and a cross channel coordinate, z:

$$F_L = 6\pi C \frac{\rho a^4 V^2}{L^2} N(z) \tag{4.4}$$

The function $N(z)$ is a numerically calculated function equal to unity on the boundaries and zero at the centre of the flow. The constant C was found analytically by Cox and Hsu [73] and numerically by Vasseur and Cox to be equal to 55/576 or about 0.1. Although the derivation of this expression is strictly only valid for small Reynolds numbers flows, it has been found to give qualitative agreement with experiments at Reynolds numbers larger than unity, as carried out by Halow and Wills [69].

The physical mechanism for the lift force on a particle near a wall was given by McLaughlin for plane Couette flow [74]. As a particle moves through a fluid it must displace the fluid to either side. If a wall is present then it resists this displacement, which has the effect of forcing the sphere away from the wall. The effect of inertia is to make the displacement of fluid irreversible at large distances from the sphere giving a lateral force even at large distances from the wall.

These are the main forces which we shall need to consider in order to construct our model of a suspension. We shall now discuss some previous models which have been suggested.

4.2 Previous Models Of Suspensions

4.2.1 The model of Nozières and Quemada

This model treats the suspension as a fluid which obeys the Navier-Stokes equations with the inclusion of the effect of a variable viscosity, η, which is a function of the local particle density, n. The density fluctuations, δn, are assumed to be small and a Taylor expansion used to write the viscosity in the form

$$\eta = \eta_0 + \frac{\partial \eta}{\partial n}\delta n. \tag{4.5}$$

The particle density is assumed to obey a diffusion equation with the additional assumption that the particles feel a lift force which is a function of the shear rate, γ: $F_L = \beta\gamma(\partial\gamma/\partial x)$. The introduction of this lift force was motivated by Ho and Leal's lift force but is not of the same form as their result.

A linear stability analysis about an equilibrium plane Couette flow was considered, allowing perturbations in the particle density and the fluid velocity parallel to the walls. The perturbations were considered to be independent of the the distance along the flow. An instability was found for shear rates above a critical value. The interpretation of this made by Nozières and Quemada was that the flow breaks up into domains for the shear rates above the critical value, γ, given by

$$\gamma^2 = \frac{\eta\mu'}{\beta\eta''}. \tag{4.6}$$

Here μ' is $\partial\mu/\partial n$ where μ is the chemical potential and η'' is $\partial\eta/\partial n$. The ratio μ'/β is effectively the ratio of the magnitudes of the diffusional forces and the lift force.

The model ignores the inertial effects of the fluid on the grounds that there is no velocity gradient along the flow. This is true at equilibrium and is consistent with the the stability analysis used. Although this is true it can be argued that a less restrictive perturbation should be considered, allowing perturbations to be

functions of the distance along the channel. In this case the inertial terms must be taken into account.

4.2.2 The model of McTigue, Givler and Nunziato

A different approach was used for the model suggested by McTigue, Givler and Nunziato. The model begins from the assumption that both the true fluid and the particulate phase can be modelled as fluids. The two phases are assumed to be inter-penetrating and able to exchange momentum by means of the hydrodynamic forces discussed earlier. The momentum equations for each phase are expressed in terms of the volume fraction of the appropriate phase, ϕ_a. The subscript a becomes p to indicate a particulate phase and f for the fluid phase. The momentum equation can be expressed in the following form.

$$\rho_a \phi_a \left(\frac{\partial \mathbf{V}_a}{\partial t} + \mathbf{V}_a \bullet \nabla \mathbf{V}_a \right) = \nabla \bullet \mathbf{T}_a + \rho_a \phi_a \mathbf{b}_a + \mathbf{m_a}. \tag{4.7}$$

Here ρ_a is the density of the appropriate phase, $\mathbf{V}_a$ the velocity field. The viscous stresses and pressure terms are denoted by $\mathbf{T}_a$, body forces by $\mathbf{b}_a$ and the interactions due to hydrodynamic forces by $\mathbf{m}_a$.

In addition to this two continuity equations are used,

$$\frac{\partial \rho_a \phi_a}{\partial t} + \mathbf{V}_a \bullet \nabla (\rho_a \phi_a) = -\rho_a \phi_a \nabla \bullet \mathbf{V}_a. \tag{4.8}$$

These equation ensure that conservation of fluid and particles are both satisfied.

The interaction terms for the solid are assumed to be of the form

$$\mathbf{m}_p = \phi_p \mathbf{F}(\mathbf{V}_f - \mathbf{V}_p) + \phi_p \mathbf{G} \nabla \bullet \mathbf{D}_f + p_f \nabla \phi_p, \tag{4.9}$$

where

$$\mathbf{F} = \alpha_1 \mathbf{1} + 2\alpha_2 \mathbf{D}_f, \qquad \mathbf{G} = \beta_1 \mathbf{1} + 2\beta_2 \mathbf{D}_f \tag{4.10}$$

with $\mathbf{D}_f$ being the symmetric tensor defined by $\mathbf{D}_f = \frac{1}{2}(\nabla \mathbf{V}_f + \nabla \mathbf{V}_f^T)$ and the symbol $\mathbf{1}$ representing the unit tensor. The α's and β's are treated as constants.

The interaction terms for the fluid are assumed to be the negative of this, in order to conserve momentum.

This form was shown by Passman [75] to be an exact second-order approximation for a general "frame-indifferent" constitutive relation for the interaction, $\mathbf{m}_p$, which is a function of $\mathbf{V}_f - \mathbf{V}_p$, $\nabla \cdot \mathbf{D}_f$ and $\mathbf{D}_f$. Frame indifference is defined by Drew [76] as the requirement that the relations are invariant under changes of reference frame. In the bulk this approach is appropriate as the variables listed are the important variables determining directions. It is not clear that this approach retains its importance near boundaries , since boundaries can impose preferred directions on the behaviour of the system.

Once this from has been chosen the interactions defined by the constants α_1, β_1, α_2 and β_2 are identified as Stokes' drag, Faxén's force, Saffman's lift force and Ho and Leal's lift force respectively. An additional term is included in the interaction term to allow for the effect of the particles on the fluid velocity. This is equivalent to using the Einstein relation mentioned in chapter 2.

The equations obtained by this approach cannot be solved in a closed form as they stand, since there are more unknowns than there are equations. This is not an uncommon problem in models of this sort and it is usually solved by postulating a constitutive relation between the fluid and particle pressure terms, p_f and p_p. Mctigue et al used a relation of the form

$$p_p = p_f + \tau + \omega(\mathbf{V}_f - \mathbf{V}_p)^2 + \zeta \text{ Trace}(\mathbf{D}_f). \tag{4.11}$$

This introduced a term, τ due to Brownian pressure, with ζ a bulk viscosity and ω a constant. This allows the equations to be solved in a closed form.

The model was solved for the case of plane Poiseuille flow using both an approximate analytic technique and a numerical approach. The results showed that a non-uniform concentration profile occurs across the channel width, due to the lift forces present. Since the exact profile is a function of shear rate, the apparent viscosity is also a function of shear rate. Thus the model behaves as a

single, non-Newtonian fluid. The stability of the resulting equilibrium solutions were not discussed.

The need for an extra constitutive relation makes this type of model rather unsatisfactory. An alternative approach was suggested by Passman [77] for dilute suspensions. Passman suggested that arguments similar to those used in the kinetic theory of gases could allow a momentum equation to be obtained for the particulate phase, giving an immediate interpretation of the particle pressure, which would remove the need for an extra constitutive relation. This is the approach used by Batchelor to describe a fluidised bed and the approach which we shall use. First we describe Batchelor's method in some detail.

4.2.3 Batchelor's model of a fluidised bed

Batchelor produced a model of a fluidised bed in order to investigate the stability of such systems [40]. In order to be as complete as possible the model was obtained in a formal manner. The approach used was similar to that used in the kinetic theory of gases. Batchelor's model is one dimensional, in that all quantities are averaged over horizontal planes normal to the direction of the fluid and particle velocities, which are vertical are driven by gravity. Because of the one-dimensional form of the equations, Batchelor showed that only the behaviour of the particles need be considered. For a mean particle velocity, V, and a volume fraction, ϕ, the flux through a control surface is $V\phi$. Hence the mean fluid flux is $-V\phi$ and the mean fluid velocity $-V\phi/(1-\phi)$ (assuming the sum of the fluid and particle volume fractions is unity).

The approach used is to consider the quantities of particle number and particle momentum, which must both be conserved. We first consider the conservation of particle number. Considering the rate of change of the number of particle centres within a cylindrical volume with a vertical axis, gives

$$\frac{\partial n}{\partial t} + \frac{\partial}{\partial x}(nV_p) = 0, \tag{4.12}$$

where n is the number density of particles and $\mathbf{V}_p$ is the velocity field associated with the particles.

A second equation is obtained by considering the momentum flux flowing in and out of a cylindrical volume. Batchelor obtained the following expression

$$m\frac{\partial(nV)}{\partial t} + m\frac{\partial(nV^2)}{\partial x} + mn\theta\left(\frac{\partial V}{\partial t} + V\frac{\partial V}{\partial x} - \zeta V\frac{\partial V}{\partial x}\right) = \tag{4.13}$$
$$-\frac{\partial(mn\langle v^2\rangle)}{\partial x} + n[F_h(V,\phi) - F_h(U,\phi)] - \frac{D}{B}\frac{\partial n}{\partial x} + \frac{\partial}{\partial x}\left(\phi\rho_f\eta'\frac{\partial V}{\partial x}\right)$$

The terms multiplied by θ and ζ are associated with virtual mass effects due to fluid inertia and are important at high Reynolds numbers. The precise form of these terms is not clear and Batchelor presents this form as a "provisional guess". The term involving $\langle v^2\rangle$ is due to perturbations in the particle velocity caused by turbulence or particle-particle interactions. The next term $F_h(V,\phi)$ is the external gravitational force acting on the particles. The contribution given by $F_h(U,\phi)$ is due to friction or drag tending to equalise the particle and fluid velocities. Next we have the diffusion forces acting on the particles characterised by the diffusion constant, D, with a mobility, B. These diffusion forces are treated as external to the particles and are important in our following calculations. The final term is equivalent to a particle viscosity which Batchelor states should be important when particles are very close together such as in a layer of sediment.

4.3 A New Model For Flowing Suspensions

4.3.1 The regime of applicability

We shall construct our model by following Batchelor's argument's for the behaviour of a distribution of particles within a one dimensional fluidised bed [40] and generalise his arguments for a system of 3 dimensions. We choose the particles to be neutrally buoyant and spherical for simplicity.

Unlike Batchelor, we shall not consider a concentrated suspension of particles. For a dilute suspension, we expect the particles to be separated sufficiently that they do not interact with each other in any direct manner. As a result of this we need only consider those interactions between the fluid and a single particle and may neglect effects which are the result of multi-particle interactions.

Before we continue the construction of the model we must note that there are two Reynolds numbers which are important in this analysis. The system Reynolds number, R_e, is given by $\rho V L/\eta$ for a fluid of density, ρ and viscosity, η, in a channel of width, L, with a scale velocity, V. There is also a particle Reynolds number, R_p, defined by $\rho V a/\eta$, where a is the particle radius. Since we expect a to be much smaller than L then we shall have $R_e \gg R_p$. (The scale velocities may also differ but this result will still be true as the particle scale velocity will not exceed the system scale velocity). In this analysis we shall assume the particle Reynolds number is small enough to allow us to use the expressions for Stokes' drag and the other forces discussed earlier. We can now discuss Batchelor's expression for conservation of particle number and fluid momentum in the light of these restrictions.

4.3.2 The particle equations

Conservation of particle number is straightforward and follows directly from Batchelor's work to give

$$\frac{\partial n}{\partial t} + \nabla \bullet (n \mathbf{V}_p) = 0, \tag{4.14}$$

where n is the particle concentration and $\mathbf{V}_p$ is the average velocity of the particles.

The momentum equations need a more careful approach. There are several effects which Batchelor considers in his model that are not appropriate for our model. We shall neglect the virtual mass effects since they are only important at a high particle Reynold's number. We may also neglect the effects of the

perturbations in the particle velocity field, $\langle v^2 \rangle$. Since we do not expect to be in a turbulent regime and we are ignoring the interactions between particles, the two possible situations which require this term do not occur.

Although the effects of gravity are essential in a fluidised bed, they are not expected to play an important role in our model since the particles are neutrally buoyant. Therefore we may ignore the term $F_h(V, \phi)$. The effects of drag ($F_h(U, \phi)$) are very important and we shall include them in the form of the Stokes' forces. The final term in Batchelor's expression is expected to be important when the particles are close together and is a form of particle-particle interaction. Because of this, we neglect this final term as with all the other particle-particle interactions.

For our system we must consider additional forces which are not present in Batchelor's model. Since the particles are not interacting, we can use the appropriate single particle results. The presence of boundaries gives rise to the previously discussed lift force, H^*, which acts in the direction normal to the walls. We must also consider Faxén's forces, $F^*\nabla^2\mathbf{V}_f$, due to the curvature of the fluid velocity profile. Unlike Mctigue, we choose not to include the Saffman lift force. This is due to the fact that the Saffman lift and the lift force of Vasseur and Cox are not compatible in their derivations. Vasseur's calculation assumes that the outer expansion is irrelevant and has a good agreement with experiment. Since Saffman's calculation relies on existence of the apparently unnecessary outer expansion we are justified in neglecting this contribution (for narrow flows).

Considering the flow of momentum through the boundary of a spherical surface (the 3-dimensional version of Batchelor's cylindrical surface) gives the following expression for the conservation of particle momentum in our system:

$$m\left(\frac{\partial(n\mathbf{V}_p)}{\partial t} + \nabla\bullet(n\mathbf{V}_p\mathbf{V}_p)\right) = -nH^*\hat{\mathbf{z}} - D^*\nabla n + nS^*(\mathbf{V}_f - \mathbf{V}_p) + nF^*\nabla^2\mathbf{V}_f. \tag{4.15}$$

Here H^*, D^*, S^* and F^* represent the lift force, diffusion forces, Stokes' drag

and Faxén forces respectively. The star indices indicate that these values are dimensional quantities. The lift force is in the z direction, denoted by the unit vector, $\hat{\mathbf{z}}$. If we now consider plane Couette flow, we assume the lift force given by Vasseur and Cox has the following form

$$H^* = \frac{6\pi}{10}\frac{\rho a^4 V^2}{L^2}\left(\frac{\partial \mathbf{V}_f}{\partial z}\right)^2 (1-2z), \tag{4.16}$$

where ρ is the density of the fluid/particles, a is the particle radius, V is the scale velocity (the velocity of the moving boundary) and L is the scale length (the width of the channel). For convenience we have defined z and $\mathbf{V}_f$ to go from 0 to 1. This expression is a reasonable analytic approximation to the numerical results of Vasseur and Cox and gives a manageable expression for our model.

The other terms are defined as

$$D^* = kT, \qquad S^* = 6\pi\eta a, \qquad F^* = \pi\eta a^3. \tag{4.17}$$

Here we have used k to be Boltzmann's constant, T the temperature and η to be the viscosity of the suspending fluid.

We can put the conservation equation into a more convenient form using the conservation of particles and the fact that $m = 4\pi a^3\rho/3$. Also the number density is proportional to the volume fraction, ϕ, such that $n = (3\phi)/(4\pi a^3)$. This gives

$$\frac{\partial \phi}{\partial t} = -\nabla\bullet(\mathbf{V}_p\phi) \tag{4.18}$$

and

$$\rho\phi\left(\frac{\partial}{\partial t} + \mathbf{V}_p\bullet\nabla\right)\mathbf{V}_p = \frac{3}{4\pi a^3}\{-\phi H^*\hat{\mathbf{z}} - D^*\nabla\phi + \phi S^*(\mathbf{V}_f - \mathbf{V}_p) + \phi F^*\nabla^2\mathbf{V}_f\}. \tag{4.19}$$

4.3.3 The fluid equations

In a 1 dimensional model there is no need to obtain the equations for conservation of fluid volume and fluid momentum. In our 3-dimensional model we must have these equations. Now we discuss how to obtain the fluid equations.

All the terms on the right hand side of the particle momentum equation 4.19 are due to interaction forces where the suspending fluid acts upon the particles. When considering the fluid equations we must take into account the resulting reaction of the particles on the fluid, which will be the negative of these terms. We must also take into account the viscosity of the fluid (which is a function of particle concentration) and the pressure gradient. The momentum of the fluid will be proportional to the voidage fraction, $1-\phi$. Any dependence on this parameter is absorbed into the definition of the viscosity for the viscous terms, and similarly the pressure gradient. This gives a conservation equation for fluid momentum as

$$\rho(1-\phi)\left(\frac{\partial}{\partial t}+\mathbf{V}_f\bullet\nabla\right)\mathbf{V}_f=\nabla\bullet\{(\eta+\eta'\delta\phi)\nabla\mathbf{V}_f\}-\nabla p \qquad (4.20)$$
$$-\frac{3}{4\pi a^3}\left\{-\phi H^*\hat{\mathbf{z}}-D^*\nabla\phi+\phi S^*(\mathbf{V}_f-\mathbf{V}_p)+\phi F^*\nabla^2\mathbf{V}_f\right\}.$$

Here we assume that for small perturbations in particle volume fraction, $\delta\phi$, from the mean volume fraction, ϕ, we can write the viscosity as $\eta+\eta'\delta\phi$ with $\eta'=\partial\eta/\partial\phi$.

The corresponding continuity equation is

$$-\frac{\partial\phi}{\partial t}=-\nabla\bullet\{\mathbf{V}_f(1-\phi)\}. \qquad (4.21)$$

It can be seen from the form of these equations that we have no form of particle viscosity or particle pressure involved. This removes the need to postulate a constitutive relation in order to close our system of equations. We now have the requisite number of equations for the unknowns $(\mathbf{V}_p,\mathbf{V}_f,p,\phi)$.

4.3.4 Boundary conditions

In order to obtain a useful solution of these equation we require the appropriate boundary conditions. The conditions on $\mathbf{V}_f$ are obviously the usual fluid boundary conditions of zero normal velocity and the no-slip condition. The conditions

for $\mathbf{V}_p$ are not so obvious. The normal velocity must be zero as for $\mathbf{V}_f$ to prevent a flow of particles through the wall. The question of the no-slip condition is not so simple. The argument for the no-slip condition is usually that any discontinuity in velocity gradient at the wall will result in large viscous stresses tending to equalise the velocities [78]. However these arguments are known not to apply to very dilute gases, which is effectively the case here. Since we have no particle viscosity it does not seem appropriate that the no-slip condition be applied. The fact that the equation of conservation of momentum for particles is of first order in $\mathbf{V}_p$ means that we will not have underspecified the boundary conditions by relaxing the no-slip condition.

The boundary condition to be applied for ϕ is more complicated. This is particularly the case when the lift force is considered since this force occurs only when particle inertia cannot be neglected. The effect of particle inertia is to introduce non-local effects, since the inertia of the particle depends on forces applied at earlier times than the time being considered. For the moment we shall merely state the physical condition that there should be no flux of momentum through the walls of the system. The mathematical implementation of this condition is discussed for specific cases in the next chapter, where certain assumptions will be made about the form of the solutions.

Chapter 5

A Suspension Undergoing Plane Couette Flow

5.1 The system to be modelled

In the previous chapter we constructed a model which describes the behaviour of a flowing suspension using the forces acting on particles on a microscopic scale. In this chapter we shall present a solution for the particular case of plane Couette flow. We shall consider first the equilibrium solution for the system and then discuss the stability of the equilibrium state.

As they stand, the equations we have are non-linear and hence solutions are very difficult to obtain. Not only do we have the non-linear terms due to inertia but also the non-linear expression for the lift force. Because of this we are forced to look for mathematical approximations which can be made in order to obtain solutions. To aid this process we first consider the equations in a dimensionless form.

The system we shall consider will consist of neutrally buoyant particles with a radius, a, of about 1μm, suspended in a fluid confined between plates with a separation, L, of 1cm. The density, ρ, and viscosity, η_0, of the suspending fluid

will be taken as the appropriate values for water at a temperature, T, of 293k. This gives $\rho = 10^3 \mathrm{kGm}^{-3}$ and $\eta_0 = 10^{-3}\mathrm{kGm}^{-1}\mathrm{s}^{-1}$. We shall also assume that that average shear rate, V/L, is approximately unity.

5.2 The equations in dimensionless form

In order to obtain the dimensionless form of the governing equations, we make the following substitutions:

$$\begin{aligned} (x, y, z) &\rightarrow (x, y, z)/L, \qquad t \rightarrow tV/L \\ (\mathbf{V}_p, \mathbf{V}_f) &\rightarrow (\mathbf{V}_p, \mathbf{V}_f)/V, \qquad p \rightarrow pL/\eta_0 V. \end{aligned} \tag{5.1}$$

Using the same definitions as in the previous chapter $\mathbf{V}_f$ and $\mathbf{V}_p$ are the fluid and particle velocities respectively. Thus using R_e as the Reynolds number, $\rho V d/\eta_0$, we obtain in dimensionless form

$$\begin{aligned} \phi R_e \left(\frac{\partial}{\partial t} + \mathbf{V}_p \bullet \nabla\right) \mathbf{V}_p &= -\phi H^* \hat{\mathbf{z}} - D\nabla\phi \\ &\quad + \phi S(\mathbf{V}_f - \mathbf{V}_p) + \phi F \nabla^2 \mathbf{V}_f \end{aligned} \tag{5.2}$$

and

$$\begin{aligned} (1-\phi) R_e \left(\frac{\partial}{\partial t} + \mathbf{V}_f \bullet \nabla\right) \mathbf{V}_f &= \nabla \bullet \{(\eta_0 + \eta' \delta\phi)\nabla \mathbf{V}_f\} - \nabla p \\ &\quad + H^* \phi \hat{\mathbf{z}} + D\nabla\phi - \phi S(\mathbf{V}_f - \mathbf{V}_p) - \phi F \nabla^2 \mathbf{V}_f. \end{aligned} \tag{5.3}$$

Here we have redefined the interaction coefficients as

$$H = \frac{18\pi}{40} R_e \left(\frac{a}{L}\right), \quad S = \frac{9}{2}\left(\frac{L^2}{a^2}\right), \quad D = \frac{kTL}{4V\eta_0 a^3}, \quad F = \frac{3}{4}. \tag{5.4}$$

The continuity equations have the same form except with dimensionless variables replacing the original variables:

$$\frac{\partial \phi}{\partial t} = -\nabla \bullet (\mathbf{V}_p \phi), \tag{5.5}$$

$$-\frac{\partial \phi}{\partial t} = -\nabla \cdot \{\mathbf{V}_f(1-\phi)\}. \tag{5.6}$$

Calculating the magnitudes of the coefficients in equation 5.4 it is found that $D \sim 1$ and that H can be considerably smaller than unity, due to the factor $(a/L) \sim 10^{-4}$. This suggests that the lift force could be treated as a perturbation to the system and an expansion in terms of the parameter H may be useful. This is convenient mathematically since the lift force corresponds to a non-linear term and a perturbation analysis will allow it to be treated in a linear fashion. We must note that H contains a factor of the system Reynolds number. Thus such a perturbation approach would require a restriction to be placed on the Reynolds number of the system. A conservative estimate would allow values of $R_e < 100$. This will still allow a wide range of realistic situations to be modelled.

Using this approach we shall now look for an equilibrium solution for Plane Couette flow.

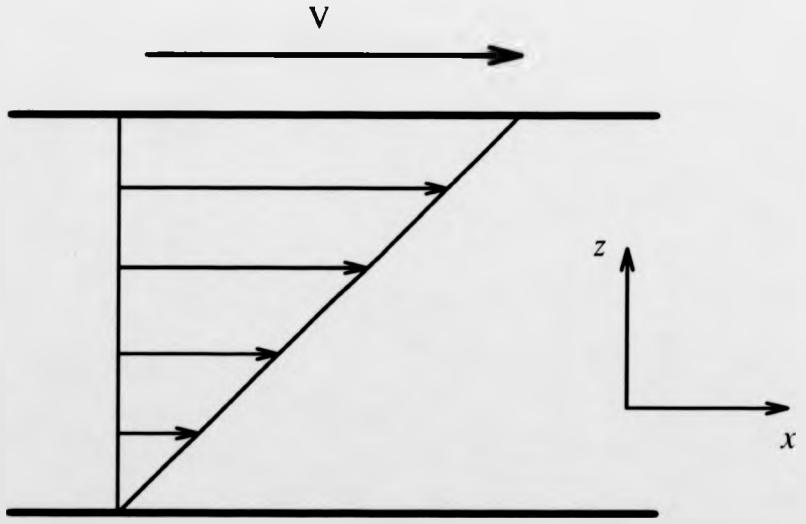

Figure 5.1: *The geometry of the problem*

5.3 The Equilibrium Solution

For an equilibrium solution we expect a time-independent, uni-directional flow. We shall use a coordinate system as shown in figure 5.1. Thus the particle and fluid velocities will take the form $\mathbf{V}_p = u_p(z)\hat{\mathbf{x}}$ and $\mathbf{V}_f = u_f(z)\hat{\mathbf{x}}$ respectively. A flow of this form will automatically satisfy the continuity conditions so we need only consider the conservation of particle and fluid momentum. In addition, it is easily seen that the non-linear terms of the form $\mathbf{V}\bullet\nabla\mathbf{V}$ are zero for uni-directional flow.

We now use an expansion such that

$$\begin{aligned} \mathbf{V}_p(z) &= \mathbf{V}_{p,0}(z) + H\mathbf{V}_{p,1}(z), \\ \mathbf{V}_f(z) &= \mathbf{V}_{f,0}(z) + H\mathbf{V}_{f,1}(z), \\ \phi &= \phi_0 + H\phi_1, \\ p &= p_0 + Hp_1. \end{aligned} \tag{5.7}$$

These expressions are then substituted into the equations of conservation of momentum and terms of like powers of H grouped together.

The zeroth order equations are

$$0 = -D\nabla\phi_0 + \phi_0 S(\mathbf{V}_{f,0} - \mathbf{V}_{p,0}) + \phi_0 F\nabla^2\mathbf{V}_{f,0}, \tag{5.8}$$

$$0 = \nabla\bullet\left(\left[1 + \frac{\eta'}{\eta_0}(\phi_0 - \bar{\phi})\right]\nabla\mathbf{V}_{f,0}\right) - \nabla p_0 + D\nabla\phi_0 - \phi_0 S(\mathbf{V}_{f,0} - \mathbf{V}_{p,0}) - \phi_0 F\nabla^2\mathbf{V}_{f,0}. \tag{5.9}$$

Using the fact that $\mathbf{V}_p = u_p(z)\hat{\mathbf{x}}$ and $\mathbf{V}_f = u_f(z)\hat{\mathbf{x}}$, equation 5.8 gives the volume fraction of particles, ϕ_0, to be a constant. This must be the average volume fraction $\bar{\phi}$. This result is then used to reduce equation 5.9 to the form

$$\nabla^2\mathbf{V}_{f,0} = -\nabla p_0. \tag{5.10}$$

This is the usual form of the equation for Couette flow of a single fluid. Since there is no external pressure gradient applied in Couette flow, we put ∇p_0 to be

equal to zero. Integrating the result and applying the boundary conditions (zero velocity at z=0 and z=1) gives

$$\mathbf{V}_{f,0} = z\hat{\mathbf{x}}, \qquad \mathbf{V}_{p,0} = z\hat{\mathbf{x}}, \qquad \phi_0 = \bar{\phi}. \tag{5.11}$$

We now require the correction to the equilibrium state to first order in H. The flow is still considered to be uni-directional. This allows the inertia terms to be neglected and ensures that the continuity equations are satisfied. The equations of conservation of particle and fluid momentum at this order are

$$0 = \phi_0(1-2z)\left(\frac{\partial u_{f,0}}{\partial z}\right)^2 \hat{\mathbf{z}} - D\nabla\phi_1 + \phi_0 S(\mathbf{V}_{f,1} - \mathbf{V}_{p,1}) + \phi_0 F\nabla^2\mathbf{V}_{f,1} \tag{5.12}$$

and

$$\begin{aligned} 0 \;=\; \nabla\cdot\left(\nabla\mathbf{V}_{f,1} + \frac{\eta'}{\eta_0}\phi_1\nabla\mathbf{V}_{f,0}\right) - \nabla p_1 - \phi_0(1-2z)\left(\frac{\partial u_{f,0}}{\partial z}\right)^2\hat{\mathbf{z}} \\ + D\nabla\phi_1 - \phi_0 S(\mathbf{V}_{f,1} - \mathbf{V}_{p,1}) - \phi_0 F\nabla^2\mathbf{V}_{f,1}. \end{aligned} \tag{5.13}$$

Using similar arguments to the case at $O(1)$, we obtain an expression for the volume fraction, which is a function of z only;

$$\phi_1 = \frac{\bar{\phi}}{D}(z - z^2) + C. \tag{5.14}$$

The constant of integration, C, is obtained by requiring that the total volume fraction of particles is a constant and hence that the integral of ϕ_1 across the channel is zero. This gives $C = -\bar{\phi}/6D$.

We can now use this expression to obtain an expression for the fluid velocity field. Thus we obtain,

$$0 = \frac{\partial}{\partial z}\left(\frac{\partial u_{f,1}}{\partial z} + \frac{\eta'}{\eta_0}\phi_1\frac{\partial u_{f,0}}{\partial z}\right) - \frac{\partial p_1}{\partial x}. \tag{5.15}$$

Again we have no pressure gradient and this expression can be integrated to obtain

$$u_{f,1} = Cz + D - \frac{\eta'}{\eta_0}\left(\frac{z^2}{2} - \frac{z^3}{3} - \frac{z}{6}\right). \tag{5.16}$$

Application of the boundary conditions ($u_{f,1}$ being zero on the boundaries) gives $C = D = 0$.

Finally, the x component of the particle equation gives

$$\phi_0 S(u_{f,1} - u_{p,1}) + \phi_0 F \nabla^2 u_{f,1} = 0. \tag{5.17}$$

This gives the particle velocity as $u_{p,1} = u_{f,1} + (\eta' \bar{\phi} a^2)(1-2z)/(\eta_0 D L^2)$. It should be pointed out that the equilibrium particle velocity does not satisfy the no-slip boundary condition only as a result of the Faxén forces, which cause the particles to lead/lag behind the fluid velocity at different points in the channel.

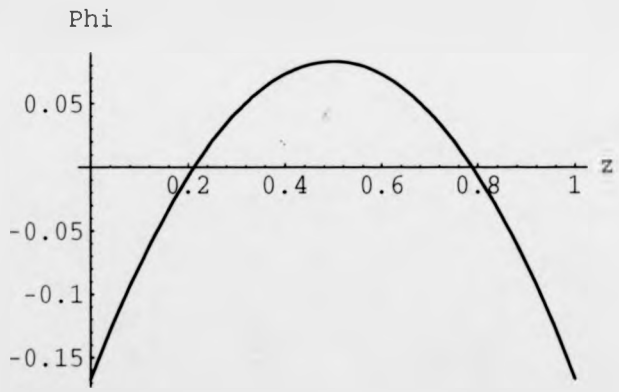

Figure 5.2: *The perturbation in volume fraction, 'Phi', across the channel due to the lift force at equilibrium*

We now have expressions for the equilibrium particle and fluid velocities and the volume fraction:

$$\phi = \bar{\phi}\left\{1 + \frac{H}{D}(z - z^2 - \tfrac{1}{6})\right\} \tag{5.18}$$

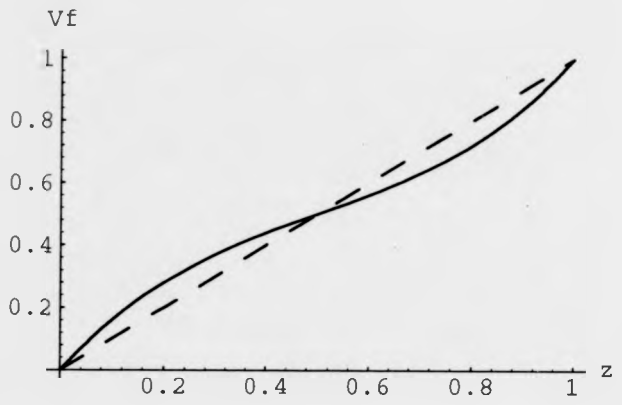

Figure 5.3: *The fluid velocity, $\mathbf{V}_f$, (dashed line) with perturbation due to the lift force (solid line). Note the magnitude of the perturbation has been exaggerated here.*

$$\mathbf{V}_f = \left\{ z - \frac{\eta' H \bar{\phi}}{\eta_0 D} \left(\frac{z^2}{2} - \frac{z^3}{3} - \frac{z}{6} \right) \right\} \hat{\mathbf{x}}$$
$$\mathbf{V}_p = \left\{ z - \frac{\eta' H \bar{\phi}}{\eta_0 D} \left(\frac{z^2}{2} - \frac{z^3}{3} - \frac{z}{6} - \frac{a^2}{L^2}(1-2z) \right) \right\} \hat{\mathbf{x}}.$$

In each of these cases the correction term is of order H since $(\eta' \bar{\phi})/(\eta_0 D)$ is of order unity.

It can be seen from figure 5.2 that the particles tend to move towards the centre of the channel, as expected. Figure 5.3 shows the effect of this on the velocity field. The shear rate is reduced in the centre of the flow where the particle volume fraction and hence the viscosity is highest. Near the edges of the flow, where the viscosity decreases, the shear rate is increased.

Now we have an equilibrium solution for plane Couette flow, we shall discuss the stability of small perturbations from the equilibrium conditions.

5.4 Linear Stability Analysis

5.4.1 The perturbations

In order to carry out a stability analysis we shall begin by writing each of the variables as the equilibrium value (designated by a hat) plus a small perturbation. These expressions are then substituted into equations 5.3, 5.4, 5.5 and 5.6. The resulting equations are then linearised with respect to the perturbation variables.

An important factor in this analysis is the form of the lift force when we are away from equilibrium. The form of the lift force used for the equilibrium calculation relied on the zeroth order flow being plane Couette, for which the lift force is well known. When we allow perturbations in the fluid velocity to occur in our system, we shall no longer have a true plane Couette (or plane Poisseuille) flow, and the correct form of the lift force is unclear. An exact calculation of the force on a particle in a time varying fluid flow would be very difficult (due to the non-local effects mentioned in the last chapter).

In the absence of any detailed calculations, we shall assume that the equilibrium form of the lift force can still be applied. In addition we shall allow for the curvature of the fluid velocity profile by including a force of the form $H\chi(\partial \mathbf{V}_f/\partial z)(\partial^2 \mathbf{V}_f/\partial z^2)\hat{\mathbf{z}}$, with χ a constant of order unity. This force is of the form noted by Ho and Leal and accounts for the tendency of particles to move away from the centre of a plane Poiseuille flow[1]. These two contributions represent the two main contributions to the lift force and will suffice to model the general behaviour of the particles.

As in chapter 3, we shall consider only a 2-dimensional system with perturbations of the form

$$(\mathbf{V}_f, \mathbf{V}_p, p, \phi) = \{\mathbf{V}_f(z), \mathbf{V}_p(z), p(z), \phi(z)\}e^{i(kx-\omega t)}. \tag{5.19}$$

[1]This behaviour is observed experimentally and predicted by the methods of both Ho and Leal and Vasseur and Cox.

The resulting linearised equations are:

Particle momentum:

$$\hat{\phi}R_e\left(\frac{\partial \mathbf{V}_p}{\partial t}+\widehat{\mathbf{V}}_p\bullet\nabla\mathbf{V}_p+\mathbf{V}_p\bullet\nabla\widehat{\mathbf{V}}_p\right)=H\hat{\phi}\chi\frac{\partial\hat{u}_f}{\partial z}\frac{\partial^2 u_f}{\partial z^2}\hat{\mathbf{z}} \tag{5.20}$$
$$+H\left\{2\hat{\phi}\left[\frac{\partial u_f}{\partial z}\frac{\partial\hat{u}_f}{\partial z}\right]+\phi\left(\frac{\partial\hat{u}_f}{\partial z}\right)^2\right\}(1-2z)\hat{\mathbf{z}}-D\nabla\phi$$
$$+S\left\{\hat{\phi}(\mathbf{V}_f-\mathbf{V}_p)+\phi(\widehat{\mathbf{V}}_f-\widehat{\mathbf{V}}_p)\right\}+F\left\{\hat{\phi}\nabla^2\mathbf{V}_f+\phi\nabla^2\widehat{\mathbf{V}}_f\right\},$$

Fluid momentum:

$$(1-\hat{\phi})R_e\left(\frac{\partial \mathbf{V}_f}{\partial t}+\widehat{\mathbf{V}}_f\bullet\nabla\mathbf{V}_f+\mathbf{V}_f\bullet\nabla\widehat{\mathbf{V}}_f\right)= \tag{5.21}$$
$$\nabla^2\mathbf{V}_f+\frac{\eta'}{\eta_0}\nabla\bullet\left\{\phi\nabla\widehat{\mathbf{V}}_f+(\hat{\phi}-\bar{\phi})\nabla\mathbf{V}_f\right\}-\nabla p$$
$$-H\chi\frac{\partial\hat{u}_f}{\partial z}\frac{\partial^2 u_f}{\partial z^2}\hat{\mathbf{z}}-H\left\{2\hat{\phi}\left[\frac{\partial u_f}{\partial z}\frac{\partial\hat{u}_f}{\partial z}\right]+\phi\left(\frac{\partial\hat{u}_f}{\partial z}\right)^2\right\}(1-2z)\hat{\mathbf{z}}$$
$$+D\nabla\phi-S\left\{\hat{\phi}(\mathbf{V}_f-\mathbf{V}_p)+\phi(\widehat{\mathbf{V}}_f-\widehat{\mathbf{V}}_p)\right\}-F\left\{\hat{\phi}\nabla^2\mathbf{V}_f+\phi\nabla^2\widehat{\mathbf{V}}_f\right\},$$

Particle conservation:

$$\frac{\partial\phi}{\partial t}=-\nabla\bullet\left(\widehat{\mathbf{V}}_p\phi+\hat{\phi}\mathbf{V}_p\right), \tag{5.22}$$

Fluid conservation:

$$-\frac{\partial\phi}{\partial t}=-\nabla\bullet\left(-\widehat{\mathbf{V}}_f\phi+(1-\hat{\phi})\mathbf{V}_f\right). \tag{5.23}$$

An inspection of these equations shows that the coefficients are not constant due to the presence of the lift force and inertial terms. This complicates any exact analysis of these equations considerably so we shall consider a further perturbation approach.

We already have a small parameter, H, but this is not sufficient to remove all the difficulties. To overcome this we shall consider an additional small parameter, k; the wavenumber for perturbations down the channel. This is the same parameter as used in Chapter 3 for our analysis of multi-layer plane Couette flow.

We therefore carry out a perturbation analysis in the two parameters; H, the lift force, and k, the wavenumber of the disturbance along the channel. To achieve this we let the quantities $\mathbf{V}_f, \mathbf{V}_p, p, \phi$ and ω be of the form

$$X = X_0 + HX_H + kX_k. \tag{5.24}$$

For the rest of this chapter we shall use the following notation for the x and z components of the velocity fields,

$$\mathbf{V}_f = u_f\hat{\mathbf{x}} + v_f\hat{\mathbf{z}}, \qquad \mathbf{V}_p = u_p\hat{\mathbf{x}} + v_p\hat{\mathbf{z}}. \tag{5.25}$$

5.4.2 Stability for H=0, K=0

Before we study the equations governing the stability of the flow, we must find the correct boundary conditions to be applied for ϕ at this level of approximation. Considering the conservation of particle momentum (equation 5.3) with $H = k = 0$, we obtain from the z component (normal to the wall)[2]

$$\bar{\phi}R_e\frac{\partial v_p^0}{\partial t} = -D\frac{\partial \phi_0}{\partial z} + \bar{\phi}S(v_f^0 - v_p^0) + \bar{\phi}F\frac{\partial^2 v_f^0}{\partial z^2}. \tag{5.26}$$

Since v_f^0 and v_p^0 are zero on the walls as stated in the last chapter and differentiating with respect to t gives only a phase factor, the condition of zero flux of momentum through the walls is

$$D\frac{\partial \phi_0}{\partial z} = \bar{\phi}F\frac{\partial^2 v_f^0}{\partial z^2}. \tag{5.27}$$

This then is the boundary condition which must be satisfied in addition to those discussed in the last chapter.

We now take the divergence of the perturbed particle momentum equation (5.21) and substitute for v_f and v_p using the perturbed continuity equations (5.23 and 5.22) which have become

$$\frac{\partial v_f^0}{\partial z} = -\frac{i\omega_0}{(1-\bar{\phi})}\phi_0, \qquad \frac{\partial v_p^0}{\partial z} = \frac{i\omega_0}{\bar{\phi}}\phi_0. \tag{5.28}$$

[2]We shall use a raised index notation for the velocity perturbation terms for clarity.

This gives for the perturbations at O(1):

$$\left[D + \frac{i\omega_0 \bar{\phi} F}{(1-\bar{\phi})}\right] \frac{\partial^2 \phi_0}{\partial z^2} + \left[R_e \omega_0^2 + \frac{i\omega_0 S}{(1-\bar{\phi})}\right] \phi_0 = 0. \tag{5.29}$$

This is an equation in ϕ_0 alone and we see that ϕ_0 must be of the form

$$\phi_0 = A\epsilon^{lz} + B\epsilon^{-lz}, \qquad l = \frac{R_e \omega_0^2 (1-\bar{\phi}) + i\omega_0 S}{D(1-\bar{\phi}) + i\omega_0 \bar{\phi} F}. \tag{5.30}$$

Differentiating the perturbed fluid continuity equation (5.28) gives

$$\frac{\partial^2 v_f^0}{\partial z^2} = -\frac{i\omega_0}{(1-\bar{\phi})} \frac{\partial \phi_0}{\partial z}. \tag{5.31}$$

Substituting this and the expression for ϕ_0 into the boundary condition we obtain

$$\left[D + \frac{i\omega_0 \bar{\phi} F}{(1-\bar{\phi})}\right] l(A\epsilon^{l} - B\epsilon^{-l}) \Big|_{z=0,1} = 0. \tag{5.32}$$

Since the quantity in square brackets cannot be zero (all the perturbations become zero if this is the case), the boundary conditions are satisfied by putting $A = -B$ and restricting l to values of $in\pi$, where n is an integer. This gives the dispersion relation:

$$\omega_0 = \frac{i}{2R_e}\left(-Q \pm \sqrt{Q^2 - 4DR_e n^2 \pi^2}\right), \qquad Q = \frac{S - n^2\pi^2 \bar{\phi} F}{(1-\bar{\phi})}. \tag{5.33}$$

From this we can see that we have two modes corresponding to the two choices of sign for the square root. Both of these modes are stable at this level of approximation as long as Q is positive. Using the known expressions for S and F, and defining the wavelength in the z direction, $\lambda = 2/n$, the condition for $Q > 0$ becomes

$$\lambda^2 > \frac{\bar{\phi}(2\pi)^2 a^2}{6L^2} \approx \frac{a^2}{L^2}. \tag{5.34}$$

For this condition to be violated, we would require physical wavelengths smaller than the particle radius. Obviously this is outside the regime of applicability of the model and we can say that in the regime where we expect the model to be valid the system is stable.

It is interesting to notice that the stability at lowest order does not depend on the form of the equations for fluid momentum conservation. At this stage particle momentum conservation is sufficient. This is not generally true and is a feature of the form of the perturbation analysis. Since at this stage the perturbed quantities are not functions of x we have effectively a one-dimensional system. This is similar to the case discussed by Batchelor [40] who noted that for a 1-dimensional fluidised bed, the fluid momentum equations are superfluous.

The eigenfunctions at this order can now be obtained in terms of ω_0 and the magnitude of the volume fraction perturbations, A. Expressions for v_f and v_p are obtained by integrating the continuity equations and these results used in the momentum equations to obtain u_f and u_p. The eigenfunctions are

$$\begin{aligned}
\phi_0 &= A\cos(n\pi z), \\
v_f^0 &= -\left(\frac{i\omega_0 A}{(1-\bar{\phi})n\pi}\right)\sin(n\pi z), \\
v_p^0 &= \left(\frac{i\omega_0 A}{\bar{\phi}n\pi}\right)\sin(n\pi z), \\
u_f^0 &= \delta\frac{A}{n\pi}\sin(n\pi z), \\
u_p^0 &= \epsilon\sin(n\pi z),
\end{aligned} \tag{5.35}$$

where δ and ϵ are real coefficients, given by

$$\begin{aligned}
\delta &= \frac{1}{\beta-(n\pi)^2\alpha}\left(\frac{\eta'}{\eta_0}(n\pi)^2 - i\omega_0 R_e\left(1-\frac{S}{S-i\omega_0 R_e}\right)\right), \\
\epsilon &= \frac{1}{(S-i\omega_0 R_e)}\left([S-(n\pi)^2 F]\delta - \frac{i\omega_0 R_e}{\bar{\phi}n\pi}\right),
\end{aligned} \tag{5.36}$$

with

$$\alpha = 1 + \frac{i\omega_0 R_e\bar{\phi}F}{S-i\omega_0 R_e}, \qquad \beta = \left(1-\bar{\phi}+\frac{\bar{\phi}S}{S-i\omega_0 R_e}\right). \tag{5.37}$$

The general form of the eigenfunction is given in figures 1.4 and 1.5 for the two possible eigenvalues. Figure 5.4 shows the case with the positive root having been chosen. This corresponds to the mode close to neutral stability and it can be seen that the particle velocities are aligned almost along the channel. There

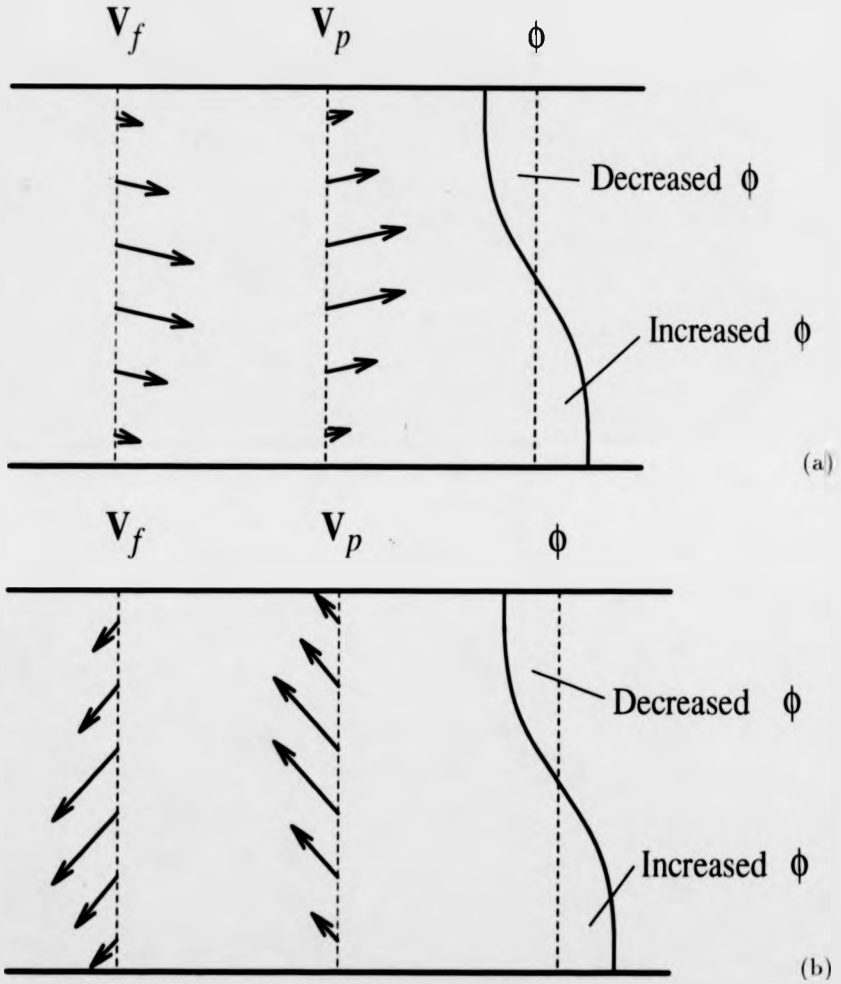

Figure 5.4: *A sketch of the eigenfunctions for $H = 0$, $k = 0$. (a) Positive root chosen. (b) Negative root chosen.*

is a small component tending to move the particles from the region of increased volume fraction to the region of decreased volume fraction, hence the mode is not exactly neutrally stable. It can be seen that the z component of the fluid velocity is oppositely directed to the z component of the particle velocity, in accordance with the conservation of fluid and particles. At this level of approximation there is no such restriction on the x components.

Figure 5.5 shows the eigenfunctions when the negative root is chosen. Again the particle and fluid velocities have opposing z components to satisfy the conservation of fluid and particles. The particle velocity is more strongly directed from the region of high volume fraction to the region of low volume fraction than for the previous case. In addition that actual velocities are considerably larger (although this cannot be shown in the figures, since the scales differ widely). These two effects demonstrate that this mode is much more strongly stabilising than the previous one.

These eigenfunctions will be required to calculate the effects of non-zero values of k and H. We begin by considering the case for $k \neq 0$.

5.4.3 Stability For Small Wavenumber Perturbations

We now consider the stability of the system including terms of order k in our analysis. Before we discuss the equations in detail we require the boundary condition to be applied for ϕ. Considering the linearised stability equations at order k, with $H = 0$ the z component of the particle momentum equation is

$$\bar{\phi} R_e \left(\frac{\partial v_p^k}{\partial t} + i z v_p^0 \right) = -D \frac{\partial \phi_k}{\partial z} + \bar{\phi} S (v_f^k - v_p^k) + \bar{\phi} F \frac{\partial^2 v_f^k}{\partial z^2}. \tag{5.38}$$

Using the boundary conditions on v_f^k and v_p^k and the known form of v_p^0 we obtain

$$D \frac{\partial \phi_k}{\partial z} = \bar{\phi} F \frac{\partial^2 v_f^k}{\partial z^2}. \tag{5.39}$$

This is of the same form as for $k = 0$ except with new indices representing terms of order k.

The analysis of the equations governing the stability begins in the same way as for zeroth order. Taking the divergence of the particle equations as before and using the continuity equations at order k:

$$\frac{\partial v_f^k}{\partial z} + iu_f^0 = -\frac{i}{(1-\bar{\phi})}\left[\omega_0\phi_k + \omega_k\phi_0 - z\phi_0\right], \tag{5.40}$$

$$\frac{\partial v_p^k}{\partial z} + iu_p^0 = \frac{i}{\bar{\phi}}\left[\omega_0\phi_k + \omega_k\phi_0 - z\phi_0\right], \tag{5.41}$$

we obtain

$$\left[D + \frac{i\omega_0\bar{\phi}F}{(1-\bar{\phi})}\right]\frac{\partial^2\phi_k}{\partial z^2} + \left[R_e\omega_0^2 + \frac{i\omega_0 S}{(1-\bar{\phi})}\right]\phi_k = \tag{5.42}$$

$$+A(\omega_k - z)\cos(n\pi z)\left(-2R_e\omega_0 - \frac{iS}{(1-\bar{\phi})} + \frac{i\bar{\phi}Fn^2\pi^2}{(1-\bar{\phi})}\right)$$

$$+2A\sin(n\pi z)\left(\frac{R_e\omega_0}{n\pi} - \frac{i\bar{\phi}Fn\pi}{(1-\bar{\phi})}\right). \tag{5.43}$$

If we note that the left hand side of the equation is satisfied by ϕ_0, then we can multiply this equation by ϕ_0 and integrate across the channel (using integration by parts) to obtain

$$\left(D + \frac{i\omega_0\bar{\phi}F}{(1-\bar{\phi})}\right)\left[\phi_0\frac{\partial\phi_k}{\partial z}\right]_0^1 = \tag{5.44}$$

$$i[\omega_k\langle\phi_0^2\rangle - \langle z\phi_0^2\rangle]\left(-2R_e\omega_0 - \frac{iS}{(1-\bar{\phi})} + \frac{i\bar{\phi}Fn^2\pi^2}{(1-\bar{\phi})}\right).$$

Here we have denoted integration across the channel by angle brackets around the integrand.

We must now consider the boundary value of $\partial\phi_k/\partial z$. If we differentiate the fluid equation of continuity (equation 5.40), and evaluate the expression at the boundary, we can write the boundary condition as

$$\left(D + \frac{i\omega_0\bar{\phi}F}{(1-\bar{\phi})}\right)\frac{\partial\phi_k}{\partial z}\bigg|_{z=0,1} = i\bar{\phi}F\left(\frac{1}{(1-\bar{\phi})} - \delta n\pi\right)A\cos(n\pi z)\bigg|_{z=0,1}. \tag{5.45}$$

This tells us that

$$\left[\phi_0\frac{\partial\phi_k}{\partial z}\right]_0^1 = 0. \tag{5.46}$$

Using this we can write ω_k as

$$\omega_k = \frac{\langle z\phi_0^2 \rangle}{\langle \phi_0^2 \rangle} = \frac{1}{2}, \tag{5.47}$$

where we have evaluated the integrals involving ϕ_0. Hence the effects of non-zero values of k are merely to allow a neutrally stable wave to pass through the system. This can be interpreted as the zeroth order perturbations being advected along the channel at the mean velocity of the fluid (mean velocity $= \frac{1}{2}$).

This approach of obtaining the dispersion relation is much more economical than solving the general equation for ϕ_0 and applying the boundary conditions. The actual eigenfunctions are simple in terms of their functional form, being products of polynomials in z with $sin(n\pi z)$ and $cos(n\pi z)$. However the coefficients are complicated expressions involving the zeroth order coefficients, making the application of the boundary conditions a lengthy procedure. This method means that we do not need to know the form of the eigenfunctions for this analysis and we shall use the same approach to calculate the stability when a small lift force is considered.

5.4.4 Stability For A Small Lift Force

As for the stability analysis at order k in the preceding section, we must begin by obtaining the boundary condition for ϕ_H. Taking the equations governing stability with $k = 0$, the boundary condition for the expansion at order H is

$$R_e \left(\bar{\phi} \frac{\partial v_p^H}{\partial t} + \tilde{\phi} \frac{\partial v_p^0}{\partial t} \right) = \left(2\tilde{\phi} \frac{\partial u_f^0}{\partial z} + \phi_0 \right) (1 - 2z) + \chi \bar{\phi} \frac{\partial^2 u_f^0}{\partial z^2} \tag{5.48}$$
$$-D \frac{\partial \phi_H}{\partial z} + \bar{\phi} S (v_f^H - v_p^H) + \bar{\phi} F \frac{\partial^2 v_f^H}{\partial z^2} + \tilde{\phi} S (v_f^0 - v_p^0) + \tilde{\phi} F \frac{\partial^2 v_f^0}{\partial z^2}.$$

Note that the equilibrium volume fraction suffers a perturbation, $\tilde{\phi}$, at order H and the effect is included here. We have assumed that the z component of the perturbations in the fluid velocity does not give a contribution to the lift force. Using the known expressions for the zeroth order functions, we can write the

boundary conditions as

$$D\frac{\partial \phi_H}{\partial z} = (2\bar{\phi}\delta l + 1)(1-2z)\phi_0 + \bar{\phi}F\frac{\partial^2 v_f^H}{\partial z^2}, \tag{5.49}$$

applied at each wall.

We now follow the same approach as for the analysis at order k. The continuity equations at order H become

$$\frac{\partial v_f^H}{\partial z} = -\frac{i}{(1-\bar{\phi})}\left[\omega_0\phi_H + \omega_H\phi_0 + i\tilde{\phi}\frac{\partial v_f^0}{\partial z}\right], \tag{5.50}$$

and

$$\frac{\partial v_p^H}{\partial z} = \frac{i}{\bar{\phi}}\left[\omega_0\phi_H + \omega_H\phi_0 + i\tilde{\phi}\frac{\partial v_p^0}{\partial z}\right]. \tag{5.51}$$

Taking the divergence of the particle equations, as before, and using the continuity equations leads to the following equation for ϕ_H in terms of known functions.

$$\begin{aligned}
&\left[D + \frac{i\omega_0\bar{\phi}F}{(1-\bar{\phi})}\right]\frac{\partial^2\phi_H}{\partial z^2} + \left[R_e\omega_0^2 + \frac{i\omega_0 S}{(1-\bar{\phi})}\right]\phi_H = \chi\bar{\phi}\frac{\partial^3 u_f^0}{\partial z^3} \qquad (5.52)\\
&+\left(2\bar{\phi}\frac{\partial^2 u_f^0}{\partial z^2} + \frac{\partial\phi_0}{\partial z}\right)(1-2z) - 2\left(2\bar{\phi}\frac{\partial u_f^0}{\partial z} + \phi_0\right) - R_e\left(\frac{\partial\tilde{\phi}}{\partial z}\frac{\partial v_p^0}{\partial z} + 2\omega_0\omega_H\phi_0\right)\\
&\quad +S\left(\frac{\partial\tilde{\phi}}{\partial z}(v_f^0 - v_p^0) - \frac{i\omega_H}{(1-\bar{\phi})}\phi_0 + \frac{\tilde{\phi}}{(1-\bar{\phi})}\frac{\partial v_f^0}{\partial z}\right)\\
&\quad +F\left(\frac{\partial\tilde{\phi}}{\partial z}\frac{\partial^2 v_f^0}{\partial^2 z} + \tilde{\phi}\frac{\partial^3 v_f^0}{\partial z^3} - \frac{i\bar{\phi}}{(1-\bar{\phi})}\left\{\omega_H\frac{\partial^2\phi_0}{\partial z^2} + i\frac{\partial^2}{\partial z^2}\left[\tilde{\phi}\frac{\partial v_f^0}{\partial z}\right]\right\}\right).
\end{aligned}$$

As for the previous case the left hand side of this equation is satisfied by ϕ_0 and we can multiply by ϕ_0 and integrate across the channel. If we denote the right hand side as a known function $f(z,\omega_H)$, we obtain after integration by parts

$$\left(D + \frac{i\omega_0\bar{\phi}F}{(1-\bar{\phi})}\right)\left[\phi_0\frac{\partial\phi_H}{\partial z}\right]_0^1 = \langle\phi_0 f(z,\omega_H)\rangle. \tag{5.53}$$

Once again, we can obtain the value of $\partial\phi_H/\partial z$ by differentiating the appropriate fluid continuity equation, substituting this result into the boundary condition expression and evaluating at the boundary to give

$$\begin{aligned}
&\left(D + \frac{i\omega_0\bar{\phi}F}{(1-\bar{\phi})}\right)\frac{\partial\phi_H}{\partial z}\bigg|_{z=0,1} = \qquad (5.54)\\
&\qquad\left((2\bar{\phi}\delta l + 1)(1-2z) - \frac{i\omega_0 F\bar{\phi}^2}{D(1-\bar{\phi})^2}(1-2z)\right)\phi_0\bigg|_{z=0,1}.
\end{aligned}$$

This gives us the condition

$$\langle \phi_0 f(z,\omega_H)\rangle = -2\left((2\bar{\phi}\delta l+1)-\frac{i\omega_0 F\bar{\phi}^2}{D(1-\bar{\phi})^2}\right). \tag{5.55}$$

Evaluating the integrals on the left hand side of this expression and rearranging gives the dispersion relation:

$$\omega_H = \mp i\left[Q^2-4l^2DR_e\right]^{-\frac{1}{2}}\times \tag{5.56}$$
$$\left[\bar{\phi}\delta l(1-\tfrac{1}{2}\chi l^2)+\tfrac{1}{2}+\frac{i\omega_0}{4(1-\bar{\phi})D}\left(\frac{S}{l^2}\left[-2+\frac{\bar{\phi}}{1-\bar{\phi}}\right]+F\bar{\phi}\left[1-\frac{\bar{\phi}}{1-\bar{\phi}}\right]\right)\right].$$

This expression involves several complicated terms found from the zeroth order stability problem. It is obvious that ω_H must be purely imaginary, although the sign of the expression is not immediately clear. Despite the fact that we can choose either sign for the denominator, the value of ω_0 is different in each case allowing the possibility that the numerator will also change sign.

The analysis of the expression is simplified if we restrict ourselves to wavelengths of a few particle radii or longer. This allows the expression for ω_0 (equation 5.33) to be expanded since $S \gg (n\pi)^2 F\bar{\phi}$. The two roots then become

$$\omega_0 = \frac{-iD(1-\bar{\phi})(n\pi)^2}{S}, \qquad \omega_0 = \frac{-iS}{R_e(1-\bar{\phi})}. \tag{5.57}$$

As expected from the form of the expression for ω_o, one is small and proportional to $1/S$, the other is of order S. The first corresponds to taking the positive value of the square root and the second to the negative root. In this limit, the denominator of the dispersion relation becomes $\pm iS$.

If we now consider the expression for ω_H for the positive root in this limit, we find the dominant terms give

$$\omega_H = -\frac{i}{S}\left(\frac{\bar{\phi}\eta'(n\pi)^2}{\eta_0(1-(n\pi)^2)}[1-\chi(n\pi)^2]+\frac{\bar{\phi}}{4(1-\bar{\phi})}\right). \tag{5.58}$$

The value for the ratio η'/η_0 is of order one and, for example, using the Einstein relation we get a ratio equal to 2.5. The first term shows the competition bewteen

the effects of the equilibrium lift force and the interaction with the curvature of the perturbation. Since the exact value of χ is unknown it is possible that this mode may be destabilising when n is small. Since χ is expected to be of order unity, such a destabilising mode is unlikely and when n becomes larger the mode is definitely stabilising. This is to be expected since as n increases, the curvature of the zeroth order solutions must increase, and the interactions with the curvature, which oppose the equilibrium lift force, must also increase. The second term in the expression is smaller than the lift force terms and is therefore not important in governing the stability.

If we now take the negative sign for the square root then then expression for ω_H becomes

$$\omega_H = \frac{-i}{(1-\bar{\phi})(n\pi)^2}\left(\frac{\chi(n\pi)^2-1}{(1-F)}+\frac{S}{2DR_e}\right). \tag{5.59}$$

This corresponds to a stabilising mode. The second term dominates the expression except for large values of n, where they may be comparable, but since both terms are of the same sign, they are both stabilising. Again the first term shows the competition between the equilibrium lift force and the force due to curvature. This time there is no chance of destabilisation occuring due to the second term, which dominates in this region.

Although this analysis shows that there is the pssibility that effect of the lift force can be destabilizing, the effect is never large enough to force the system into an unstable regime. Since the total dispersion relation is

$$\omega = \omega_0 + H\omega_H + k\omega_k, \tag{5.60}$$

where H is small, it can be seen that the stabilizing effect of the zeroth order mode will always dominate any destabilizing effect of the lift force.

The fact that the damping of the system is does not depend on the wavenumber along the channel implies that the damping is dominated by local effects at this level of approximation. Thus we would expect that local, single particle effects are dominating the behaviour of the system.

5.5 Discussion

This analysis has shown that under an imposed shear, our model predicts a stable equilibrium flow with a small curvature of the normally flat velocity profile. The stability of this equilibrium state is apparently in disagreement with the result of Nozières and Quemada but in fact this is not the case.

The critical shear rate predicted by Nozières and Quemada is very high due to the factor η/η^*. Since $\eta^* = \partial\eta/\partial n$ and $n = \phi/v$ for a volume fraction, ϕ and the volume of a single sphere, v, then in the dilute limit $\eta^* = 2.5\eta v$. This makes the ratio η/η^* of order 10^{18} and the critical shear rate corresponding high. Such a shear rate is obviously well out the regime in which our perturbation analysis can be applied. To make any accurate comparison of our model with Nozières result would require a fully non-linear analysis, probably by numerical means.

Chapter 6

Conclusions

In this thesis we have theoretically investigated the rheological properties of various types of materials undergoing shear flows. In chapter 2 we obtained the effective shear modulus of an elastic medium filled with a distribution spherical inclusions. We have shown that a single elastic inclusion can be treated in a similar way to a polarisable molecule in an electric field. Following the approach used by Clausius and Mossotti for dielectric materials, we have obtained the effective shear modulus of a material in terms of the polarisability of a single inclusion. The resulting expression was in agreement with bounds found by Hashin using a variational approach. This demonstrated some useful links which can be made between elasticity theory and electromagnetic theory, two subjects which would normally be thought of as unrelated areas of interest.

This last result was used to model a gel as an elastic medium containing spherical voids representing regions of failed bonds. Using a phenomenological model for the yield stresses of bonds within a gel, in conjunction with this, we obtained the stress-strain behaviour of a gel subjected to shear. This model showed that a gel will support a maximum stress given by the yield stress of the strongest bonds within its structure. These mean field arguments were augmented by considering the energy density near a single void. This showed that bond

failures are likely to occur along planes parallel to the plates providing a shearing force. Thus we have obtained a model of the softening and eventual failure of a gel.

In addition to the analogy made with electromagnetic theory, we showed in chapter 2 that very useful comparisons can be made between the equations of elasticity and those of Stokes' or Creeping flows. We used this to obtain the displacement field of a spherical cavity near a fixed wall. In the incompressible limit it was shown that the problem of a point force in an elastic medium is virtually identical to the problem of a point force in a fluid undergoing creeping flow.

In chapter 3 we studied a model of layered colloidal structures observed by Buscall in a sheared suspension of colloidal particles. The layers were assumed to be fluidised and of an alternating viscosity. A numerical linear stability analysis of the flow, using long wavelength perturbations, showed that the stability of the fluid flow depends strongly on the number of layers that are present. A resonance instability was identified, which is analogous to that obtained by Li for three layers. This instability occurs for three or more layers. The regimes in which this instability is important were found to depend strongly on the number of layers, with the topological structure of the neutral stability curves changing abruptly when going from five to six layers.

Where a resonance instability does not occur, a different instability was identified for four or more layers. This is analogous to the instability found by Yih for two layers and is due to the discontinuity in vorticity at the interfaces between the layers. In the limit of many layers it was found that the flow is unstable and hence that the experimentally observed layers should be unstable. The growth rate of the instability is such that a time scale of greater than 100s would be required for any effect to evolve to an observable scale. Since the timescale of the experiment is not known to the author it is not possible to to draw a firm conclusion as to whether this is in agreement with observations.

In chapter 4 we have constructed a microscopic model of a dilute, flowing suspension of neutrally buoyant colloidal particles. To achieve this we followed the approach used by Batchelor for a fluidised bed. This approach uses the conservation of particles and particle momentum in a spherical volume to obtain governing equations for the particle motions. The effects of Vasseur and Cox's lift force were included as well as Stokes' drag and Faxén forces. Since the particles were assumed to be approximately 1μm in size the effects of Brownian diffusion were also included. Using this approach we avoid the need to postulate a constitutive relation involving the particle pressure, since all the contributions to the particle momentum are obtained explicitly.

In chapter 5 we investigated our model for the case of a sheared suspension. We showed that an equilibrium flow is obtained, with small changes from the simple shear solution. These are due to the non-uniformity of the particle distribution, brought about by the lift forces. This equilibrium flow is shown to be linearly stable to small perturbations in the particle concentrations and the equilibrium flow.

Appendix A

Oscillatory Rheological Measurements

Oscillatory rheological measurements are very useful for observing the visco-elastic properties of materials. Measurements of this kind involve subjecting a material to a periodic shear strain, γ, of a given frequency, ω, such that

$$\gamma = \gamma_0 \sin \omega t. \tag{A.1}$$

Here the amplitude of the oscillation is given by γ_0. The response to this shear strain is also periodic with the same frequency, provided that the magnitude of the oscillation is small enough for the material to respond linearly. The response stress, $S(t)$, can therefore be written in the form,

$$S(t) = \gamma_0(G' \sin \omega t + G'' cos\ \omega t). \tag{A.2}$$

G' and G'' are dimensionally of the form of elastic moduli. They represent the in-phase and out of phase parts of the response respectively. The in-phase component, G', is known as the shear storage modulus, and represents the elastic behaviour of the material. G'' is called the shear loss modulus, and represents the losses due to viscous dissipation with the material. This is illustrated in figure A.1.

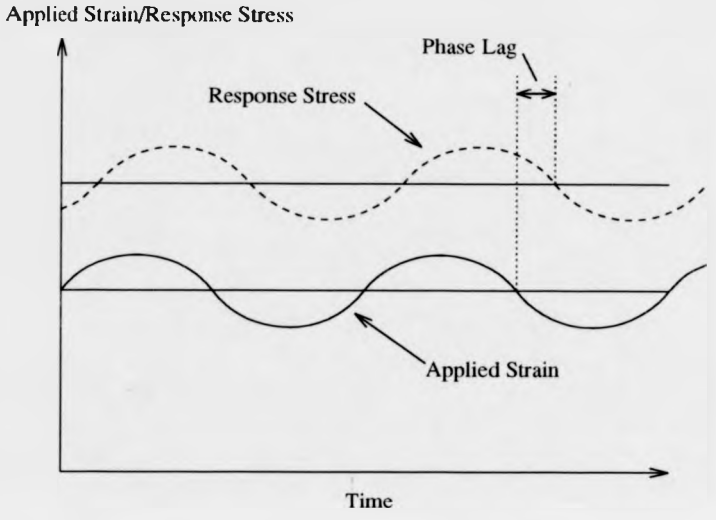

Figure A.1: *The applied strain and response stress for oscillatory rheological measurements*

The general visco-elastic behaviour of a material is usefully described by the definition of the phase angle, δ, where

$$\tan \delta = \frac{G''}{G'}. \tag{A.3}$$

A purely elastic body will have a response precisely in phase with the applied strain, and hence have $\delta = 0$. A purely viscous body will respond out of phase with the applied force, giving a δ of 90 degrees.

Appendix B

The Green's Function For An Elastic Medium

The equation of equilibrium for a distribution of body forces, $\mathbf{F}$, throughout an elastic body is,

$$\mu\nabla^2\mathbf{u} + \frac{\mu}{(1-2\nu)}\nabla(\nabla\cdot\mathbf{u}) = -\mathbf{F}. \tag{B.1}$$

Here we denote Poisson's ratio by ν and the shear modulus by μ. If we Fourier transform this equation, denoting transformed quantities with tildes, we obtain

$$\mu\mathbf{k}^2\tilde{\mathbf{u}} + \frac{\mu}{(1-2\nu)}\mathbf{k}(\mathbf{k}\cdot\tilde{\mathbf{u}}) = \tilde{\mathbf{F}}. \tag{B.2}$$

Using index notation and inverting this equation gives

$$\tilde{u}_i = \left(\delta_{ij} - \frac{k_i k_j}{2k^2(1-\nu)}\right)\frac{\tilde{F}_j}{\mu k^2}, \tag{B.3}$$

where δ_{ij} here is the Kronecker delta, which is zero unless its indices are equal. Equation B.3 can now be reverse Fourier transformed to give a convolution integral

$$u_i = \frac{1}{16\pi\mu(1-\nu)}\int F_j(\mathbf{r}')\left(\frac{(3-4\nu)\delta_{ij}}{|\mathbf{r}-\mathbf{r}'|} + \frac{(\mathbf{r}-\mathbf{r}')_i(\mathbf{r}-\mathbf{r}')_j}{|\mathbf{r}-\mathbf{r}'|^3)}\right)d\mathbf{r}' \tag{B.4}$$

where $\partial_i = \partial/\partial x_i$.

This expression is equivalent to the Green's function given by Landau and Lifshitz [43] , but has been derived by a more direct method here.

Appendix C

Macroscopic Elastic Polarisation

First we consider from the Green's function for the displacement vector, $u_i(\mathbf{r})$, due to a distribution of forces, $F_k(\mathbf{r}')$ (See Appendix A).

$$u_i = \frac{1}{4\pi\mu}\int F_k\left[\frac{\delta_{ik}}{|\mathbf{r}-\mathbf{r}'|} - \frac{1}{4(1-\nu)}\partial_i\partial_k|\mathbf{r}-\mathbf{r}'|\right]dr'^3. \tag{C.1}$$

Here μ is the shear modulus and ν is Poisson's ratio.

A Taylor expansion of the terms in the square brackets is equivalent to replacing the force distribution by the appropriate multipole distributions. Here we consider only the first two terms in such an expansion,

$$F_k = F_k^0 - \partial_j F_{kj}^1, \tag{C.2}$$

where F_k^0 is the distribution of point forces, and F_{kj}^1 is the distribution of dipolar contributions. Once this expansion is made, we calculate the strain, u_{ik}, in the usual way, using

$$u_{ik} = \tfrac{1}{2}\left(\partial_i u_k + \partial_k u_i\right). \tag{C.3}$$

The stress field, σ_{ik}, is then obtained using Hooke's law,

$$\sigma_{ik} = 2\mu^0\left(u_{ik} + \frac{\nu}{(1-2\nu)}u_{ll}\delta_{ik}\right). \tag{C.4}$$

If we now take the divergence of the stress, after a fairly lengthy calculation, we obtain,

$$\partial_i\sigma_{ik} = \partial_i F_{ik}^1 - F_k^0. \tag{C.5}$$

This has used the the fact that derivatives of the radius vector have delta function components, with the following weights.

$$\partial_i \partial_j \left(\frac{1}{|\mathbf{r} - \mathbf{r}'|} \right) \sim -\frac{4\pi}{3} \delta_{ij} \delta(\mathbf{r} - \mathbf{r}') \tag{C.6}$$

$$\partial_i \partial_j \partial_k \partial_l |\mathbf{r} - \mathbf{r}'| \sim -\frac{8\pi}{15} (\delta_{ij}\delta_{kl} + \delta_{ik}\delta_{jl} + \delta_{il}\delta_{jk}) \delta(\mathbf{r} - \mathbf{r}') \tag{C.7}$$

We now define the *elastic displacement field*, G_{ik}, by analogy with the electric displacement vector, $\mathbf{D}$, such that,

$$\partial_i G_{ik} = -F_k^0 \tag{C.8}$$

Hence the divergence of G_{ik} gives us the point force distribution. This gives us,

$$G_{ik} = \sigma_{ik} - F_{ik} \tag{C.9}$$

which is the elasticity analogue of $\mathbf{D} = \mathbf{E} + 4\pi\mathbf{P}$ as used in electromagnetic theory.

Appendix D

The numerical stability analysis for multi-layer flows

D.1 The zeroth order calculation

The Orr-Sommerfeld equation at zeroth order is

$$\frac{\partial^4 \phi_{0,j}}{\partial y^4} = 0, \tag{D.1}$$

where $\phi_{0,j}$ is the perturbed stream function in the jth layer of fluid. This has a polynomial solution in each layer:

$$\phi_{0,j} = A_{0,j} + B_{0,j}\, y + C_{0,j}\, y^2 + D_{0,j}\, y^3. \tag{D.2}$$

Applying the boundary conditions described in Chapter 4 gives the following set of recurrence relations;

$$\begin{aligned} A_{0,j+1} &= A_{0,j} + y_j(B_{0,j} - B_{0,j+1}) + y_j^2(C_{0,j} - C_{0,j+1}) \\ &\quad + y_j^3(D_{0,j} - D_{0,j+1}), \end{aligned} \tag{D.3}$$

$$\begin{aligned} B_{0,j+1} &= B_{0,j} + 2y_j(C_{0,j} - C_{0,j+1}) + 3y_j^2(D_{0,j} - D_{0,j+1}) \\ &\quad + F_j(A_{0,j} + y_j B_{0,j} + y_j^2 C_{0,j} + y_j^3 D_{0,j}), \end{aligned} \tag{D.4}$$

$$C_{0,j} = C_{0,1}\frac{\mu_1}{\mu_j}, \tag{D.5}$$

and

$$D_{0,j} = D_{0,1}\frac{\mu_1}{\mu_j}, \tag{D.6}$$

where $F_j = (\bar{b}_j - \bar{b}_{j+1})/\epsilon_{0,j}$, and y_j is the position of the jth interface.

If we take $A_{0,1}$ to be unity then the boundary conditions at $y = 1$ are

$$1 + B_{0,1} + C_{0,1} + D_{0,1} = 0, \qquad B_{0,1} + 2C_{0,1} + 3D_{0,1} = 0. \tag{D.7}$$

The boundary conditions at $y = 0$ are

$$A_{0,N} = 0, \qquad B_{0,N} = 0. \tag{D.8}$$

We can calculate $C_{0,1}$ and $D_{0,1}$ in terms of B_1 to get

$$C_{0,1} = -(2B_{0,1} + 3), \qquad D_{0,1} = B_{0,1} + 2. \tag{D.9}$$

All the $C_{0,j}$ and $D_{0,j}$ are now known using the recurrence relations D.4 and D.5.

We now use the substitution

$$A_{0,j} = \hat{A}_{0,j} + B_{0,1}\tilde{A}_{0,j}, \qquad B_{0,j} = \hat{B}_{0,j} + B_{0,1}\tilde{B}_{0,j}. \tag{D.10}$$

This leads to a set of four recurrence relations which after substituting for $C_{0,1}$ and $D_{0,1}$ become

$$\begin{aligned}\hat{A}_{0,j+1} &= (1 - F_j y_j)\hat{A}_{0,j} - F_j y_j^2 \hat{B}_{0,j} + \nu y_j^2(-1)^j(3 - 4y_j) \\ &\quad + F_j y_j^3 Q_j(3 - 2y_j),\end{aligned} \tag{D.11}$$

$$\begin{aligned}\hat{B}_{0,j+1} &= (1 + F_j y_j)\hat{B}_{0,j} - F_j \hat{A}_{0,j} + \nu y_j(-1)^j(6y_j - 6) \\ &\quad + F_j y_j^2 Q_j(2y_j - 3),\end{aligned} \tag{D.12}$$

$$\begin{aligned}\tilde{A}_{0,j+1} &= (1 - F_j y_j)\tilde{A}_{0,j} - F_j y_j^2 \tilde{B}_{0,j} + \nu y_j^2(-1)^j(2 - 2y_j) \\ &\quad + F_j y_j^3 Q_j(2 - y_j),\end{aligned} \tag{D.13}$$

$$\hat{B}_{0,j+1} = (1+F_j y_j)\hat{B}_{0,j} - F_j \hat{A}_{0,j} + \nu y_j (-1)^j (3y_j - 4) + F_j y_j^2 Q_j (y_j - 2), \tag{D.14}$$

where $\nu = (1/m) - 1$ for a viscosity ratio, m, and $Q_j = [1 + \frac{1}{2}\nu(1 + (-1)^j)]$.

The transformed boundary conditions become

$$\hat{A}_{0,1} = 1, \quad \hat{A}_{0,1} = 0, \quad \hat{B}_{0,1} = 0, \quad \hat{B}_{0,1} = 1 \tag{D.15}$$

and

$$\hat{A}_{0,N}\hat{B}_{0,N} - \hat{B}_{0,N}\hat{A}_{0,N} = G(c_0) = 0. \tag{D.16}$$

We now have a set of recurrence relations which have we can iterate with a single unknown, c_0. Thus solving this eigenvalue problem is now equivalent to finding the zeroes of $G(c_0)$.

Inspection of the recurrence relations shows that $G(c_0)$ is a polynomial of order $N-1$ in $1/c_0$. It can also be seen that all the coefficients in the recurrence relations are real. Thus if less than $N-1$ roots exist then the other roots must exist in complex conjugate pairs. In this case one of the pairs of roots will correspond to an unstable mode. Using this approach of looking for real roots only allows us to use only real variables, which is a considerable simplification compared to using complex variables. Finally, the values of the zeroes are obtained using a bisection algorithm.

When $N-1$ real roots have been obtained then we know that the system is neutrally stable at this order. In this case we must consider the first order correction to c.

D.2 The first order calculation

The first order stream function satisfies

$$\frac{\partial^4 \phi_{1,j}}{\partial y^4} = i\alpha R_j \left\{ (\bar{u}_j - c)\frac{\partial^2 \phi_{0,j}}{\partial y^2} - \frac{\partial^2 \bar{u}_j}{\partial y^2}\phi_{0,j} \right\}. \tag{D.17}$$

This gives the following form for $\phi_{1,j}$,

$$\phi_{1,j} = A_{1,j} + B_{1,j}\, y + C_{1,j}\, y^2 + D_{1,j}\, y^3 + i\alpha R_j h_j(y). \tag{D.18}$$

The functions $h_j(y)$ are defined by

$$h_j(y) = C_{0,j}(\bar{a}_j - c_0)\frac{y^4}{12} + \{C_{0,j}\bar{b}_j + 3D_{0,j}(\bar{a}_j - c_0)\}\frac{y^5}{60} + D_{0,j}\bar{b}_j\frac{y^6}{60}. \tag{D.19}$$

As for the zeroth order calculation, application of the interfacial boundary conditions results in a set of recurrence relations which cannot be separated to obtain a general solution. These are,

$$\begin{aligned} A_{1,j+1} \;=\; & A_{1,j} + y_j(B_{1,j} - B_{1,j+1}) + y_j^2(C_{1,j} - C_{1,j+1}) \\ & + y_j^3(D_{1,j} - D_{1,j+1}) + i\alpha R_j\left(h_j - \frac{\mu_j}{\mu_{j+1}}h_{j+1}\right), \end{aligned} \tag{D.20}$$

$$\begin{aligned} B_{1,j+1} \;=\; & (1 + F_j y_j)B_{1,j} + F_j A_{1,j} + 2y_j(C_{1,j} - C_{1,j+1}) \\ & + 3y_j^2(D_{1,j} - D_{1,j+1}) + F_j y_j^2(C_{1,j} + y_n D_{1,j}) \\ & + i\alpha R_j\left\{\frac{\partial h_j}{\partial y} - \frac{\mu_j}{\mu_{j+1}}\frac{\partial h_{j+1}}{\partial y} + F_j h_j\right\} - \frac{F_j\phi_{0,j}}{e_{0,j}}c_1, \end{aligned} \tag{D.21}$$

$$D_{1,j+1} = \frac{\mu_j}{\mu_{j+1}}D_{1,j} + \frac{i\alpha R_{n+1}}{6}\left(\frac{\partial^3 h_j}{\partial y^3} - \frac{\partial^3 h_{j+1}}{\partial y^3}\right), \tag{D.22}$$

and

$$C_{1,j+1} = \frac{\mu_j}{\mu_{j+1}}C_{1,j} + \frac{i\alpha R_{n+1}}{2}\left\{\frac{\partial^2 h_j}{\partial y^2} - \frac{\partial^2 h_{j+1}}{\partial y^2} + y_n\left(\frac{\partial^3 h_{j+1}}{\partial y^3} - \frac{\partial^3 h_j}{\partial y^3}\right)\right\}. \tag{D.23}$$

The boundary conditions at the walls are,

$$B_{1,1} + C_{1,1} + D_{1,1} + i\alpha R_1 h_1(1) = 0, \tag{D.24}$$

$$B_{1,1} + 2C_{1,1} + 3D_{1,1} + i\alpha R_1\frac{\partial h_1(1)}{\partial y} = 0, \tag{D.25}$$

at $y = 1$ and

$$A_{1,N} = 0, \qquad B_{1,N} = 0, \tag{D.26}$$

at $y = 0$.

We now make a transformation similar to that for the zeroth order problem. This time it is more convenient to transform all the variables such that

$$X_{1,j} = i\alpha R_1 \tilde{X}_{1,j} + B_{1,1} \tilde{X}_{1,j}. \tag{D.27}$$

The recurrence relations for the variables $\tilde{X}_{1,j}$ are identical to the equations for the zeroth order problem with $\tilde{X}_{0,j}$ being replaced by $\tilde{X}_{1,j}$. These equations are simply iterated using the known values of c_0.

The recurrence relations in $\tilde{X}_{1,j}$ become

$$\begin{aligned} \hat{A}_{1,j+1} &= (1 - F_j y_j)\hat{A}_{1,j} - F_j y_j^2 \hat{B}_{1,j} - y_j^2(\hat{C}_{1,j} - \hat{C}_{1,j+1}) \\ &\quad -2y_j^3(\hat{D}_{1,j} - \hat{D}_{1,j+1}) - F_j y_j^3(\hat{C}_j + y_j \hat{D}_j) + Q_j(h_j - y_j \frac{\partial h_j}{\partial y} - F_j y_j h_j) \\ &\quad -Q_{j+1}(h_{j+1} - y_j \frac{\partial h_{j+1}}{\partial y}) + \frac{F_j}{\epsilon_{0,j}} y_j \phi_{0,j} c_1^*, \end{aligned} \tag{D.28}$$

$$\begin{aligned} \hat{B}_{1,j+1} &= (1 + F_j y_j)\hat{B}_{1,j} - F_j \hat{A}_{1,j} + 2y_j(\hat{C}_{1,j} - \hat{C}_{1,j+1}) \\ &\quad +3y_j^2(\hat{D}_{1,j} - \hat{D}_{1,j+1}) + F_j y_j^2(\hat{C}_j + y_j \hat{D}_j) + Q_j(\frac{\partial h_j}{\partial y} + F_j h_j) \\ &\quad -Q_{j+1}\frac{\partial h_{j+1}}{\partial y} + \frac{F_j}{\epsilon_{0,j}} \phi_{0,j} c_1^*, \end{aligned} \tag{D.29}$$

$$\mu_{j+1}\hat{C}_{j+1} = \mu_j \hat{C}_j + \frac{1}{2}\left\{ \frac{\partial^2 h_j}{\partial y^2} - \frac{\partial^2 h_{j+1}}{\partial y^2} + y_j \left[\frac{\partial^2 h_j}{\partial y^2} - \frac{\partial^2 h_{j+1}}{\partial y^2} \right] \right\}, \tag{D.30}$$

and

$$\mu_{j+1}\hat{D}_{j+1} = \mu_j \hat{D}_j + \frac{1}{6}\left(\frac{\partial^3 h_j}{\partial y^3} - \frac{\partial^3 h_{j+1}}{\partial y^3} \right), \tag{D.31}$$

where $c_1^* = i\alpha R_1 c_1$.

The boundary conditions at $y = 1$ are

$$\begin{aligned} \hat{A}_{1,1} &= 0, & \hat{B}_{1,1} &= 0, \\ \hat{C}_{1,1} &= \frac{\partial h_1}{\partial y} - 3h_1, & \hat{D}_{1,1} &= -\frac{\partial h_1}{\partial y} + 2h_1. \end{aligned} \tag{D.32}$$

Finally, the boundary condition at $y = 0$ becomes

$$\hat{A}_{1,N}\hat{B}_{1,N} - \hat{B}_{1,N}\hat{A}_{1,N} = H(c_1^*) = 0. \tag{D.33}$$

It can be seen from these relations that all the variables $\hat{X}_{1,j}$ must be entirely real and that c_1^* is also real. From this we see that the first order eigenvalue c_1 must be entirely imaginary and of the form

$$c_1 = i\alpha R_1 J, \tag{D.34}$$

where J is a real function.

The problem is now similar to the zeroth order case. We must find the zeroes of the function $H(c_1^*)$. This is more simple that for the zeroth order case since H is linear in c_1^* and the zeroes can be calculated directly without using a bisection algorithm.

Bibliography

[1] J.P. Humm *Unpublished*

[2] P.K. Vinson, Y. Talmon. *J. Colloid Interface Sci.* V133 p288 (1989)

[3] H.C. Hamaker. *Physica* **4** p1058 (1937) **133** p288 (1989)

[4] H.P.G. Casimir, D. Polder. *Phys. Rev.* **73** p360 (1948)

[5] P. Langevin. *Comptes Rendus Acad. Sci.* (Paris) **146** p530 (1908)

[6] H. Haken. *Synergetics* Springer-Verlag (1978)

[7] R.H. Weiland, Y.P. Fessas, B.V. Ramarao. *J. Fluid Mech.* **142** p383 (1984)

[8] G.K. Batchelor, R.W. Janse Van Rensburg. *J. Fluid Mech.* **166** 379 (1986)

[9] K. Almdal, J. Dyre, S Hvidt. O. Kramer. *Polymer Gels and Networks* **1** p5 (1993)

[10] R. Buscall. I.J. McGowan, P.D. Mills, R.F. Stewart, D. Sutton, L.R. White, G.E. Yates. *J. Non-Newtonian Fluid Mech.* **24** p183 (1987)

[11] R. Buscall, P.D.A. Mills, J.W. Goodwin, D.W. Lawson. *J. Chem. Soc. Faraday Trans.* **84** p4249 (1988)

[12] C. Allain, L. Salomé. *Macromolecules* **23** p981 (1990)

[13] M. Adam, M. Delsanti, J. Munch, D. Durand. *J. Phys.* **48** (1987) p1809

[14] D. Stauffer *Percolation Theory*

[15] M. Adam, M. Delsanti, D. Durand, G. Hild, J.P. Munch. *Pure and Appl. Chem* **53** p1489 (1981)

[16] M.F. Thorpe. *J Non-Cryst. Solids* **76** p109 (1985)

[17] M.F. Thorpe. *J Non-Cryst. Solids* **57** p355 (1983)

[18] P.M. Duxbury, P.L.Leath, P.D. Beale. *Phys. Rev. B* **36** p367 (1987)

[19] D.A. Denny, R.S.Brodkey. *J. Appl. Phys.* **33** p2269 (1962)

[20] J.D. Eshelby. *Proc. Roy. Soc. Lond.* **A241** p376 (1957)

[21] Z. Hashin. *J. Appl. Mech.* **29** p143 (1962)

[22] R.L. Hoffman. *Trans. Soc. Rheol.* **16** p155 (1972)

[23] R.L. Hoffman. *J. Colloid Interface Sci.* **46** p491 (1974)

[24] M. Tomita, T.G.M. Van De Ven. *J. Colloid Interface Sci.* **99** p374 (1984)

[25] B.J. Ackerson, P.N. Pusey. *Phys. Rev. Lett.* **61** p1033 (1988)

[26] R. Buscall. *Private Communication*

[27] G.I. Taylor. *Proc. Roy. Soc.* (London) **A132** p499 (1931)

[28] H.B. Squire. *Proc. Roy. Soc.* (London) **A142** p621 (1933)

[29] C.S. Yih. *J. Fluid Mech.* **27** p337 (1967)

[30] C.H. Li. *Phys. Fluids* **12** p2473 (1969)

[31] G. Stokes. *Trans. Cambridge Philos. Soc.* **9** p8 (1851)

[32] H. Faxén. *Arkiv. Mat. Astron. och Fys.* **17**, No. 1 (1922) ; **20**, No. 8 (1927)

[51] G.K. Batchelor *J. Fluid Mech.* **41** p545 (1970)

[52] I.S. Gradshteyn, I.M. Ryzhik. *Table Of Integrals, Series and Products* (Academic Press) p64 (1965)

[53] G. Rowlands. *Appl. sci. Res.* **8** Section B p62 (1959)

[54] J.R. Blake. *Proc. Camb. Phil. Soc.* **70** p303 (1971)

[55] H. Hasimoto, O. Sano. *Ann. Rev. Fluid Mech.* **12** p335 (1980)

[56] N. Phanthien. *J. Elasticity* **13** p231 (1983)

[57] J.R. Blake, A.T. Chwang. *J Eng. Math.* **8** p23 (1974)

[58] S.J. Weinstein, M.R.Kurz. *Phys. Fluids* A **3** p2680 (1991)

[59] A.P. Hooper, R. Grimshaw. *Phys. Fluids* **28** p37 (1985)

[60] C.S. Yih. *Fluid Mechanics* (McGraw-Hill) p511 (1969)

[61] E.J. Hinch. *J. Fluid Mech.* **144** p 463 (1984)

[62] P.G. Drazin, W.H. Reid. *Hydrodynamic Stability* (Cambridge University Press) Sec. 25. (1989)

[63] W.H. Press, B.P. Flannery, S.A. Teulolsky, W.T. Vetterling. *Numerical Recipes* (Cambridge University Press) p579.

[64] D.D. Joseph. *J. Fluid Mech.* **33** p617 (1968)

[65] G. Segré, A. Silverberg. *J. Fluid Mech.* **14** p115 (1962)

[66] G. Segré, A. Silverberg. *J. Fluid Mech.* **14** p136 (1962)

[67] G. Segré, A. Silverberg. *J. Colloid Sci.* **18** p312 (1963)

[68] J.S. Halow, G.B. Wills. *A.I.Ch.E* **16** p281 (1970)

[69] J.S. Halow, G.B. Wills. *Ind. Eng. Chem. Fundam.* **9** p603 (1970)

[70] M.A. Jefri, A.H. Zahed. *J. Rheology* **33** p691 (1989)

[71] S.I. Rubinow, J.B. Keller. *J. Fluid Mech.* **11** p447 (1961)

[72] H.A. Lorentz. *Abhandl. Theoret. Phys.* **1** p23 (1907)

[73] R.G. Cox, S.K. Hsu. *Int. J. Multiphase Flow* 3 p201 (1977)

[74] J.B. McLaughlin. *J. Fluid Mech.* 224 p261 (1991)

[75] S.L. Passman. *J. Rheology* **30** p1077 (1986)

[76] D.A. Drew. *Ann. Rev. Fluid Mech.* **15** p261 (1983)

[77] S.L. Passman. *Two Phase Flows And Waves* IMA Volumes In Mathematics Volume 26 p80 Springer-Verlag (1990)

[78] G.K. Batchelor. *An Introduction To Fluid Mechanics* p 149 (Cambridge University Press) (1967)